UNIVERSITY OF SZEGED

Doctoral School of Geosciences

Faculty of Science and Informatics

Department of Physical and Environmental Geography

PERFORMANCE OF SHALLOW GEOPHYSICAL TECHNIQUES IN THE ASSESSMENT OF EARTH AND ROAD STRUCTURES

PhD DISSERTATION

ENAS MUHAMMED ABDELRAZEK ABDELSAMEI

Supervisor:

Dr. GYÖRGY SIPOS

associate professor

Szeged

2025

Table of Contents

Abbreviations and acronyms

GPR: Ground Penetrating Radar

ERT: Electrical Resistivity Tomography

RMS: Root Mean Square

DMI: Distance Measuring Instrument

SR: Surface Reflection

RD: Relative Density

HMA: Hot Mix Asphalt

AC: Asphalt Concrete

EM: Electromagnetic

$\mathbf{G_{mb}}$: Bulk Specific Gravity

$\boldsymbol{\varepsilon_r}$**:** Relative Dielectric Permittivity

$\boldsymbol{\varepsilon}$: Dielectric Permittivity

W: Water Content

D50: Median Grain Size

$\boldsymbol{\varphi}$: Porosity

$\boldsymbol{\rho}$: Density

K: Saturated Hydraulic Conductivity

f: Volume Fraction of Water

$\mathbf{h_{GT}}$: Ground Truth-derived Thickness

$\mathbf{h_{amp}}$**:** Amplitude-derived Thickness

SIR: Subsurface Interface Radar

$\mathbf{A_1}$**:** Reflected amplitude from the top of the subsequent layer

$\mathbf{A_m}$**:** EM wave reflection amplitude of the metal plates

Aa: EM wave reflection amplitude of the asphalt surface

$\boldsymbol{\varepsilon_a}$**:** Dielectric value of the asphalt layer

$\boldsymbol{\varepsilon_{eff}}$**:** Effective permittivity

$\boldsymbol{\varepsilon_i}$**:** Permittivity of the inclusion

$\boldsymbol{\varepsilon_e}$**:** Permittivity of the environment

Tr: Proportion of energy transmitted

R: Reflection coefficient MSZ

MSZ-EN: Hungarian Standard

e-UT: Hungarian Road technical regulations in force

FIR: Finite Impulse Response

Dz: Depth of the water-bearing zone

Wz: Width of the water-bearing zone

Rz: True resistivity of the water-bearing zone

nV: Volume fraction of the inclusions in the mixture

1 Preliminaries

1.1 Parameters affecting the performance of GPR and ERT

Ground Penetrating Radar (GPR) and Electrical Resistivity Tomography (ERT) are non-destructive geophysical methods widely used for assessing the condition of built infrastructure such as roads and levees. However, the effectiveness of these techniques is significantly influenced by various environmental and intrinsic parameters. The understanding of the effects of these parameters on GPR and ERT measurements across different applications is crucial to making reliable interpretations, utilising the full potential of non-destructive geophysical methods and assessing their limitations

The key parameters affecting the performance of geophysical methods, particularly GPR and ERT, include mineral moisture content, temperature, composition, porosity, air void content, density, compaction, grain size, clay content, bitumen content, and structural heterogeneity, with moisture content and aggregate type having the most significant influence on dielectric properties and resistivity measurements.

1.1.1 Impact of Environmental parameters

Moisture content is one of the most critical environmental factors affecting GPR and ERT measurements across all types of applications, including infrastructures. Its influence is profound and multifaceted, impacting materials' electromagnetic and electrical properties in ways that significantly alter geophysical readings.

In pavements, moisture content plays a crucial role in GPR measurements, as it directly affects the dielectric properties of asphalt. Moisture content is significantly influenced by material composition and physical characteristics, such as aggregate type, bulk density, bitumen content, and air void content. Loken (2007) elaborated on the concept of moisture impact, noting that water has a greater dielectric constant (81) than either air (1) or soil materials (4-20), which significantly affects the dielectric characteristics of materials. This difference in dielectric properties makes moisture content a key factor in interpreting GPR data from aged road structures. Daniels (2004) highlighted this relationship by reporting that dry asphalt's dielectric constant (ε) typically ranges from 2 to 4, while wet asphalt exhibits significantly higher values, ranging from 6 to 10. Building on this, Evans et al. (2007) demonstrated that even when asphalt materials appear similar, their dielectric constants can vary under comparable conditions, further emphasizing the complex interplay between moisture, material properties, and GPR responses. Al-Qadi et al. (2002) observed that changes in dielectric constant values were

attributed to test site moisture content variations. This finding highlights the sensitivity of GPR to moisture fluctuations in older road structures as well. The impact of moisture on aged road assessments is further emphasized by (Al-Qadi et al., 2005), who found that the age of the pavement increased the GPR thickness error, with a 4.4% error for pavements 0-5 years old versus a 5.8% error for pavements older than 20 years. This increase in error with age can be partially attributed to the cumulative effects of moisture infiltration and retention in older pavement structures. The sensitivity of GPR to moisture in aged roads was further demonstrated by Saarenketo and Scullion (2000), who found that GPR can identify and decipher various subsurface reflections from asphalt layers with a buried moisture barrier. For newly constructed roads, moisture content remains a significant factor in GPR assessments, particularly in the context of compaction quality control.

Leng et al. (2012) and Shangguan et al. (2016) suggested that GPR can be utilized as a non-nuclear method to assess compaction quality and monitor the compaction process during asphalt pavement construction. The ability of GPR to detect moisture variations makes it a valuable tool for ensuring proper compaction, as excess moisture can lead to inadequate compaction and subsequent pavement deterioration. Saarenketo (1997) and Saarenketo & Roimela (1998) reported that compaction of the asphalt layer minimizes the presence of low-dielectric air in the asphalt mixture, while the volumetric ratios of high-dielectric asphalt and rock are augmented, leading to elevated dielectric constant values. This relationship between compaction, moisture, and dielectric properties underscores the importance of considering moisture content when using GPR for quality control in new road construction. Many tests were done to assess the repeatability of GPR on dry and wet pavements (Willett et al., 2006). Soil moisture in the surrounding area can affect the overall moisture conditions of the studied structures. Al-Qadi et al. (2002) reported soil moisture values at 10 cm depth for different survey dates, which correlated with the observed dielectric values of pavement materials.

When assessing earth structures. The impact of moisture on ERT and GPR measurements is particularly pronounced. Antoine et al. (2015) successfully coupled GPR with permeability logging to identify seepage zones. This approach demonstrates the effectiveness of GPR in detecting moisture-related issues in levee structures. Sentenac et al. (2017) used ERT surveys to map historical earthworks for structural heterogeneity and post-flood damage, further illustrating the sensitivity of ERT to moisture variations in levee materials. Tresoldi et al. (2019) employed ERT to identify seepage zones and

sections experiencing intense water saturation, demonstrating that the technique is suitable for structural assessments and long-term monitoring. This application of ERT highlights its capability to detect and monitor moisture-related issues in levee structures over time.

Dielectric permittivity measured by GPR is strongly influenced by water content in levee materials. Perri et al. (2014) observed a clear relationship between water content and dielectric permittivity, with higher water content leading to increased permittivity values. Water content significantly affects both resistivity and dielectric permittivity measurements. Jodry et al. (2019) found a strongly negative correlation between resistivity and water content, especially after infiltration. The study also noted that materials with higher water content tended to have lower resistivity. Several researchers explored the relationship between moisture content and resistivity in levee materials (Fukue et al. (1999), Michot et al. (2000), Yoon and Park (2001), and Loke (2004)); all of them observed an inverse relation between resistivity and water content. This consistent finding across multiple studies underscores the reliability of ERT in assessing moisture conditions within levee structures. Jodry et al. (2019) utilized ERT and temperature profiles to monitor changes in soil moisture within a levee, which they subsequently used to generate models to estimate seasonal variations in resistivity. This approach demonstrates the potential for using these techniques in ongoing infrastructure health assessments, particularly in changing moisture conditions. Precipitation history is a crucial environmental parameter significantly influencing GPR and ERT measurements, particularly in earth structure and road condition evaluations. Its impact is closely related to moisture content but represents a more dynamic and immediate environmental factor. For aged road structures, precipitation can significantly impact GPR measurements due to the potential for water infiltration into deteriorated pavement layers. In the context of new road construction and assessment, precipitation can affect GPR measurements by altering the moisture content of pavement materials. Liu and Guo (2003) reported that moisture content significantly influenced dielectric permittivity and electromagnetic wave velocity under different conditions. This finding suggests that recent precipitation events could impact GPR measurements on newly constructed roads. Tresoldi et al. (2019) use of ERT to identify seepage zones and sections experiencing intense water saturation demonstrates the technique's sensitivity to precipitation-induced moisture variations in levee structures. The impact of precipitation on levee assessments is further emphasized by studies that observed higher dielectric values in GPR measurements

following periods of high precipitation. This relationship underscores the importance of considering recent precipitation events when planning and interpreting GPR and ERT surveys for levee assessment.

Temperature is another significant environmental parameter that affects GPR and ERT measurements, albeit often in more subtle ways than moisture content. Its impact is particularly notable in road assessments, where temperature variations can alter material properties and influence geophysical readings. For aged pavements, temperature variations can exacerbate existing structural issues, potentially affecting GPR measurements. Al-Qadi et al. (2005) observed it can be inferred that temperature fluctuations could contribute to the increased GPR thickness error in older pavements. In new road construction and assessment, temperature plays a crucial role in material properties and subsequent GPR measurements. Kassem et al. (2012) found that lower compaction temperatures increased air voids in both Hot Mix Asphalt (HMA) and Warm Mix Asphalt (WMA). This relationship between temperature and material properties directly impacts GPR measurements, as changes in air void content affect the dielectric properties of the asphalt mixture. The impact of temperature on GPR measurements in road assessments was further explored by (Al-Qadi et al., 2002), who noted that temperature variations could contribute to changes in dielectric constant values. This observation highlights the need to consider temperature as a factor when interpreting GPR data for road condition assessment. It can be inferred that temperature variations could impact ERT measurements in levees, particularly in conjunction with moisture content. Jodry et al. (2019) suggest that using temperature profiles alongside ERT for monitoring soil moisture in levees is also a relevant factor in levee assessment.

Seasonal changes encompass variations in environmental parameters, including temperature, precipitation, and overall moisture conditions. These cyclical changes can significantly impact GPR and ERT measurements across all types of infrastructure. Seasonal variations can exacerbate the challenges of assessing aged road structures using GPR and ERT. Al-Qadi et al. (2002) found that thickness inaccuracies showed significant variations in measurements taken at the same location but at different times. This observation highlights the need to consider seasonal fluctuations when planning and interpreting GPR surveys for old road assessments. For newly constructed roads, seasonal variations can impact GPR and ERT measurements by altering material properties and moisture conditions. While not explicitly mentioned in the provided text, it can be inferred that the relationship between moisture, temperature, and air void content observed by

(Kassem et al., 2012) would be subject to seasonal fluctuations, potentially affecting GPR measurements. Seasonal variations have a particularly significant impact on levee assessments using GPR and ERT. Jodry et al. (2019) use ERT and temperature profiles to generate models estimating seasonal variations in resistivity, demonstrating the importance of considering seasonal changes in levee monitoring and assessment.

The variability introduced by environmental parameters underscores the need for robust calibration methods. Loizos and Plati (2007a; 2007b) evaluated various calibration approaches, including core calibration, reflection amplitude calibration, and laboratory dielectric constant calculations. These methods are crucial for accurately interpreting GPR and ERT data in varying environmental contexts. The ability of GPR and ERT to detect moisture variations makes them valuable tools for long-term infrastructure monitoring. (Jodry et al., 2019) utilized ERT and temperature profiles to monitor changes in soil moisture within a levee, which they subsequently used to generate models to estimate seasonal variations in resistivity. This approach demonstrates the potential for using these techniques in ongoing infrastructure health assessments. This comprehensive literature review reveals that environmental parameters, particularly moisture content, temperature, precipitation, and seasonal variations, significantly impact GPR and ERT measurements across old roads, new roads, and levees. Understanding these environmental effects is essential for accurately interpreting GPR and ERT data and developing effective infrastructure assessment and management strategies. For old roads, the cumulative effects of environmental factors over time pose challenges for accurate GPR assessments. In new road construction, considering environmental parameters is crucial for quality control and long-term performance prediction. In levee assessments, environmental factors are critical in detecting and monitoring seepage and structural integrity issues. These findings underscore the importance of considering environmental parameters when planning, conducting, and interpreting GPR and ERT surveys for infrastructure assessment. Future research should focus on developing more robust methods to account for these parameters, improving the accuracy and reliability of non-destructive testing techniques for infrastructure evaluation. As climate change continues to alter environmental conditions, the ability to accurately assess and monitor infrastructure using these non-destructive methods will become increasingly valuable. Advances in data processing techniques, integration with other assessment methods, and developing long-term monitoring strategies that account for environmental variability

offer promising avenues for enhancing our understanding and management of critical infrastructure.

1.1.2 Impact of intrinsic parameters

Air void content is a crucial parameter in assessing the quality and performance of asphalt pavements. (Roberts et al., 1996) the ideal range for air void content is between 3% and 8%. (Brown, 1990) highlights that higher air void content can lead to moisture damage, binder oxidation, pavement ravelling, and cracking.

Lower air void content increases stiffness and reduces rutting potential but may cause bleeding. In dense-graded asphalt mixtures, if the air void content falls below 3%, it can lead to significant permanent deformation and shoving (Brown, 1990; Roberts et al., 1996). Compaction is critical in achieving the desired density and air void content, with each compactor passing decreasing the air void content. GPR measurements can monitor these parameters, providing valuable information about the pavement's structural integrity and potential for long-term performance. Al-Qadi et al. (2005) found that variations in asphalt moisture content can impact GPR outcomes. At the same time (Porubiaková and Komačka, 2015) noted that the sources of variations in dielectric constants include asphalt composition and material characteristics such as bitumen content, aggregate bulk density, and air void content. As compaction increases, the presence of low-dielectric air in the asphalt mixture is minimized, while the volumetric ratios of high-dielectric asphalt and rock are augmented, leading to elevated dielectric constant values (Saarenketo, 1997; Saarenketo & Roimela, 1998). This relationship directly impacts GPR measurements, as the dielectric constant is a key input parameter for calculating layer thickness (Al-Qadi & Lahouar, 2005). In the context of levee assessment, porosity is closely related to grain size and moisture content, which significantly influence resistivity measurements in ERT surveys (Samouelian et al., 2005; Cosenza et al., 2006; Sudha et al., 2009; Oludayo 2021). Understanding these complex interactions is crucial for accurately interpreting geophysical data and assessing the condition of both pavements and levees.

The mineral composition of materials plays a significant role in geophysical measurements, particularly in pavement and levee assessments (Keller, 2017). The aggregate type has the greatest influence on the dielectric constant among the constituents of asphalt mixtures. Different rock types used as aggregates, such as dolomite and limestone, are preferred due to their resistance to fragmentation and polishing (Šernas et

al., 2016). These rock types have densities similar to volcanic and crystalline rocks but exhibit notably different dielectric constants (ElShafie & Heggy, 2013; Hartlieb et al., 2016). In the context of earthen levee assessment, the mineral composition of sedimentary layers and deposits significantly influences their resistivity, which is crucial for Electrical Resistivity Tomography (ERT) surveys (Samouelian et al., 2005; Cosenza et al., 2006; Sudha et al., 2009; Oludayo, 2021). The clay content in levees has been particularly noted to affect the performance of Ground Penetrating Radar (GPR), often limiting its ability to investigate deeper structures (Busato et al., 2016; Perri et al., 2014). Therefore, understanding the mineralogical composition of materials is essential for accurately interpreting geophysical data and assessing the condition of both pavements and levees, as it directly impacts the dielectric and resistivity properties measured by GPR and ERT techniques.

Grain size plays a crucial role in the geophysical properties of materials, particularly in the context of pavement engineering; aggregate size is a critical factor affecting the physical properties of the asphalt mixture and its geophysical response. The type and size of aggregates used in pavement construction significantly impact the dielectric properties measured by GPR (Keller, 2017). The aggregate type has the greatest influence on the dielectric constant among the constituents of asphalt mixtures. Different rock types used as aggregates, such as dolomite and limestone, are preferred due to their resistance to fragmentation and polishing (Šernas et al., 2016). These rock types have densities similar to volcanic and crystalline rocks but exhibit notably different dielectric constants (ElShafie & Heggy, 2013; Hartlieb et al., 2016). The aggregate bulk density, along with bitumen and air void content, contributes to variations in dielectric constants (Porubiaková & Komačka, 2015). These variations directly impact GPR measurements, as the dielectric constant is a key input parameter for calculating layer thickness (Al-Qadi & Lahouar, 2005). Therefore, understanding the relationship between aggregate size, composition, and geophysical PR properties is essential for accurately interpreting GPR data and assessing pavement quality and performance.

In the context of levee assessment and soil characterization. Several studies have observed a proportional relationship between resistivity and grain size (Samouelian et al., 2005; Cosenza et al., 2006; Sudha et al., 2009; Oludayo, 2021). This relationship is particularly important in Electrical Resistivity Tomography (ERT) surveys, where the grain size distribution of sedimentary layers and deposits significantly influences the measured resistivity values. Fine-grained materials, especially clay, have been noted to

limit the effectiveness of Ground Penetrating Radar (GPR), reducing its ability to investigate deeper structures (Busato et al., 2016; Perri et al., 2014). This limitation highlights the importance of considering grain size when selecting and interpreting geophysical methods for level assessment.

Thickness is a critical parameter in assessing pavement quality and remaining life. Ground Penetrating Radar (GPR) has proven to be highly accurate in determining the thickness of asphalt layers, particularly when using air-coupled antennas (Al-Qadi & Lahouar, 2005; Al-Qadi et al., 2005; Domitrović & Rukavina, 2013; Domitrović et al., 2019; Flintsch et al., 2005; Holzschuher et al., 2007; Loizos & Plati, 2007b; Sener et al., 1998; Willett et al., 2006; Hugenschmidt, 1996). The accuracy of GPR thickness measurements has been extensively studied, with various researchers reporting different levels of precision. Al-Qadi et al. (2005) found that the age of the pavement increased the GPR thickness error, with pavements older than 20 years showing a 5.8% error compared to 4.4% for pavements 0-5 years old. For older pavements with thicknesses ranging from 280 to 350 mm, Al-Qadi et al. (2005) reported an average error of 6.8%. The impact of these parameters on GPR measurements differs between old and new roads and earth structures. This could be due to the accumulation of moisture, changes in material properties over time, and the development of cracks and other defects.

Pavement layer thickness is critical in estimating the remaining pavement life and ensuring quality assurance during and after construction (Bezina et al., 2021). The accuracy of GPR in thickness measurement is crucial for assessing pavement conditions and planning maintenance activities. However, the effectiveness of GPR in measuring thickness can be influenced by various factors, including the age of the pavement and environmental conditions. Previous studies have used field data to demonstrate the anticipated physical constraints associated with the use of GPR technology for pavement thickness detection (Al-Qadi & Lahouar, 2005), with some authors addressing the accuracy issues associated with using GPR to assess the surface layer thickness of various pavement layers (Sener et al., 1998; Willett et al., 2006; Domitrović & Rukavina, 2013). In the case of levees, Sentenac et al. (2017) studied an old levee system in Hungary, and the age and lack of comprehensive construction documentation complicated the assessment of its effectiveness. The study demonstrated that GPR and ERT could successfully delineate seepage pathways and identify subsurface features in these older structures.

The age of the pavement has been found to affect the accuracy of GPR thickness measurements. Al-Qadi et al. (2005) investigated the thickness error of newly constructed pavement. They found that GPR data from several locations revealed an increase in thickness inaccuracy with the age of the pavement. This finding suggests that as pavements age, their properties may change in ways that affect GPR measurements. Conversely, Ožbolt et al. (2012) found that the error in new motorway pavements was mostly less than that of regional/county roads with several years of service. These contrasting findings highlight the complex relationship between pavement age and GPR measurement accuracy and underscore the need for careful calibration and interpretation of GPR data, especially when assessing older pavements.

The age of infrastructure, particularly in the case of levees, can also impact geophysical assessments. In Hungary, for example, artificial levees were constructed along water channels decades ago, and over time, multiple interventions have been conducted at various locations in response to specific flood events (Szűcs et al., 2019; Kiss et al., 2021). The advanced age of these levees means that information on their structural attributes, composition, and resilience against floods is often limited. This lack of historical data can complicate the interpretation of geophysical measurements and necessitates a comprehensive approach to assessment. Using multiple geophysical methods, such as combining GPR with Electrical Resistivity Tomography (ERT), can provide a more complete picture of the condition of aged infrastructure. Additionally, integrating geophysical measurements with geotechnical data and historical records, where available, can enhance the accuracy and reliability of assessments for older structures.

1.2 Knowledge Gaps

The use of shallow geophysical methods is becoming increasingly widespread in infrastructure assessment. However, in some applications, there is limited information on the accuracy and reliability of these methods and the obtained results (Perri et al., 2014; Rahimi et al., 2018; Dezert et al., 2019; Jodry et al., 2019; Tresoldi et al., 2019; Lee et al., 2020). Consequently, the performance of these methods needs to be tested, and geophysical results must be validated in various applications. This study addresses several interconnected problems across flood protection levees, aged roads, and new roads.

The assessment of levees faces significant challenges, including the lack of high-resolution measurements during flood conditions to accurately assess seepage

characteristics, which limits our understanding of levee behaviour under critical stress. Additionally, the scarcity of direct measurements on seepage pathways poses a considerable challenge in levee assessment, as highlighted by the absence of geotechnical measurements to serve as control data in numerous instances, which has hindered the validation of geophysical methods such as ERT.

There is a scarcity of comprehensive studies comparing geophysical survey results across different seasons and moisture conditions for aged roads despite evidence that environmental parameters significantly affect the obtained geophysical results. The lack of extensive reproducibility measurements under varying environmental conditions for older road structures limits our ability to quantify the reliability and consistency of geophysical methods, such as GPR, in assessing aged infrastructure over time and under different climatic scenarios.

The quality of newly constructed pavement depends largely on compaction, which ensures pavement longevity and performance. Traditional methods of evaluating pavement compaction and density, such as core sampling and nuclear gauge measurements, are often time-consuming and invasive and provide only limited data points at a low spatial resolution. A non-destructive method is needed to assess the specific gravity of asphalt mixtures at different degrees of compaction and generate relative density maps to visualize the spatial homogeneity of asphalt density.

1.3 Research objectives and questions

The study aimed to evaluate the impact of seepage on the integrity of artificial levees in low-lying regions, with a particular focus on Hungary, by applying advanced geophysical methods to assess levee integrity and seepage dynamics. Additionally, it investigated the applicability of Ground Penetrating Radar (GPR) in road assessments, particularly for aged roads with complex structures, while examining the influence of environmental conditions on GPR results and the relationship between GPR parameters and road composition. Furthermore, the research focused on assessing the specific gravity of a dolomitic asphalt mixture at different degrees of compaction using GPR techniques, aiming to generate relative density (RD) maps to visualize the spatial homogeneity of asphalt density and develop a method for density assessment by surveying asphalt at varying levels of compaction.

Considering the theoretical framework and objectives, the following scientific questions were developed:

1. How effective are electrical resistivity tomography (ERT) and ground-penetrating radar (GPR) in delineating seepage pathways and accurately identifying subsurface features in levees?
2. How do the results of geophysical surveys, particularly Ground Penetrating Radar (GPR) and Electrical Resistivity Tomography (ERT), compare with validation through drilling, and what are the relative strengths and limitations of these methods in assessing infrastructures such as levees and pavements?
3. How accurate and reproducible are GPR measurements for assessing road thickness and structure in aged pavements with a complex multilayer structure?
4. How do different environmental conditions and pavement properties affect GPR measurements and the obtained dielectric constant values?
5. What is the optimal procedure to map dielectric constants and related physical properties through field and laboratory comparisons?
6. How can Ground Penetrating Radar (GPR) be effectively utilized to determine the specific gravity and relative density of asphalts?
7. Is it possible to develop a general function between dielectric properties and specific gravity for dolomitic pavements to facilitate compaction quality mapping?

1.4 Dissertation outlines

The chapters draw upon scientific articles published in peer-reviewed journals. Each chapter outlined below articulates its research objectives, with the overall conclusions and future outlook provided in the comprehensive conclusion and perspectives section. Furthermore, each chapter can be regarded as exploring an independent research query.

Chapter 1: This chapter presents a summary of the dissertation, featuring a concise literature review that addresses the primary topics of the study. It also defines the problem statement, explains the research objective, formulates the hypotheses, and outlines the overall structure of the dissertation.

Chapter 2: Begins by introducing the challenges of assessing older levee structures and the importance of non-destructive evaluation techniques. It then describes the study area along the Körös River and the experimental setup using a tank to simulate flood conditions. The methodology section details the use of Electrical Resistivity Tomography (ERT), Ground Penetrating Radar (GPR), and borehole drilling for validation. Results

present the 3D ERT and GPR profiles showing seepage pathways and zones. The discussion evaluates the effectiveness of these geophysical methods in levee assessment and their implications for flood risk assessment, as well as addresses limitations. The conclusion summarizes key findings and offers recommendations for future levee integrity assessments.

Chapter 3: Addresses the challenges of assessing aged roads with complex structures and introduces GPR as a potential solution. It describes the study area, a 1 km section of a secondary road near Gyöngyös, Hungary. The methodology covers GPR data collection using a SIR-30 unit with multiple antennas, surveys under different environmental conditions, data processing techniques, thickness calculation methods, and dielectric analysis. Results present the accuracy of GPR thickness measurements, dielectric variations under different conditions, and relationships between GPR parameters and road composition. The discussion explores the applicability of GPR for aged road assessment, the impact of environmental conditions on results, and implications for road maintenance. The conclusion summarizes findings and provides recommendations for future aged road assessments using GPR.

Chapter 4: Introduces the importance of compaction in asphalt pavement quality and the potential of GPR in assessing it. It describes the study area comprising two recently paved roads in Szeged, Hungary. The methodology section covers GPR techniques using horn antennas and surface reflection methods, calibration with nuclear density gauging, validation using core samples, data analysis, relative density mapping, and the development of a compaction assessment method. Results present relationships between dielectric constants, specific gravity, aggregate size, and relative density maps showing spatial homogeneity of asphalt density. The discussion evaluates the applicability of GPR for assessing asphalt compaction quality, its advantages over traditional methods, and implications for pavement construction and quality control. The conclusion summarizes key findings and recommends implementing GPR in asphalt compaction quality assessment.

Chapter 5: Describes the dissertation's main conclusions, implications, limitations, and suggestions.

2. Detection of seepage zones in artificial levees: a case study at the Körös River, Hungary

This article is published in Open Geosciences Journal as:
Enas Abdelsamei, Attila Timar, Diaa Sheishah, Viktória Blanka-Végi, Alexandru Hegyi, Boglárka Runa, Olivér Balogh, Ahmed M. Ali, György Sipos
Detection of seepage zones in artificial levees: a case study at the Körös River, Hungary," in *Open Geosciences 2024; 16: 20220744*
DOI:10.1515/geo-2022-0744
Journal Impact Factor:1.99 (2023-2024)

Research Article

Enas Abdelsamei, Attila Tímár, Diaa Sheishah, Viktória Blanka-Végi, Alexandru Hegyi, Boglárka Runa, Olivér Balogh, Ahmed M. Ali, and György Sipos*

Detection of seepage zones in artificial levees: A case study at the Körös River, Hungary

https://doi.org/10.1515/geo-2022-0744
received September 09, 2024; accepted November 26, 2024

Abstract: This study evaluates the impact of seepage on the integrity of artificial levees in low-lying regions, with a particular focus on Hungary, where levees built over a century ago lack comprehensive construction documentation, complicating current assessments of their effectiveness. Advanced geophysical methods – electrical resistivity tomography (ERT) and ground-penetrating radar (GPR) – were applied in a controlled tank experiment designed to simulate varied flood conditions along a 37-m levee section. The three-dimensional (3D) ERT profiles successfully delineated seepage pathways as the tank filled, while the 3D GPR profiles indicated areas of increased amplitude, corresponding to seepage zones and the water table. Validation through drilling confirmed the geophysical findings, underscoring the accuracy of ERT and GPR in non-destructively identifying subsurface features and seepage channels. The results highlight the applicability of these methods for evaluating levee integrity and seepage dynamics, offering a reliable approach for flood risk assessment in Hungary and similar flood-prone areas worldwide.

Keywords: artificial levee, seepage, electrical resistivity tomography, ground-penetrating radar, drilling

*** Corresponding author: György Sipos,** Department of Geoinformatics, Physical and Environmental Geography, University of Szeged, Egyetem u. 2-6., 6722 Szeged, Hungary; National Laboratory for Water Science and Water Safety, Herman Ottó út 15, 1022 Budapest, Hungary, e-mail: gysipos@geo.u-szeged.hu
Enas Abdelsamei: Department of Geoinformatics, Physical and Environmental Geography, University of Szeged, Egyetem u. 2-6., 6722 Szeged, Hungary; National Research Institute of Astronomy and Geophysics, El Marsad st., Helwan, 11421, Cairo, Egypt, e-mail: enas.mohammed@nriag.sci.eg
Attila Tímár: Department of Flood Protection and River Engineering, Körös District Water Directorate, Városháza u. 26., 5700 Gyula, Hungary, e-mail: atimar82@gmail.com
Diaa Sheishah: Department of Geoinformatics, Physical and Environmental Geography, University of Szeged, Egyetem u. 2-6., 6722 Szeged, Hungary; National Research Institute of Astronomy and Geophysics, El Marsad st., Helwan, 11421, Cairo, Egypt, e-mail: geo_diaa@nriag.sci.eg
Viktória Blanka-Végi: Department of Geoinformatics, Physical and Environmental Geography, University of Szeged, Egyetem u. 2-6., 6722 Szeged, Hungary; National Laboratory for Water Science and Water Safety, Herman Ottó út 15, 1022 Budapest, Hungary, e-mail: blankav@geo.u-szeged.hu
Alexandru Hegyi: Department of Geography, Applied Geomorphology and Interdisciplinary Research Centre (CGACI), West University of Timisoara, 300223 Timisoara, Romania, e-mail: alexandru.hegyi@e-uvt.ro
Boglárka Runa: Roden Engineering Office Ltd., Villám u. 13, 1089 Budapest, Hungary, e-mail: runaboglarka@gmail.com
Olivér Balogh: Roden Engineering Office Ltd., Villám u. 13, 1089 Budapest, Hungary, e-mail: balogholiver1993@gmail.com
Ahmed M. Ali: Department of Geoinformatics, Physical and Environmental Geography, University of Szeged, Egyetem u. 2-6., 6722 Szeged, Hungary; National Research Institute of Astronomy and Geophysics, El Marsad st., Helwan, 11421, Cairo, Egypt, e-mail: ahmed.mahmoud@nriag.sci.eg

1 Introduction

Floods are a major type of natural hazard, and flood events comprised half of all natural disasters globally in 2018 [1]. Artificial levees are linear earthworks constructed along riverbanks and have emerged as an integral protective measure against the flooding of urban and agricultural regions. Levee construction requires the consideration of various factors, including the type and availability of materials used, their efficacy at flood protection, the distinct characteristics of the riverside and protected side, and the potential strength of flood events [2–5]. Because the collapse of a levee can cause extensive and severe damage, numerous studies have focused on evaluating its stability. Salazar et al. [6] employed a predictive model, while Chen and Zhang [7] and Lee et al. [8] investigated water seepage through a levee body. Although detecting external changes in levees is relatively straightforward, assessing their subsurface properties is considerably challenging. Levees are critical and expansive infrastructures, rendering the use of invasive and time-intensive measurement techniques impractical owing to their localized nature. Consequently, nondestructive shallow geophysical techniques that can

Abstract

This study evaluates the impact of seepage on the integrity of artificial levees in low-lying regions, with a particular focus on Hungary, where levees built over a century ago lack comprehensive construction documentation, complicating current assessments of their effectiveness. Advanced geophysical methods—electrical resistivity tomography (ERT) and ground-penetrating radar (GPR)—were applied in a controlled tank experiment designed to simulate varied flood conditions along a 37-meter levee section. The three-dimensional (3D) ERT profiles successfully delineated seepage pathways as the tank filled, while the 3D GPR profiles indicated areas of increased amplitude, corresponding to seepage zones and the water table. Validation through drilling confirmed the geophysical findings, underscoring the accuracy of ERT and GPR in non-destructively identifying subsurface features and seepage channels. The results highlight the applicability of these methods for evaluating levee integrity and seepage dynamics, offering a reliable approach for flood risk assessment in Hungary and similar flood-prone areas worldwide.

Keywords

artificial levee, seepage, electrical resistivity tomography, ground-penetrating radar, drilling

2.1 Introduction

Floods are a major type of natural hazard, and flood events comprised half of all natural disasters around the world in 2018 (Mezősi 2022). Artificial levees are linear earthworks constructed along riverbanks and have emerged as an integral protective measure against the flooding of urban and agricultural regions. Levee construction requires the consideration of various factors, including the type and availability of materials used, their efficacy at flood protection, the distinct characteristics of the riverside and protected side, and the potential strength of flood events (Lászlóffy 1982; Kiss et al. 2019; Sheishah et al. 2023a, Sheishah et al. 2023b). Because the collapse of a levee can cause extensive and severe damage, numerous studies have focused on evaluating their stability. Salazar et al. (2016) employed a predictive model, while Chen and Zhang (2006) and Lee et al. (2011) investigated water seepage through a levee body. Although detecting external changes in levees is relatively straightforward, assessing their subsurface properties is considerably challenging. Levees are critical and expansive infrastructures, rendering the use of invasive and time-intensive measurement techniques impractical owing to their localized nature. Consequently, nondestructive shallow geophysical techniques that can rapidly and continuously evaluate physical parameters over a wide spatial range have gained widespread attraction (Perri et al. 2014; Rahimi et al. 2018; Dezert et al. 2019; Jodry et al. 2019; Tresoldi et al. 2019; Lee et al. 2020).

Ground-penetrating radar (GPR) and electrical resistivity tomography (ERT) are the most widely employed geophysical techniques. Both of them have their own distinct advantages, and their integration with geotechnical measurements can contribute to a comprehensive understanding of a levee's condition. For instance, Antoine et al. (2015) successfully coupled GPR with permeability logging to identify seepage zones. Sentenac et al. (2017) used ERT surveys to map historical earthworks for structural heterogeneity and post-flood damage. Tresoldi et al. (2019) used ERT to identify seepage zones and sections experiencing intense water saturation, demonstrating that the technique is suitable not only for structural assessments but also for long-term monitoring. Other researchers have used ERT to establish correlations between the water content and resistivity, enabling the resistivity profiles to be transformed into water content maps. Perri et al. (2014) employed geotechnical measurements to validate findings from geophysical surveys. Jodry et al. (2019) utilized the ERT and temperature profiles to monitor changes in soil moisture within a levee, which they used subsequently to generate models to estimate seasonal variations in resistivity. Compositional and localized defects

can diminish the flood protection capacity of earthworks. Chlaib et al. (2014) showed that cracks in levees caused by contraction and animal burrows increase the flood risk. Rahimi et al. (2018) employed GPR, ERT, and the multichannel analysis of surface waves to identify cavities responsible for piping and the development of sand boils on the protected side of levees. Lee et al. (2020) utilized an integrated approach involving three-dimensional (3D) resistivity inversion to interpret the cause and identify the seepage pathways within a damaged levee.

Various researchers have found that GPR has a limited capability to investigate the depth of levee structures because of their high clay content. Hence, they have frequently used ERT as an alternative owing to its greater penetration depth and ability to provide comprehensive information regarding the sedimentary composition (Busato et al. 2016; Perri et al. 2014). However, ERT has the disadvantages of a lower spatial resolution. In addition, the lack of geotechnical measurements to serve as control data in numerous instances has hindered the validation of ERT measurements (Dezert et al. 2019; Lee et al. 2020; Radzicki et al. 2021). Moreover, in ERT, interpretation challenges often arise from the "3D effect," where resistivity variations outside the survey plane impact readings along the ERT line. This effect is especially notable in complex environments like river embankments, where nearby resistive features, topographic variations, and changing river conditions (e.g., water level and conductivity due to tides) can distort the data. Because 2D ERT assumes resistivity is uniform perpendicular to the profile, these 3D effects introduce inaccuracies, shaped by each site's unique geometry, resistivity distribution, and boundary conditions such as air and water. Unless otherwise noted, references to 3D effects will specifically address river-induced distortions (Ball et al. 2023; Hojat 2024). The resistivity of sedimentary layers and deposits in earthworks is notably influenced by the water content and grain size, which are closely related to porosity. Many studies reveal a linear relation between the resistivity and grain size (Samouelian et al. 2005; Cosenza et al. 2006; Sudha et al. 2009; Oludayo 2021) and an inverse relation between the resistivity and water content (Fukue et al. 1999; Michot et al. 2000; Yoon and Park 2001; Loke 2004). Furthermore, a linear empirical relation is proposed between the resistivity and water content (Gupta and Hanks 1972; Goyal et al. 1996). Owing to the large contrast between the dielectric constants of water, air, and soil, the dielectric constant is affected by the presence of water in porous sediments. Therefore, many researchers used dielectric permittivity measurements to determine the volumetric water content (Birchak et al. 1974; Topp et al. 1980). Thus, dielectric permittivity can be

used to study the proportion of energy transmitted through levee materials and to evaluate its condition.

In Hungary, artificial levees were constructed along water channels decades ago to protect against flood events, and they predominantly comprise densely compacted, fine-grained, and impermeable sediments such as silt and clay. Over time, multiple interventions were conducted at various locations in response to specific flood events (Szűcs et al. 2019; Kiss et al. 2021). Because of the advanced age of these levees, information available on their structural attributes, composition, and resilience against floods is limited. The aim is to identify the effects of seepage on artificial levees and to reveal the advantages and weaknesses of the application of geophysical techniques in analyzing the structure and seepage pathways through artificial levees. A controlled tank experiment was performed along the riverside of the levee to simulate flood scenarios and to analyze water seepage. The effects of various parameters on the resistivity of borehole samples collected before and after filling the tank were evaluated to identify any relations that can be used to represent the levee integrity.

2.2 Materials and methods

2.2.1 Study site

The study site was situated along the Körös River in southeastern Hungary, a major tributary of the Tisza River. The present research was conducted at a 37-m-long levee section with a height of approximately 4.5 m (Figure 2.1). At the center of the studied levee section, a tank with a length of 12.6 m and a width of 6.6 m was fixed on the riverside slope of the investigated levee to simulate a flood scenario.

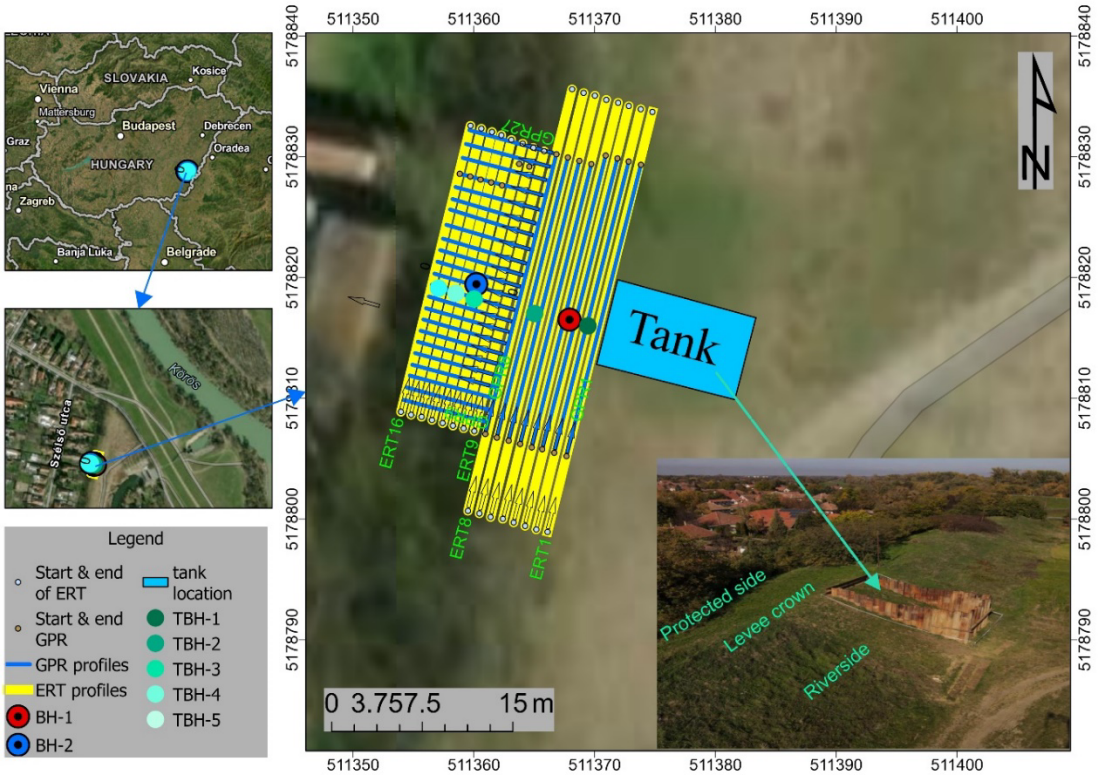

Figure 2.1 Study area map showing the locations of the ERT and GPR measurements boreholes (BH) and test boreholes (TBH)

2.2.2 Data collection and processing

A geophysical survey was conducted at the test site using ERT and GPR, as shown in Figure 2.1. Measurements were performed at the levee crown and protected side before (14 June 2023) (Figure 2.2a) and one month after (Figure 2.2b) the tank was filled with water (14 July 2023) to detect the seepage pathways and changes in the physical properties of the levee materials. Two boreholes were drilled to measure the water table and validate the interpretation of the geophysical data (Figure 2.2f). The coordinates of the start and end points of each profile were collected using a TopCon Hyper Pro real-time kinematic global positioning system (RTK GPS).

The coordinates and elevation data of each ERT profiles and the boreholes were accurately measured using TopCon Hyper Pro RTK GPS.

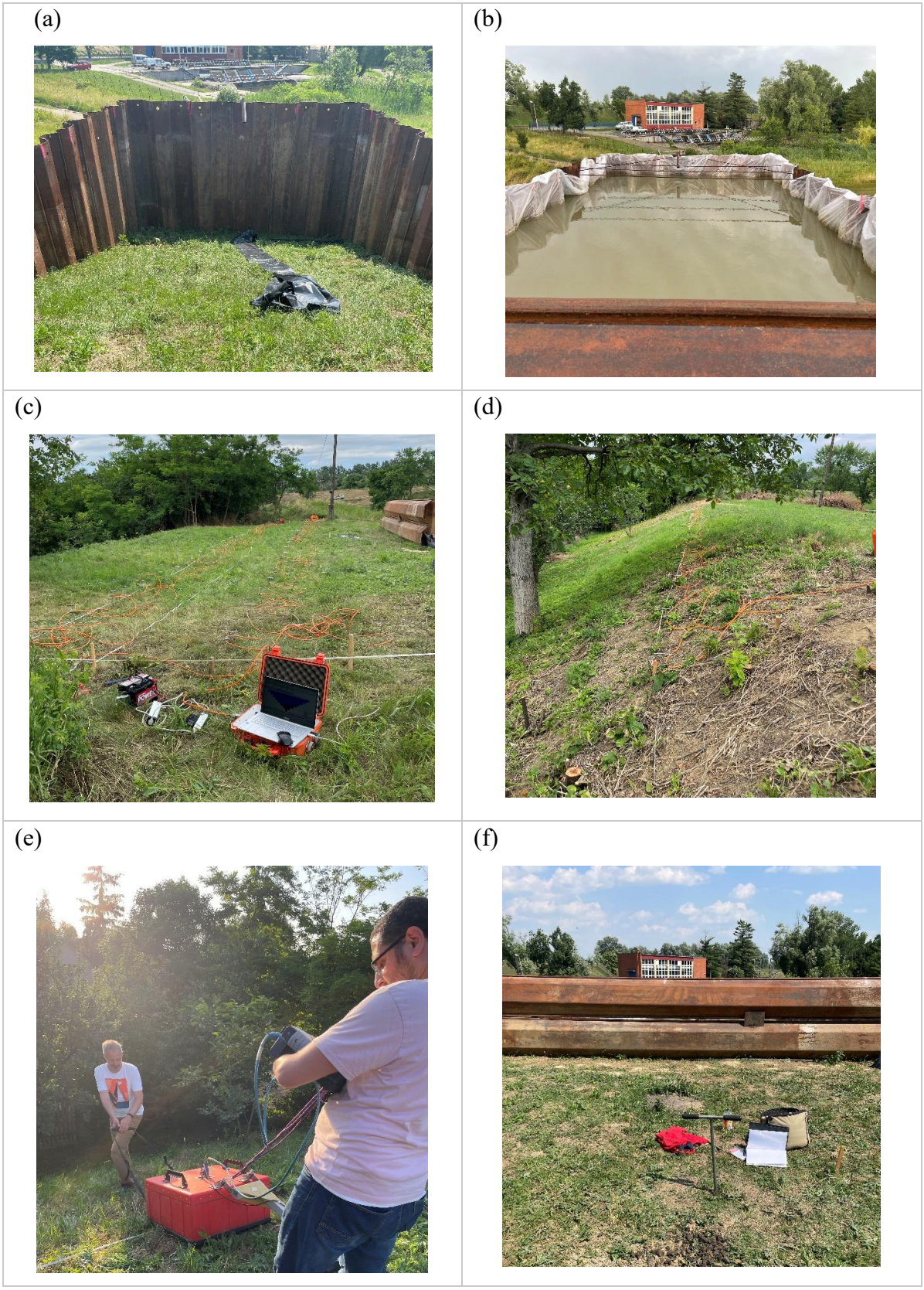

Figure 2.2 Field photos of the tank (**a**) before and (**b**) after filling with water; ERT data acquisition on the (**c**) levee crown and (**d**) protected side; (**e**) GPR data acquisition; and (**f**) borehole drilling

2.2.2.1 ERT

ERT was performed using a GeoTom MK8E100 apparatus connected to a multi-electrode system. Measurements were conducted on the levee crown and the protected side, but not on the riverside flank, as significant 3D effects are likely when ERT surveys are conducted on the riverside flank of an embankment, whereas surveys on the protected side are less likely to be impacted, as noted by Ball et al. (2023). Measurements at the levee crown were conducted using 37 electrodes (ERT profiles 1–8) (Figure 2.2c); however, only 25 electrodes were used on the protected side (ERT profiles 9–16). This is because vegetation restricts the profile length (Figure 2.2d). In total, 32 ERT profiles were obtained (Table 2.1), of which 16 ERT profiles were measured before filling the tank and the remaining 16 after filling the tank. Each profile was centered at the center of the tank. Data were collected using Wenner and Schlumberger arrays because of their high sensitivity to vertical and horizontal changes, respectively, where the subsurface resistivity was below the center of the array. The obtained profiles were parallel and equally spaced at 1 m. The electrodes were also spaced 1 m apart. A coupling test was conducted in the field before each ERT measurement to ensure good contact between each electrode and the levee. The contact resistance for all electrodes was maintained within a similar range and kept below 4 kΩ. The ERT data were used to monitor seepage through the levee body over time. The Wenner array was set to 12 depth levels, while the Schlumberger array was set to 17 depth levels. Consequently, these two arrays acquired 210 and 306 data points, respectively, for each profile. As noted by Ball et al. (2023): there is unlikely to be any significant 3D effect for the Wenner array with a spacing of 1 m and it is noticeable at river distances less than 4.5 m in lateral distance from the electrode array, consequently, we prioritized the use of the Wenner array in our analysis to minimize potential misinterpretations related to 3D effects and the lateral distance from the electrode array was more than 4.5 m.

Table 2.1 Details on collected geophysical data

Method	Location	Profile numbers	Profile spacing (meter)	Measurements regarding the tank case
ERT	Levee crown	1-8	1	Before filling the tank
	Protected side	9-16	1	
	Levee crown	1-8	1	After filling the tank

	Protected side	9-16	1	
GPR	Levee crown	1-8	1	Before filling the tank
	Protected side	9-27	1	
	Levee crown	1-8	1	After filling the tank
	Protected side	9-27	1	

The apparent resistivity values obtained from the ERT profiles were converted into true resistivity values for subsurface layers using the inversion software RES2DINV 3.4 (Loke, Barker, 1996). A few outlying data points were modified before inversion. Systematic noise was observed but was easily identifiable within the dataset, appearing in only a limited number of readings. Data points affected by systematic noise manifested as spots with unusually high values, making them stand out clearly in profile form and allowing for straightforward manual removal from the dataset. This methodology follows the approach outlined by Loke (2004). The least-square smoothness-constrained iterative optimization algorithm was used for the inversion (Constable et al. 1987; De Groot-Hedlin & Constable 1990).

Furthermore, a unified color scale was applied to all profiles The estimated RMS error for all 2D ERT profiles was very low, ranging from 0.86% to 2.7% (average 1.69%) for pre-tank filling ERT measurements, and from 0.71% to 2.9% (average 1.63%) for post-tank filling ERT measurements. Subsequently, the data were exported, gridded, and blanked for further analysis using the software Surfer. A 3D model was constructed from parallel 2D lines obtained in the inversion using the modeling software ResIPy (Blanchy et al., 2020). Additionally, a triangular mesh was used in this study owing to its suitability for complicated geometry such as the topography and geometric features within the study area. The estimated RMS error for 3D models was also low and showed 1.9% for pre-tank filling measurements and 2.3% for post-tank filling measurements.

The low RMS error values observed during our 2D ERT measurements indicate less impact on the overall data quality and interpretation. For 3D the values are still within a reasonable range, confirming that the errors do not significantly influence the inversion results or the derived resistivity models.

2.2.2.2 GPR

GPR measurements were conducted on the levee crown and protected side using a GSSI SIR 3000 apparatus in the distance mode connected to an antenna with a central frequency of 200 MHz (Figure 2.2e). In total, 56 profiles were collected (Table 2.1), of which 28 profiles were measured before filling the tank and the remaining 28 profiles after filling the tank. A total of 8 parallel profiles with lengths of 25 m were measured longitudinally on the levee crown, 19 parallel profiles with lengths of 8 m were measured transversely on the protected side, and 1 profile with a length of 20 m was measured longitudinally on the levee foot. To facilitate comparison, the start and end points of these profiles were made the same during both the surveys (i.e., surveys before and after filling the tank). Data were collected over a time range of 170 ns. A total of 64 scans were obtained per second, 40 scans were obtained per meter, and 1024 samples were obtained per scan. From the GPR profiles measured after filling the tank, the water table was clearly observed, and its reflectivity was strongly positive. Conversely, reflectivity was not observed in profiles measured before filling the tank. The measured water table depth was 3.1 m, which allowed dielectric permittivity (ε) to be accurately estimated as 11. The water table was monitored regularly at the location where the boreholes were drilled on the levee, and the depth was found to change over time. Once a slight change was observed in the water table depth, measurements were repeated at the same profile locations one month after the tank was filled.

The collected GPR data contained various types of noise because no filters were used in the field. Such noise needed to be eliminated. The following processes were applied to the GPR cross-sections by using GSSI, RADAN 7 version 7.6.19.11260 software: time zero correction to move the data to an effective time zero, infinite impulse response filtering, stacking, range gain setting, and migration. RADAN 7 was also used to identify the strong reflectivity of the water table and other positive peaks with high amplitudes to clarify the interfaces between layers with different dielectric permittivity values. The 3D GPR analysis was performed by using the software GPR-Slice **(**Goodman, D. (2017). The parallel GPR profiles were processed by time zero correction, bandpass frequency, migration, and Hilbert transform. Then, the data measured on the levee crown and on the protected side before and after the tank was filled were sliced and gridded.

2.2.2.3 BH

Two boreholes were drilled using an Eijkelkamp drilling system with a 5-cm-diameter drilling head to investigate the physical properties of levee materials and to validate the GPR and ERT data. One borehole was drilled on the levee crown (BH1), while the other was on the slope of the protected side (BH2) (Figures 2.1 and 2.2f), with a depth of 5.2 and 3.8 m, respectively. Additionally, five more boreholes were drilled along the same line as BH1 and BH2 as test boreholes (TBH) to measure the water table depth in the levee body (Figure 2.1).

Samples were collected from boreholes at a depth interval of 40 cm to compare the vertical changes in the gravimetric water content of the levee body and protected side. The samples were packed in airtight bags, and their wet weights were measured. Subsequently, the samples were dried at a temperature of 105°C in the laboratory, and their dry weights were estimated. Furthermore, their grain size distributions were analyzed using a Fritsch Analysette 22 laser analyzer with a measurement range of 0.08–2000 μm. The samples were then subjected to ultrasonic homogenization, and all measurements were repeated thrice to examine for further disintegration. Furthermore, the samples were categorized according to their mean grain size (D_{50}) using the Udden–Wentworth scale.

Eight samples were collected from BH1 and placed in undisturbed soil cylinders to measure the saturated hydraulic conductivity (K) of the levee section, which is an important parameter for flood water retention. These samples were collected at the depth of observed composition changes. K was calculated according to the Darcy's law, which states that the flow through a medium is directly proportional to the height of the hydraulic head and inversely proportional to the flow path length. The flow was determined using the coefficient K, which depends on the porosity of the medium. K was measured using an infiltrometer and the falling-head method, which is suitable for fine-grained samples such as silts (Dane and Hopmans 2002; Reynolds and Elrick 2002). Following the measurements, the samples were dried at 100°C, and their weights were measured using a precision scale. The bulk density was measured by dividing the dry sample weight with the cylinder volume. Subsequently, the total porosity n (%) was estimated as follows:

$$n = 100\ [1 - \rho_b/\rho_d] \quad (2.1)$$

where n is the total porosity (%), ρ_b is the bulk density of the material (g/cm^3), and ρ_d is the particle density of the material (g/cm^3). The particle density was adopted from a previous study and was set to 2.65 g/cm^3 (Fetter, 2001).

2.2.2.4 Meteorological data

For the preceding periods of the ERT and GPR surveys, meteorological data were also collected from Békés station to describe the hydrological characteristics of the period that can have an effect on the wetness condition of the levee. According to the available meteorological data in the vicinity of the study area, the average temperature during the week preceding the first survey (14 June 2023, i.e. before the tank was filled) was 17.84 °C., and the precipitation sum during the previous week was 1.04 mm. During the week preceding the second survey (14 July 2023, i.e., after the tank was filled), the average temperature was 23.36°C, and the precipitation sum was 1.7 mm (Table 2.2). As relevant precipitation did not occur in the preceding periods of the surveys, it did not have significant effect on the field measurement results.

Table 2.2 Meteorological conditions near the investigated levee section during the surveys conducted before and after filling the tank collected from Békés station

Day of survey	Daily mean temperature(°C)	Precipitation in the previous 1 week (mm)	Mean temperature in the previous 1 week (°C)
14. June	16.44	1.04	17.84
14. July	22.58	1.7	23.36

2.2.2.5 Dielectric permittivity calculation

Various empirical models are available for determining the dielectric constant (ε) of sediments, and they commonly have either a logarithmic or a polynomial structure. The Topp equation is widely used to relate the dielectric constant to the water content:

$$\varepsilon = 3.03 + 9.30(\Theta_w) + 146.00(\Theta_w)^2 - 76.70(\Theta_w)^3 \qquad (2.2)$$

where Θ_w is the volumetric water content of the levee material. In this study, Eq. (2.2) was used to evaluate the effect of water from the tank on the levee body and the physical properties of the levee materials during the geophysical surveys.

The water content increased suddenly at depths of 3.1 m and lower in the levee crown, which was defined as the water table. Therefore, the transmission of electromagnetic energy through the levee body was investigated above and below that depth to differentiate between the levee conditions before and after filling the tank. Variations in the levee material affect the transmission of electromagnetic waves. Incident electromagnetic waves are reflected when adjacent layers have different relative dielectric constants. A greater contrast results in higher reflection. The reflection coefficient (R)

represents the proportion of reflected energy and is influenced by discrepancies in the wave velocities and the relative dielectric constants of adjacent media (Reynolds, 2011):

$$R = \frac{\sqrt{\varepsilon 2} - \sqrt{\varepsilon 1}}{\sqrt{\varepsilon 2} + \sqrt{\varepsilon 1}} \quad (2.3)$$

The proportion of energy transmitted is equal to $1 - R$. The bulk relative dielectric constant (ε_r) and bulk conductivity at a given frequency (σ) largely affect attenuation. These properties are influenced by the material composition, electrical behavior, and relative abundance of each constituent. The loss factor is directly proportional to conductivity and is inversely proportional to the relative dielectric constant and frequency. The dielectric permittivity was calculated for borehole samples to a depth of 4.8 m at intervals of 0.4 m using Equation (2.2). Further, the average dielectric permittivity was calculated above (ε_1) and below (ε_2) the water table, which was at a depth of 3.1 m. The reflection coefficient for the levee body was calculated before and after filling the tank using Equation (2.3), which could then be used to estimate the proportion of transmitted energy.

2.3 Results

2.3.1 ERT measurements

The ERT measurements indicated that the levee had a layered structure. The topmost layer had a higher resistivity than the rest of the levee body because of its dryness, which resulted in tensile cracks. The ERT profiles measured on the levee crown exhibited three layers: a thin layer on the top with a thickness of 0.8 m and resistivity of 18–27 Ω-m, another thin layer with a thickness of 0.4–0.6 m and slightly higher resistivity of 28–40 Ω-m, and a very thick layer extending from a depth of 1 m to the bottom of the levee with a very low resistivity of 9–17 Ω-m (Figure 2.3). The ERT profiles on the levee crown had a maximum survey depth of 6 m, which exceeded the levee height of 4.5 m. Before filling the tank, the ERT profiles indicated a layered structure that reflected the resistivity of levee materials (Figure 2.3a). After filling the tank, the profiles close to the tank had distinctly oval shapes with substantially lower resistivity values of 2–7 Ω-m (Figure 2.3b). These shapes progressively became narrower and deeper with increasing distance from the tank until they completely disappeared in the ERT profile 9, which corresponded to a location on the protected side at 1 m from the edge. This disappearance, which occurred within one month, indicates that water seeped from the tank into the protected side.

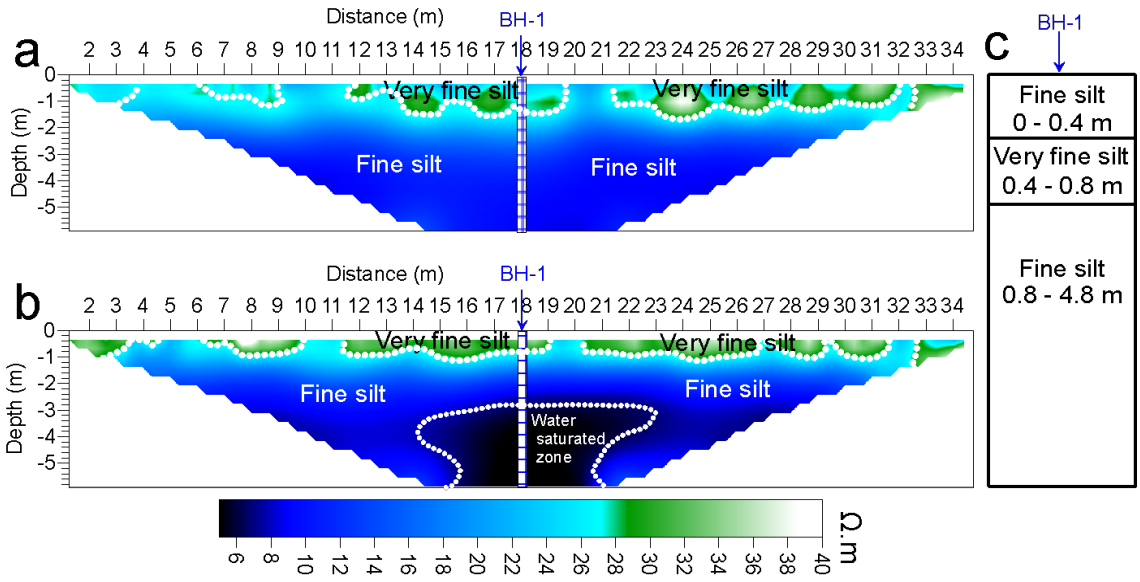

Figure 2.3 ERT profile 3 measured in the middle of the levee crown (**a**) before and (**b**) after filling the tank showing section of resistivity changes

From the ERT profiles, depth (D_z), width (W_z), and true resistivity (R_z) of the water-bearing zone were derived (Table 4.3). The depth values indicate that the water-bearing zone descended away from the tank, implying that water flowed downward through the levee body with increasing distance from the water source. The water-bearing zone was widest within 2 m of the tank and progressively diminished in size with increasing distance from the tank. The true resistivity values were low (3–5 Ω-m) within 2 m of the tank, increased to 3–7 Ω-m at 3–5 m from the tank, and narrowed to 5–7 Ω-m at 6–8 m from the tank. These results indicate that the levee was highly saturated with water near the tank and that the water content decreased with increasing distance from the water source, particularly near the protected side.

Table 2.3 Depth, width, and true resistivity of water-bearing zones in successive ERT profiles

ERT No.	D_z (m)	W_z (m)	R_z range (Ωm)
1	1.6	6.5	3 – 5
2	2.2	8.5	3 – 5
3	2.8	8	3 – 7
4	3.2	5.5	3 – 7
5	3.4	5	3 – 7
6	3.6	4.5	5 – 7
7	3	5.5	5 – 7
8	3.6	3	5 – 7

The ERT profiles of the levee crown and protected side were used to calculate the specific resistivity ranges for distinct materials and the water-bearing zone to compare the levee conditions before and after the tank was filled. In general, the levee materials had a lower range of resistivities after the tank was filled than before the tank was filled. The specific resistivities observed before the tank was filled had a minimum of 5 Ω-m, a mean of 24 Ω-m, and a maximum of 180 Ω-m. After the tank was filled, these values changed to a minimum of 2 Ω-m, a mean of 20 Ω-m, and a maximum of 110 Ω-m. The resistivity ranges were monitored across all ERT profiles in detail to compare the levee conditions before and after the tank was filled (Figure 2.4). Most of the ERT profiles exhibited a decrease in mean resistivity after the tank was filled except for profile 10, which showed a slight increase. The highest interquartile range was observed at profile 9 both before and after the tank was filled, which can likely be attributed to the measurement location at the edge of the protected side where the levee materials were less compacted and air gaps were present. Conversely, the lowest interquartile range was observed at profile 16, which was at the bottom of the protected side. This location had a higher water content that increased further after the tank was filled because of the shallow water table resulting from seepage.

Three distinct trends were observed in the mean resistivity of each profile before and after the tank was filled: profiles 1–5 showed a constant mean resistivity, profiles 6–9 showed an increase in the mean resistivity, and profiles 10–16 showed a decrease in the mean resistivity. The stability of the first group was attributed to their proximity to the tank, where seepage affected the adjacent levee side uniformly. The second group was further from the tank and was less affected by seepage, which resulted in an increasing trend. The third group was situated on the protected side slope, and the decreasing trend can be attributed to the rising water table caused by seepage. Joint analysis of both levee conditions revealed that the interquartile resistivity ranges of the ERT profiles were broader on the levee crown than on the protected side. This can be attributed to several factors. First, the water table was at greater depth on the levee crown (depth of 3.1–3.4 m) than on the protected side (depth of 0.5–1.9 m), which resulted in larger drier zones in the levee crown and consequently a wider resistivity range. Second, the variability in compaction of the levee materials was greater at the levee crown than on the protected side. Finally, disturbances due to erosion and human activities on the levee crown increased the variability of the measured resistivity compared to on the protected side.

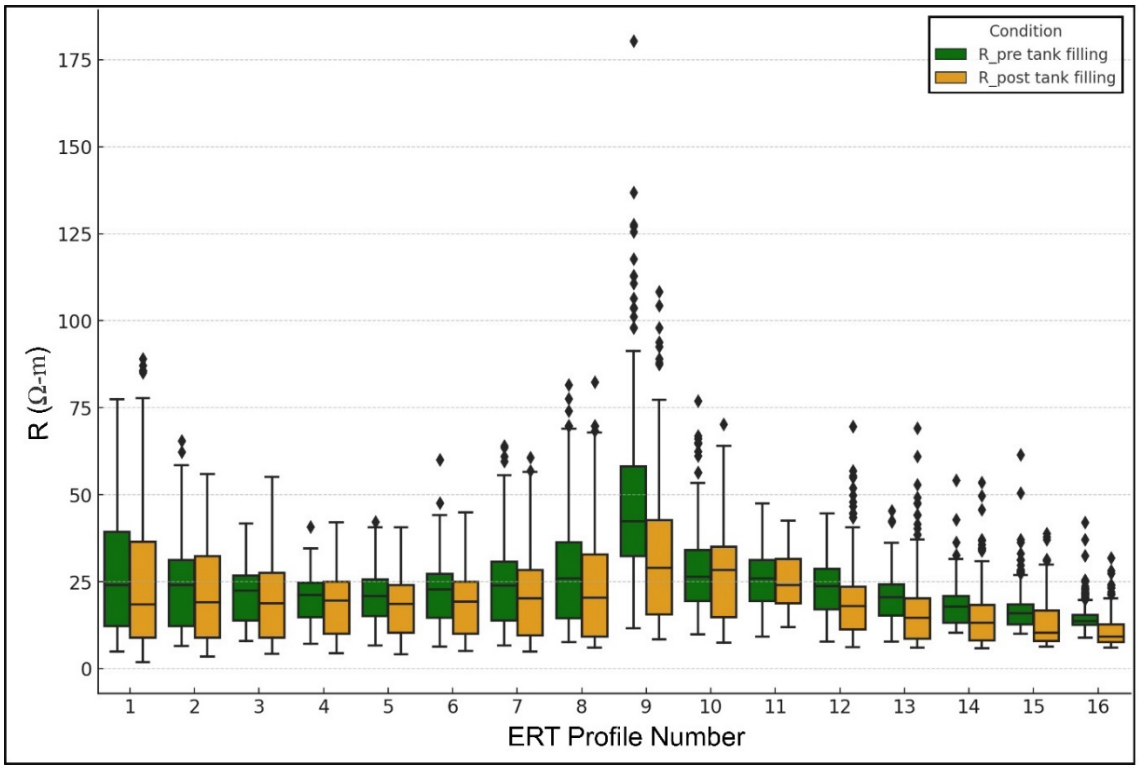

Figure 2.4 Resistivity ranges of every ERT profile measured before and after filling the tank

3D depth slice maps at 4 m derived from ERT profiles indicate a distinct contrast in anomalies before and after the tank was filled. Before filling the tank, the higher and medium resistivity values corresponded to the composition of the levee body under dry conditions, which predominantly comprised fine-grained materials (Figure 2.5a). After filling the tank, the lower resistivity values reflected water seeping from the tank through the levee body and its protected side to manifest as a blue anomaly starting at a depth of 3.1 m (Figure 2.5b). This anomaly widened with increasing depth until the maximum survey depth. Notably, the initial depth of the anomaly closely agreed with the water table measurements obtained using a measurement tape connected to light-emitting diodes with high brightness. This convergence supports the correlation between the ERT data and direct water table measurements for a better understanding of the water seepage dynamics after the tank was filled.

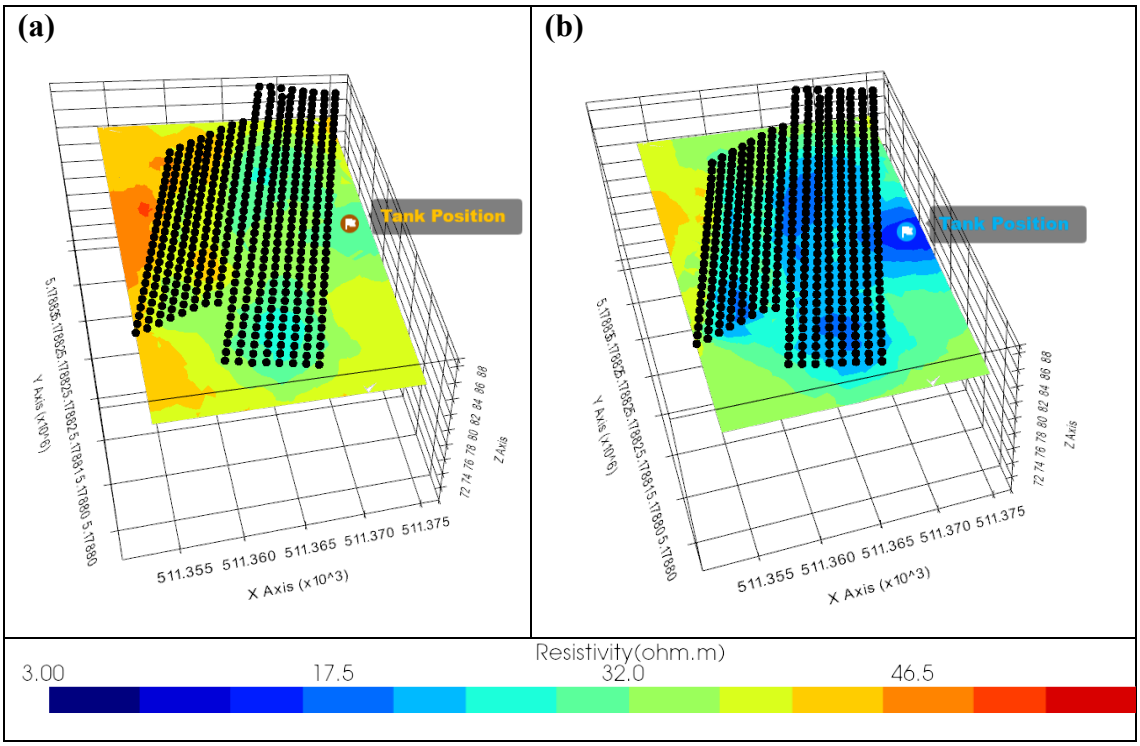

Figure 2.5 Depth slice maps at 4 m of the levee body and protected side (**a**) before and (**b**) after filling the tank. The black points represent electrode locations on the levee body. An anomaly with a blue color in Figure 5b is interpreted as a zone of lower resistivity values reflecting water seeping from the tank.

4.3.2 GPR measurements

GPR measurements at the levee crown indicated that the material of the levee body generally homogeneous (Figure 2.6). Before the tank was filled, an interface was consistently identified at a depth of 0.8–1.0 m, which extended horizontally through the levee body (Figures 2.6a and b). Consequently, the levee could be delineated into three primary units: the topmost unit had an average thickness of 0.8 m, middle unit had a thickness of 0.4 m, and third unit extended beyond the survey depth. After filling the tank, the same interface was observed. In addition, a robust reflection was identified at an approximate depth of 3–3.2 m, which was interpreted as the water table following seepage from the tank. This prominent reflection was notably absent in measurements taken before filling the tank (Reynolds, 2011). Similarly observed the water table as a horizontal reflection with a substantial amplitude. Beyond the water table, three additional interfaces were observed at depths of 3.6, 4.2, and 4.9 m (Figures 2.6c and d). The signal floor tool in RADAN 7 was used to detect the approximate depth reached by the GPR signal. Before filling the tank, the GPR signal reached a maximum depth of 4.6 m on average.

Meanwhile, after filling the tank, the maximum depth decreased to 4.4 m, which was attributed to wave attenuation resulting from water seepage through the levee body.

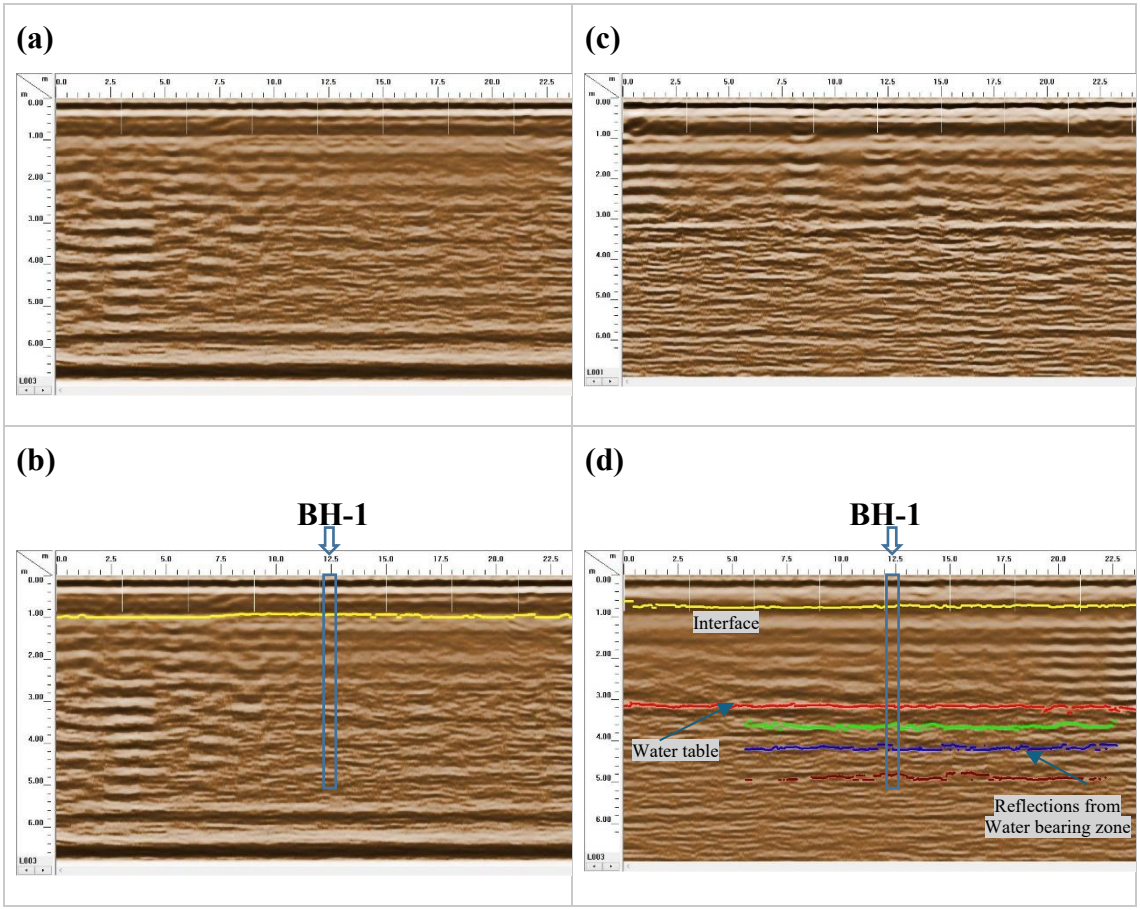

Figure 2.6 GPR profiles measured along the middle of the levee crown before filling the tank and (**a**) before and (**b**) after picking the interface as well as after filling the tank and (**c**) before and (**d**) after picking the interface

The reflection coefficient at the detected water table depth of ~3.2 m was 0.07 before the tank was filled and 0.19 after the tank was filled. Thus, the proportion of energy transmitted (Tr) was 0.93 (Figure 2.7a) and 0.81 (Figure 2.7b) before and after the tank was filled, respectively. The reduction in energy transmitted through the levee body after the tank was filled was attributed to water seepage from the tank saturating the levee materials, especially in the lower part. The calculated energy transmitted through the levee body showed good agreement with previous studies (Reynolds, 2011), which indicates that the conductivity and relative dielectric constant of the saturating fluid dominated the matrix values in the saturated granular media. A higher relative dielectric constant increases attenuation. Similarly, a higher content of fine silt and clay increases

the loss factor and attenuation because of the bound water within the clay lattice and electrical properties of clay minerals owing to their physicochemical structure.

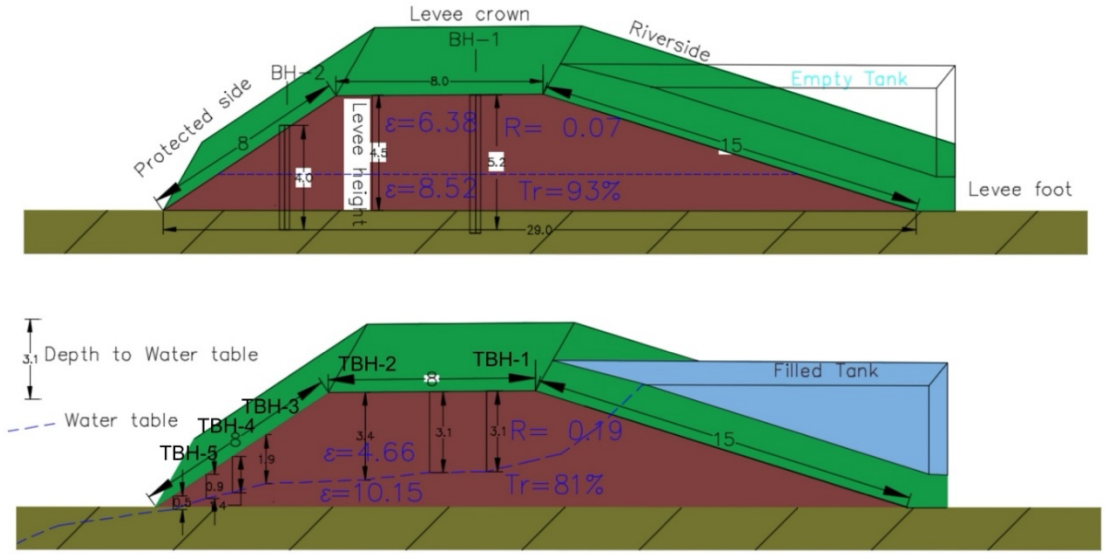

Figure 2.7 Calculated reflection coefficients, energy transmitted of the levee and the detected water table (**a**) before and (**b**) after filling the tank

The horizontal time slices extracted from the 3D representation of the GPR data allow a comparison of the levee conditions before and after the tank was filled. The profiles obtained on the protected side and levee crown had lower amplitudes before the tank was filled (Figures. 2.8a and b, indicated by blue) than after the tank was filled (Figures 2.8 c and d, indicated by red and yellow). This disparity was primarily attributed to water seepage from the tank. The change in amplitude was directly connected to changes in the dielectric permittivity and hence loss factor of the soil, which are affected by both the temperature and water content. An increase in temperature reduces the peak frequency of the dielectric relaxation while an increase in the water content increases the loss factor and decreases the peak frequency. The dielectric relaxation has generally been observed to have a lower peak frequency and to occur over a more limited frequency range for soils than for conductive media.

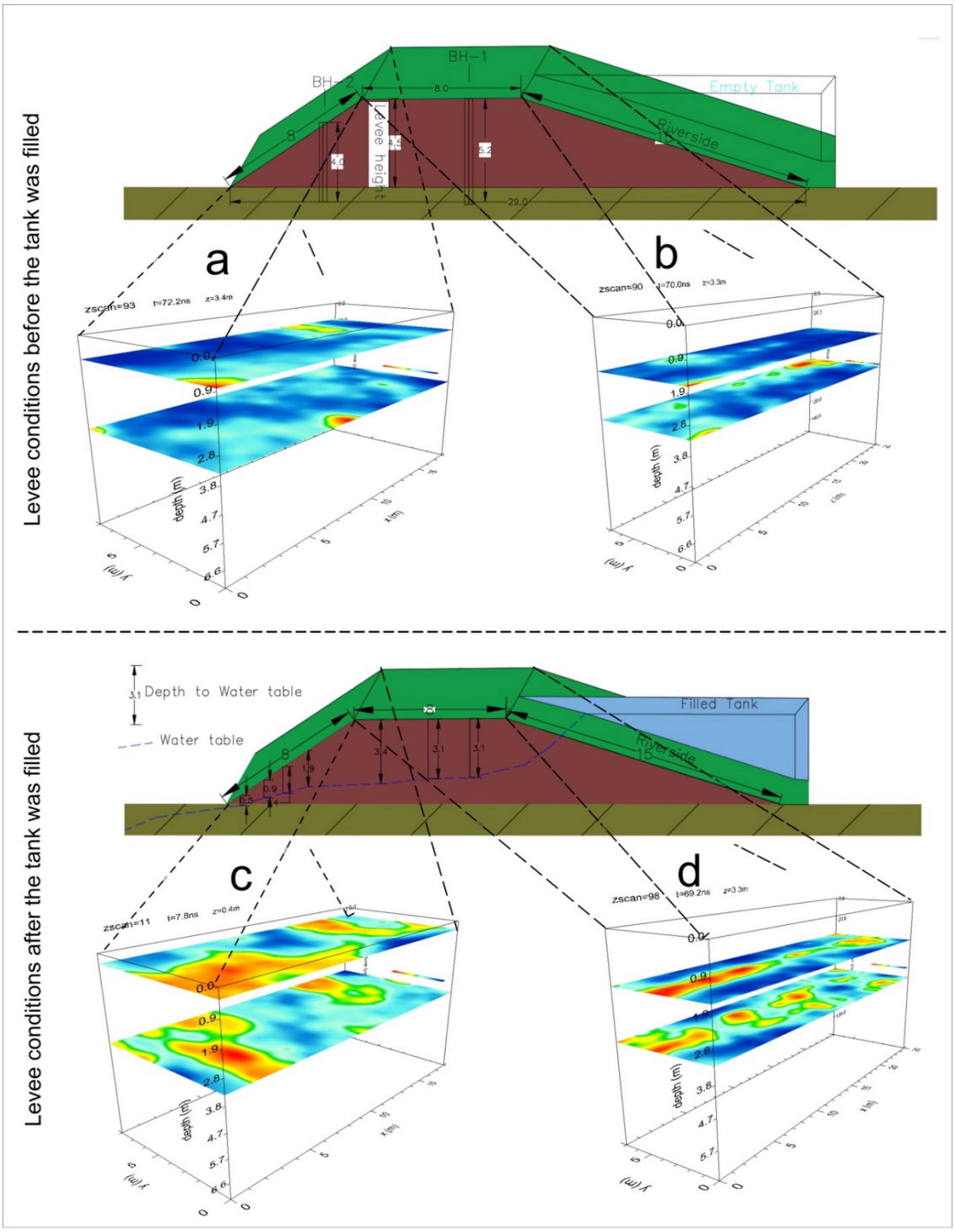

Figure 2.8 3D cube showing horizontal slices on the (**a**) protected side and (**b**) levee crown before the tank was filled and on the (**c**) protected side and (**d**) levee crown after the tank was filled. Anomalies shown in red and yellow in Figures 8c and d are interpreted as increased amplitudes of electromagnetic waves, attributed to water seepage from the tank.

2.3.3 Sedimentological data

2.3.3.1 BH samples

The BH drilled in the middle of the levee crown (BH1) showed three main units (Figure 2.9a). The first unit extended from the surface to a depth of 0.4 m was formed of fine silt (mean grain size D_{50} = 12 µm). The second unit comprised a very fine silt (D_{50} = 7 µm) and had a depth of 0.4–0.8 m, while the third unit was fine silt (D_{50} = 9–15 µm with an average of 11 µm) and was observed at depths below 0.8 m. The grain size of the third unit increased with the depth but remained within the range of fine silt. The D_{50} values of individual units indicated that the levee body generally comprised very fine and fine silts with some differences in grain size. The borehole drilled on the protected slope of the levee (BH2) had three units (Figure 2.9b). The first unit comprised a fine silt (D_{50} = 9–10 µm) and extended from the surface to a depth of 2 m. The second unit was a very fine silt (D_{50} = 7 µm) and had a depth of 2–2.4 m, while the third unit comprised a fine silt (D_{50} = 9 µm) and had a depth of 2.4–2.8 m.

The water content (W) of the BH1 samples varied substantially with the depth before the tank was filled (Figure 2.9c). The topmost samples had a water content of 14% to a depth of 0.8 m. Samples from depths of 0.8–2 m had a lower water content (10%) with little variations. Samples from depths of 2–4.8 m showed an increased water content of up to 15.7% on average. Furthermore, the water content of samples obtained from a borehole drilled 0.2 m from BH1 after filling the tank showed substantial differences (Figure 2.9d). The topmost samples had a low water content of 8% to a depth of 3.2 m, while those from depths of 3.2–4.4 m had a high water content of 20%. The higher water content at higher depth can be attributed to the formation of a water-bearing zone from which the samples were collected.

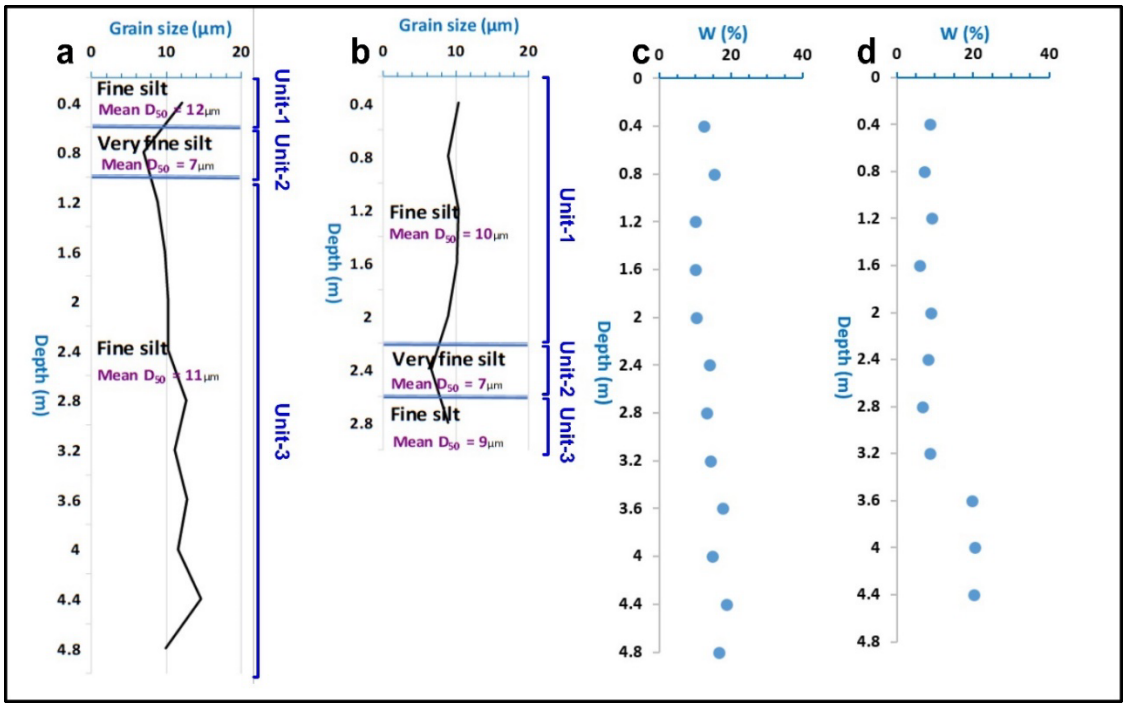

Figure 2.9 Mean grain size (D_{50}) along the vertical axes of BH (**a**) BH1 and (**b**) BH2; water content in borehole BH1 (**c**) before and (**d**) after filling the tank

2.3.3.2 Saturated hydraulic conductivity

The correlations of the water content W, mean grain size D_{50}, porosity φ, and density ρ for correlations with the resistivity R obtained from the ERT profiles and their degree of significance was analysed using IBM SPSS. Here, the subscripts "dry" and "wet" are used to distinguish parameters measured before and after the tank was filled, respectively. As expected, R_{dry} showed a strongly negative correlation with W_{wet} at a high degree of significance ($R^2 = -0.73$). R_{wet} showed the same correlation with W_{wet} at an even higher degree of significance ($R^2 = -0.76$) because of the high conductivity of water compared to the dry fine materials of the levee. In addition, the water created continuous conductive pathways by filling the pore spaces in the levee materials, which decreased the resistivity. Meanwhile, R_{dry} had a moderately negative correlation with W_{dry} ($R^2 = -0.57$), and R_{wet} had a negligible correlation with W_{dry} because of the lack of conductive media restricting the passage of the electric current in the levee before the tank was filled. Unexpectedly, D_{50} had a moderately negative correlation with R_{dry} and a negligible correlation with R_{wet}. This result was attributed to the homogeneity of the levee materials, which were mainly fine silt. φ had a strongly negative correlation with R_{wet} at a high degree of significance ($R^2 = -0.77$). This was expected because the presence of pores facilitates the movement of water through the levee materials, which in turn affects

electrical resistivity. This also explains why φ had a negligible correlation with R_{dry} ($R^2 = -0.25$). The collected samples showed that R_{wet} had higher values than R_{dry} at the upper part of the levee (depth of <1 m). This can be attributed to two reasons. First, the daily mean temperature was higher after the tank was filled (22.58°C) than before the tank was filled (16.44°C) (Table 2.2). Therefore, the top part of the levee was drier, which increased the tensile cracks and thus the resistivity. Second, the seepage has no effect on the upper part of the levee. Below a depth of 1 m, R_{wet} had lower values than R_{dry} because this part of the levee was affected by seepage. The K values indicated that all collected samples were non-aquitard (Table 4.4), which means that the levee was built from a material that does not restrict the flow of water during floods. This is an important observation of its health and ability to protect against floods. The lowest filtration velocity was observed for a sample collected at a depth of 0.8 m. A weakly positive correlation was observed between R_{dry} and K ($R^2 = 0.373$) while a negligible correlation was observed between R_{wet} and K. These results indicate no direct connection between the resistivity and saturated hydraulic conductivity of the levee materials.

Table 2.4 Properties of the collected samples used to evaluate the saturated hydraulic conductivity

ID	Location	D (m)	W_{dry} (%)	W_{wet} (%)	D50	φ (m/m%)	ρ (g/cm^3)	K (m/s)	Material type	R_{dry} (Ω.m)	R_{Wet} (Ω.m)
1	levee crown	0.3	12.5	8	13.44	43.6	1.61	1.3*10^-7	not aquitard	22.04	33.16
2	levee crown	0.4	12.5	8.8	12.14	44.9	1.61	2.4*10^-7	not aquitard	22.77	32.17
3	levee crown	0.5	13.1	10.5	10.84	46.2	1.55	2.4*10^-6	not aquitard	23.51	31.20
4	levee crown	0.8	15.4	12.4	6.93	49.4	1.53	4.7*10^-8	not aquitard	25.71	28.23
5	levee crown	1.2	10.1	11	8.87	50.2	1.39	5.1*10^-6	not aquitard	27.50	22.27
6	levee crown	1.6	10.1	9.9	9.78	50.4	1.45	4*10^-7	not aquitard	26.01	16.16
7	levee crown	2	10.3	11.9	10.3	45.9	1.46	2.8*10^-7	not aquitard	22.40	11.60
8	levee crown	3.4	15.5	18.5	11.97	52.9	1.44	5.2*10^-7	not aquitard	12.30	5.45

Notes: D: depth; W_{dry}: water content before filling up the tank; W_{wet}: water content after filling up the tank; D50: mean grain size, φ: porosity; ρ: bulk density; K: saturated hydraulic conductivity; material type, R_{dry}: resistivity based on ERT profiles measured before filling up the tank, and R_{wet}: resistivity based on ERT profiles measured after filling up the tank.

2.3.4 Analysis of physical parameters

The seepage after the tank was filled influenced the physical parameters used to investigate the current levee section: the resistivity and dielectric permittivity. The water content indicated an inversely proportional relationship with the resistivity and a proportional relationship with the dielectric permittivity. Therefore, the relationship between the resistivity and dielectric permittivity of the levee section was investigated. After the tank was filled, water flowed through the levee body, increasing the saturation of the levee material at lower depths, which increased the relative dielectric permittivity. This observation confirmed a direct relationship between the water content and dielectric permittivity. A strongly negative correlation was observed between the resistivity and dielectric permittivity before the tank was filled ($R^2 = -0.6$) because the water content of the levee materials was homogeneously distributed. However, the correlation weakened after the tank was filled ($R^2 = -0.25$) because of a heterogeneous water distribution where some areas of the levee were fully saturated, others areas were partially saturated, and the upper part was unaffected by seepage.

2.4 Discussion

To study the effect of seepage on artificial levees, a tank was fixed on the riverside slope, and measurements obtained using two geophysical techniques that complement their respective advantages and drawbacks before and after filling the tank with water were compared. The geophysical techniques were then applied for identifying the main units of the levee from the borehole data because the structure and composition are important parameters for evaluating the effectiveness of the levee for flood protection. The results from geophysical techniques were then compared with borehole data, which were used as the ground truth. The borehole data indicated the presence of a very fine silt layer with a thickness of 0.4 m; however, this layer appeared as an interface separating fine silt materials in the GPR profiles, rather than a layer. In the ERT profiles, the bottom of this thin layer appeared as an interface at a depth of ~1 m. Thus, the GPR and ERT profiles could not resolve the very fine silt layer. Meanwhile, a second interface was clearly observed at 3–3.2 m, almost at the same position in the ERT and GPR profiles, corresponding to the water table originating due to water seepage from the tank. The collected samples confirmed a sharp increase in the water content at this interface after the tank was filled; conversely, this interface was not observed before the tank was filled. Thus, the results confirmed that the levee body comprised three major units: fine silt at the top, very fine silt in the middle, and fine silt again at the bottom. Therefore, the levee

body was generally homogeneous and comprised fine silts. Moreover, fewer layers and increased homogeneity are generally advantageous for the health of a levee because they indicate that it does not have a complex structure (Zorkóczy 1987; Schweitzer 2001, Szlávik 2000). The simple structure of the levee section under study was similar to that observed for a levee section along the Tisza River (Sheishah et al. 2023; DWMS, 2024). However, saturated hydraulic conductivity measurements indicated that the levee body had a non-aquitard nature in all samples, which may facilitate concentrated seepage through the levee body.

The resistivity values of the levee body were low and matched those observed in previous studies on alluvial materials (Sheishah et al., 2023; Loke, 2004; Sheishah et al. 2022; Keller & Frischknecht, 1966; Abu-Hassanein & Benson 1996; Giao et al. 2003; Tabbagh et al. 2007). This indicates that the levee primarily comprised fine-grained materials. Specific resistivities obtained using the ERT profiles had mean values of 24 Ω-m before the tank was filled and 20 Ω-m after the tank was filled. These values are below the range reported by Ball et al., 2023, who observed resistivity values of 50–100 Ω-m in a levee comprising clayey sand under low-moisture conditions. This correspondence is consistent with findings indicating that fine-grained materials within levee structures typically exhibit specific resistivity values below 100 Ω-m (Jodry et al. 2019; Himi et al. 2018).

Previous studies revealed a correlation between the electrical resistivity and porosity (Tabbagh et al. 2007; Himi et al. 2018; Robain et al. 1996; Alakukku 1996; Richards & Reddy 2010, Pereira & Defossez & Richard 2007). Increasing resistivity can be attributed to the soil compaction process, which increases bulk density while diminishing the volume of larger pores. This relation is widely acknowledged in literature, and Keller & Frischknecht (1966) proposed a typical association between resistivity and coarse-grained materials. In this study, a decrease in porosity was strongly correlated to lower resistivity in the levee section, as expected. The borehole measurements confirmed that sediments with a high water content after the tank was filled tended to have lower resistivity, especially in the lower half of the levee body. This agreed with the observations of Loke (2004). The inversely proportional relation between resistivity from the ERT data and dielectric permittivity calculated from the water content agreed with the results reported by (Iravani et al. 2020a; Iravani et al. 2020b).

The compaction of levee materials primarily manifests as an increase in soil bulk density and decrease in microporosity, which reduce electrical resistivity (Zhu et al.,

2007). Furthermore, Beck et al. (2011) demonstrated that dry density considerably influences the resistivity of fine-grained soils, rendering resistivity measurements a promising tool for discerning structural disparities resulting from soil compaction. Jerabek et al. (2017); García-Tomillo et al. (2018); Hadzick et al. (2011) noted that there is no direct connection between resistivity and saturated hydraulic conductivity because resistivity is more strongly influenced by other soil parameters such as the particle size and bulk density.

2.5 Conclusion

In this study, the seepage was monitored by fixing a water-filled tank on the riverside slope of an investigated levee section using geophysical techniques (ERT and GPR) and measurements of the physical parameters, which provided useful information regarding the levee and its ability to protect against floods. The levee body was found to primarily comprise fine silts, suggesting that the levee was in good health. The low-to-medium resistivity values indicated that the levee section has a homogeneous nature. The 3D analysis of the ERT profiles helped to identify water pathways through the levee body before and after the tank was filled, while the GPR profiles clearly indicated the presence and position of the water table by indicating an increase in amplitude values after the tank was filled, which can be attributed to water seeping through the levee body. Calculations of the reflection coefficient and the proportions of EM energy transmission are important parameters in studying water seepage through the levee body during flood events, as they provide information about the loss factor and attenuation of EM waves and clarify the differences in the levee condition before and after the tank was filled. Analysis of the physical parameters of levee materials confirmed significant changes before and after the tank was filled with water. Despite the homogeneous structure and fine-grained materials of the levee body, the saturated hydraulic conductivity measurements indicated that it has a non-aquitard nature, rendering it susceptible to concentrated seepage. These results demonstrate the importance of studying the physical properties of levee materials to gain a complete understanding of the levee's health and its ability to provide protection against floods.

3. Application of Ground Penetrating Radar in the Assessment of Aged Roads: Focus on Complex Structures Under Different Weather Conditions

This article is published in Pure and Applied Geophysics Journal as:
Enas Abdelsamei, Diaa Sheishah, Boglárka Runa, Olivér Balogh, Csaba Tóth, Péter Primusz, Sándor Trenka, Boudewijn Van Leeuwen, Zalán Tobak, Dávid Gergely, Páll, György Sipos
Application of Ground Penetrating Radar in the Assessment of Aged Roads: Focus On Complex Structures Under Different Weather Conditions," in *Pure Appl. Geophys. 181 (2024), 3633–3651 2024*
https://doi.org/10.1007/s00024-024-03604-y
Journal Impact Factor: 1.9 (2023)

Pure Appl. Geophys. 181 (2024), 3633–3651

https://doi.org/10.1007/s00024-024-03604-y

Pure and Applied Geophysics

Application of Ground Penetrating Radar in the Assessment of Aged Roads: Focus On Complex Structures Under Different Weather Conditions

Enas Abdelsamei,[1,2] Diaa Sheishah,[1,2] Boglárka Runa,[3] Olivér Balogh,[3] Csaba Tóth,[4] Péter Primusz,[4] Sándor Trenka,[3] Boudewijn van Leeuwen,[1] Zalán Tobak,[1] Dávid Gergely Páll,[1] and György Sipos[1]

Abstract—Ground penetrating radar (GPR) has been widely used to assess asphalt and pavement, especially in quality testing for newly constructed roads. However, its usage has been limited in regard to aged roads. Thus, this study focuses on the applicability of GPR to extract diverse information regarding structure, thickness, and various conditions, including the moisture content of an aged road section that has undergone repeated renewals. First, two methods were employed to calculate the thickness and dielectric values; the reflection amplitude and ground truth methods. The analysis was done by RADAN 7 software. Based on the findings, the average error of thickness on the same day between continuous GPR and the core data were 2.87% and 8.72%, respectively. Second, dielectric analysis of three structural units was performed under different moisture conditions. As a result, the average dielectric values of macadam (3, 3.3, and 4), surface asphalt layer (4, 7.06, and 8.31), and cement-treated base (4.83, 10.88, and 11.88) were determined under dry, medium-wet, and wet conditions, respectively. The volumetric water difference (f) within the pavement was also estimated. As for the asphalt, macadam, and cement-treated base, the difference in the volume fraction of water (f) was 0.06, 0.01, and 0.1, respectively, under dry and wet conditions, and 0.04, 0.004, and 0.09, respectively, under dry and medium-wet conditions. Overall, the findings demonstrate that reasonably accurate assessments of the pavement thickness, structure, dielectric values, and amplitude of aged roads can be achieved by using a GPR survey under various conditions.

Keywords: Ground penetrating radar, Aged roads, Thickness, Dielectric analysis, Volumetric water content.

1. Introduction

Ground penetrating radar (GPR) has been successfully used in pavement engineering for various applications, from determining layer thickness and moisture content to analyzing the quality of pavement construction during maintenance assessments (Ameri et al., 2014). Pavement layer thickness is a key factor in estimating the remaining pavement life and strengthening quality assurance during and after construction (Bezina et al., 2021). In this regard, GPR has proven to be very accurate in determining the thickness of asphalt layers, as shown in the use of GPR with air-coupled antennas (Al-Qadi & Lahouar, 2005; Al-Qadi et al., 2005; Domitrović & Rukavina, 2013; Domitrović et al., 2019; Flintsch et al., 2005; Holzschuher et al., 2007; Loizos & Plati, 2007b; Sener et al., 1998; Willett, et al., 2006; Hugenschmidt, 1996). Meanwhile, Al-Qadi et al. (2005) investigated the thickness error of newly constructed pavement and found that the GPR data from several locations revealed an increase in thickness inaccuracy with age of the pavement, while Ožbolt et al. (2012) found that the error in new pavements for motorways was mostly less than that of regional/county roads with several years of service. Previous studies also used field data to demonstrate the anticipated physical constraints associated with the use of GPR technology for pavement thickness detection (Al-Qadi & Lahouar, 2005), with some authors addressing the accuracy

[1] Department of Geoinformatics, Physical and Environmental Geography, University of Szeged, Egyetem U. 2-6., 6722 Szeged, Hungary. E-mail: enas.mohammed@nriag.sci.eg; geo_diaa@nriag.sci.eg; leeuwen@geo.u-szeged.hu; tobak@geo.u-szeged.hu; pall.david.gergely@gmail.com; gysipos@geo.u-szeged.hu
[2] National Research Institute of Astronomy and Geophysics, El Marsad St., Helwan 11421, Cairo, Egypt.
[3] Roden Engineering Office Ltd, Villám U. 13, 1089 Budapest, Hungary. E-mail: runaboglarka@gmail.com; balogholiver1993@gmail.com; trenka.sandor@roden.hu
[4] Department of Highway and Railway Engineering, Budapest University of Technology and Economics, Műegyetem Rakpart 3., 1111 Budapest, Hungary. E-mail: toth.csaba@epito.bme.hu; primusz.peter@emk.bme.hu

Abstract

Ground penetrating radar (GPR) has been widely used to assess asphalt and pavement, especially in quality testing for newly constructed roads. However, its usage has been limited in regard to aged roads. Thus, this study focuses on the applicability of GPR to extract diverse information regarding structure, thickness, and various conditions, including the moisture content of an aged road section that has undergone repeated renewals. First, two methods were employed to calculate the thickness and dielectric values; the reflection amplitude and ground truth methods. The analysis was done by RADAN 7 software. Based on the findings, the average error of thickness on the same day between continuous GPR and the core data were 2.87% and 8.72%, respectively. Second, dielectric analysis of three structural units was performed under different moisture conditions. As a result, the average dielectric values of macadam (3, 3.3, and 4), surface asphalt layer (4, 7.06, and 8.31), and cement-treated base (4.83, 10.88, and 11.88) were determined under dry, medium-wet, and wet conditions, respectively. The volumetric water difference (*f*) within the pavement was also estimated. As for the asphalt, macadam, and cement-treated base, the difference in the volume fraction of water (*f*) was 0.06, 0.01, and 0.1, respectively, under dry and wet conditions, and 0.04, 0.004, and 0.09, respectively, under dry and medium-wet conditions. Overall, the findings demonstrate that reasonably accurate assessments of the pavement thickness, structure, dielectric values, and amplitude of aged roads can be achieved by using a GPR survey under various conditions.

Keywords: Ground penetrating radar, aged roads, thickness, dielectric analysis, volumetric water content

3.1. Introduction

Ground penetrating radar (GPR) has been successfully used in pavement engineering for various applications, from determining layer thickness and moisture content to analyzing the quality of pavement construction during maintenance assessments (Ameri et al., 2014). Pavement layer thickness is a key factor in estimating the remaining pavement life and strengthening quality assurance during and after construction (Bezina et al., 2021). In this regard, GPR has proven to be very accurate in determining the thickness of asphalt layers, as shown in the use of GPR with air-coupled antennas (Al-Qadi & Lahouar, 2005; Al-Qadi et al., 2005; Domitrović & Rukavina, 2013; Domitrović et al., 2019; Flintsch et al., 2005; Holzschuher et al., 2007; Loizos & Plati, 2007b; Sener et al., 1998; Willett, et al., 2006; Hugenschmidt, 1996). Meanwhile, Al-Qadi et al. (2005) investigated the thickness error of newly constructed pavement and found that the GPR data from several locations revealed an increase in thickness inaccuracy with age of the pavement, while Ožbolt et al. (2012) found that the error in new pavements for motorways was mostly less than that of regional/county roads with several years of service. Previous studies also used field data to demonstrate the anticipated physical constraints associated with the use of GPR technology for pavement thickness detection (Al-Qadi & Lahouar, 2005), with some authors addressing the accuracy issues associated with using GPR to assess the surface layer thickness of various pavement layers (Sener et al., 1998; Willett et al., 2006; Domitrović & Rukavina, 2013). Collectively, this evidence still demonstrates the successful application of GPR in assessing various road structures.

In related research, it has been reported that GPR can identify and decipher various subsurface reflections from asphalt layers that have a buried moisture barrier (Saarenketo & Scullion, 2000). As for moisture content within pavement layers, it can result in a variety of issues, such as material deterioration and a loss of structural strength, as seen in one study on concrete (Laurens et al., 2005). It is important to note that the material's dielectric constant is significantly influenced by its moisture content, hence it is important to compare values directly between locations, even this should be done carefully because local moisture conditions can differ from site to site. Because water has a greater dielectric constant (81) than either air (1) or soil materials (4–20), moisture content affects the dielectric characteristics of materials (Loken, 2007). Thus, lower dielectric constants may indicate a material with less stiffness (Evans et al., 2007), while higher dielectric constants is explained by high moisture values.

When using GPR, the foundation layer and pavement materials' dielectric characteristics are important input parameters for calculating layer thickness, as seen through applying calibrations in the field (Al-Qadi & Lahouar, 2005) and independent test devices (Loizos & Plati, 2006; 2007; 2007b). Specifically, an evaluation of calibration methods conducted by Loizos and Plati (2007a; 2007b) involved calibration of the cores, calibration of the reflection amplitude (i.e., by only using GPR data), and calculations of the dielectric constants in the laboratory. However, according to some studies (Al-Qadi et al., 2003; Al-Qadi & Lahouar, 2005; Loizos & Plati, 2007b; Al-Qadi, et al., 2010), variations in asphalt moisture content can have an impact on the outcomes. The sources of these variations in dielectric constants are the asphalt composition and material characteristics (such as bitumen content, aggregate bulk density, and air void content) (Porubiaková & Komačka, 2015).

In general, road sections are extremely long, some of which are old with complex structures, making the evaluation of their composition and defects challenging. For instance, as highlighted in Solla et al. (2014), GPR was used to examine an old road characterized by complex crack structures resulting from various maintenance activities (Barnes & Trottier, 2002). Additionally, research has been done on the reproducibility of GPR measurements. In this regard, conducting repeated measurements in the same section under different environmental conditions can help understand their effect on the GPR data's quality and determine the importance of environmental parameters in such assessments. According to Al-Qadi et al. (2002), in which three datasets were gathered in one place, but in different times, thickness inaccuracies showed significant variations. Additionally, the changes in the dielectric constant values were attributed to variation in the test site's moisture content, while measurements at the same day illustrated good repeatability. In another study (Liu & Guo, 2003), GPR was used to determine the condition of hot mix asphalt (HMA) specimens under three different environmental conditions. They found that moisture content has a significant impact on dielectric permittivity and electromagnetic wave velocity under different conditions. In related research, many tests were done to assess the repeatability of GPR on dry and wet pavements (Willett et al., 2006).

Based on this discussion, the main objectives of the present research are as follows:

1- To determine the applicability of using GPR in road assessments, especially regarding aged roads.

2- To study the impact of environmental conditions on the GPR results.

3- To examine the relationship between GPR parameters (e.g., dielectric constants) and road composition (e.g., asphalt quality and water content).

3.2. Site description

The subject of focus in this research was a secondary road located near the town of Gyöngyös in Northern Hungary, Europe (see Figure 3.1). This road, with a macadam structure, was constructed in the 1970s and renewed in 2006 and 2007, when it received a binding asphalt layer and surface course. In certain sections, the macadam was replaced by a cement-treated base. These interventions resulted in a complex road structure. According to the plans, the road will be upgraded to a high-traffic road, since it will become part of a new bypass around the town.

For the purpose of this study, a 1-kilometer (km) long, 5-meter (m) wide section between 1,000 and 2,000 m from the starting point of the road was selected for the detailed GPR survey. The road consists of two lanes, referred to in my study as the right and left sides of the road, with one lane in each direction. At 11 locations, 15-centimeter (cm) diameter boreholes were drilled in the middle of the right and left lanes of the road (see Figure 3.1). The thicknesses of the cores varied between 8 and 25.5 cm, and showed high compositional diversity, indicating a challenge for an accurate survey of the road structure through traditional methods. In other words, the GPR measurements were performed on a structurally complicated old road, with considerable variations in asphalt thickness. In this relatively short section, two visual asphalt defects were detected: longitudinal and transversal cracks (see Figure 3.1).

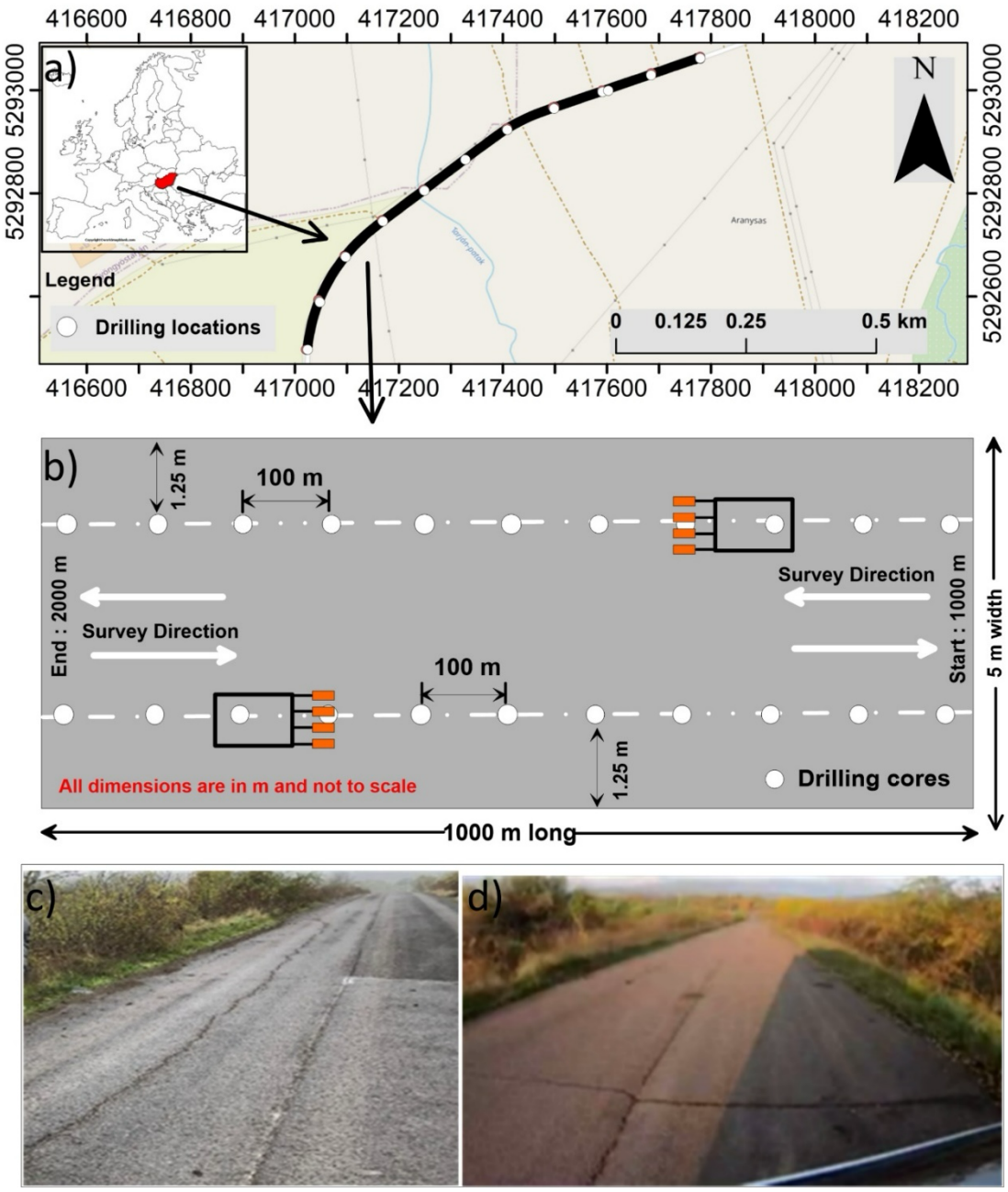

Figure 3.1 a) The location of the test site b) location of the survey lines and drillings, c) and d) photos of the road showing two types of cracks (longitudinal and transverse)

3.3 Materials and Methods

3.3.1 GPR data collection

The GPR data was collected by using a multichannel unit (SIR-30) connected to four air-coupled antennas manufactured by Geophysical Survey Systems, Inc. (GSSI). The air-coupled antennas enabled high speed collection of the GPR data, with each antenna used as both a transmitter and receiver. The antennas were installed at the back of the vehicle by using a distance measuring instrument (DMI) on one of the rear wheels.

In this case, two antennas had a center frequency of 1 GHz, while the other two had a center frequency of 2 GHz. The antenna arrangement (from left to right) was 1, 2, 1, and 2 GHz, depending on the center frequency. With Channel 1 as a reference point, Channel 2 was 0.56 m from Channel 1, Channel 3 was 1.12 m from Channel 1, and Channel 4 was 1.68 m from Channel 1 (see Figure 3.2).

We also used two different center frequency antennas to cover the resolution and penetration depth. A Leica global positioning system (GPS) unit was fixed to the top of the vehicle to provide accurate coordinates, along with the GPR data. Inline and cross-line offsets were manually measured at the beginning of the survey to correct the GPS locations by using GPR horn antennas. In this case, the inline offset was 3.3 m, which was the distance from the GPS antenna to the first 1 GHz horn antenna on the left side of the antenna arrangement. Meanwhile, the cross-line offset for each antenna was measured from the first 1-GHz horn antenna to the other horn antennas.

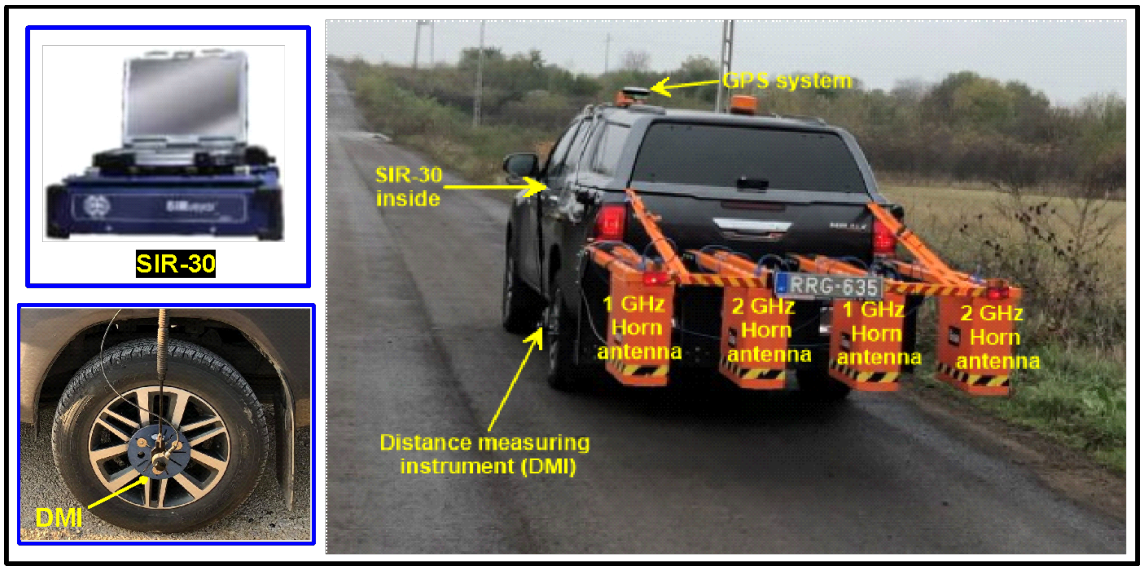

Figure 3.2 GPR data collection using SIR-30 equipped with four horn antennas.

In this study, several tests were conducted to identify the repeatability of GPR on dry and wet pavements. A total of 15 multichannel GPR profiles (60 separate GPR profiles) were performed on three different dates throughout the year. The 1 GHz horn antenna measured 30 profiles, while the 2 GHz horn antenna measured the other 30 profiles. Additionally, the GPS device was connected to the SIR-30 unit to perform the high-resolution survey and fixed to the top of the vehicle in front of the channels with a 3.3 m shift, after which the inline and cross-line offsets were adjusted. The GPR data was collected at 50 scans/unit for a total of 2,048 samples/scans.

At the beginning of the assessment, four metal plates were installed below the horn antennas and the calibration profiles were collected in the time mode. In the first survey**,** the time range was 20 nanoseconds (ns) for all antennas, while in the second and third surveys, it was 30 ns for the 1 GHz antennas and 25 ns for the 2 GHz antennas. The road was basically empty during all of the measurements, with only a few instances in which cars appeared and had to exit from the planned measuring lane and return later.

Overall, the surveys were performed on three different dates: October 27, 2020 (1st survey), January 27, 2021 (2nd survey), and June 8, 2021 (3rd survey**)**, each with four runs. The surveys were conducted under different weather conditions varying from wet (first and second measurement) to dry (third measurement) to show the applicability of GPR in different environmental conditions. A total of 38 GPR repeated profiles were collected from the right and left lanes of the road. The surveys were performed at a speed of 16 km/h.

3.3.2 Meteorological data

According to the meteorological data collected near the investigated site on October 27, 2020, the daily mean temperature was 13.1°C, the precipitation in the previous two weeks was 100 millimeters (mm), the precipitation of the previous week was 13.9 mm, and the soil moisture at 10 cm was 35.5%. On January 27, 2021, the daily mean temperature was −0.5°C, the precipitation in the previous two weeks was 11.9 mm, the precipitation of the previous week was 9.2 mm, and the soil moisture at 10 cm was 40.4%. On June 8, 2021, the daily mean temperature was 21.8°C, the precipitation in the previous two weeks was 16.7 mm, the precipitation in the previous week was 0 mm, and the soil moisture at 10 cm was 30.1% (DWMS, 2024).

3.4 Data processing and interpretation

3.4.1 GPR data processing

The collected GPR data was processed by using GSSI RADAN 7 software. First, the raw data (Figure 3.3a) underwent a filtering process to improve the signals and remove the noise. We included the metal plates at the beginning because horn antennas were used to collect the data, which removed a pocket of air on top of the pavement. Thus, we first calibrated the horn antennas and then applied a reflection picking step, which corrected the RoadScan data. This process eliminated the unwanted noise and enhanced the reflections from the pavement layers, making them easier to track. It also measured the

return times of the reflections and calculated the two-way travel time for each pavement layer.

Second, we applied a finite impulse response filter. In this step, we chose horizontal and vertical filters, with the former including stacking and the latter including low- and high-pass frequency filtering. In this case, the stacking in the horizontal filters applies a simple running average to stack the data. Stacking also combines the adjacent radar scans and outputs the data into a single scan. In this study, we used a length (scans) of 7. Meanwhile, the vertical low-pass frequency filter eliminated high-frequency noise often seen in deep radar profiles. As for the vertical high-pass frequency filter, we used a 2,000 and 4,000 MHz filter for the 1 and 2 GHz antennas, respectively. This filter rejected the frequencies above an established threshold. For the 1 and 2 GHz antennas, we used 250 and 600 MHz, respectively (GSSI RADAN 7 manual, 2017).

Third, we applied Gain, which is used to increase the data amplitudes of lower interfaces. In this case, the Gain was set to 7 points, with exponential values between 1.5 and 20. We also employed a background removal horizontal filter in some profiles. Here, the length of the filter should always be a greater number than the length of the longest horizontal “real” reflector in the data (GSSI RADAN 7 manual, 2017).

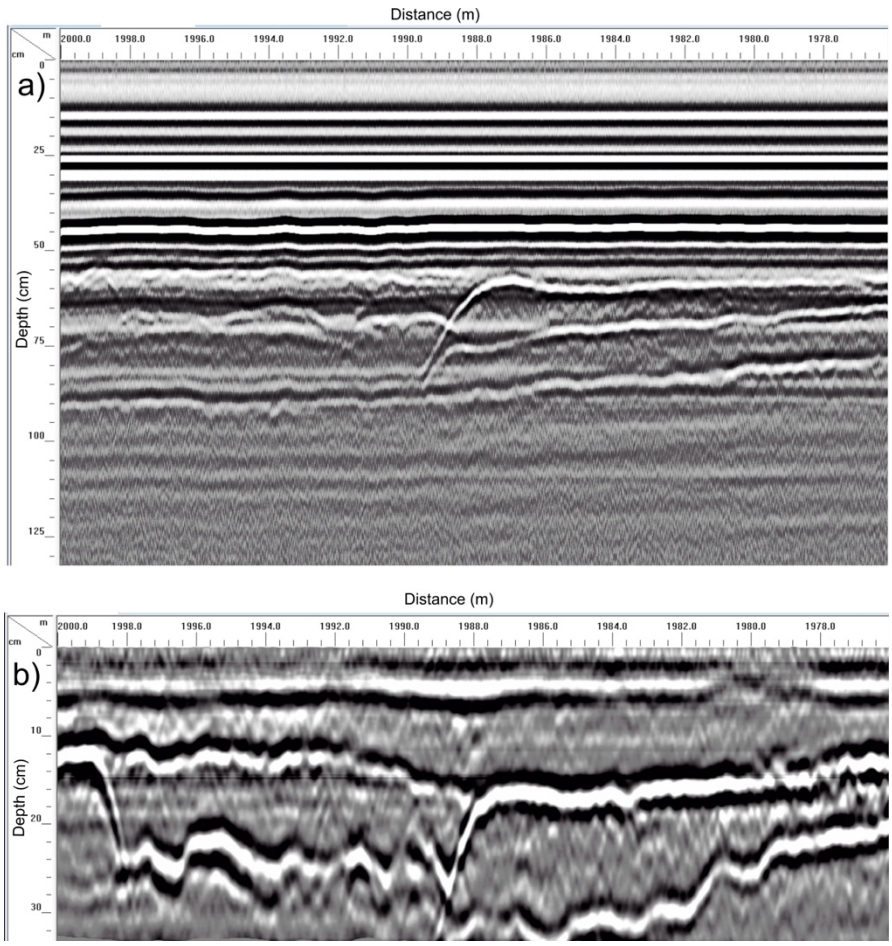

Figure 3.3 A section of the GPR profile illustrates the data a) before and b) after applying the processing steps

Finally, after carrying out these steps (Figure 3.3b), the interfaces between the layers in the asphalt and below them became clear, after which the "select block" option in the RADAN software was used to select the interfaces. The ground truth method was then used as an input tool for the exact thickness of the core samples in their specific locations. This was achieved by fitting the coordinates of the drilling information with the exact locations of the multichannel GPR profiles collected by the high-resolution coordinates. Furthermore, the core data and automatic velocity methods were used to export the picking information for data interpretation and analysis.

3.4.2 Interpreting the GPR data

The relationships between the layer thicknesses, dielectric constants, and the reflection amplitudes have been described by Scullion and Briggs (1991). First, the GPR data determined the thickness of the surface asphalt layers for each survey. The reproducibility of the repeated thickness measurements on the same day and under different meteorological conditions was assessed by using the 2 GHz channels closest to

the track of drilling points during the surveys. In this case, the reproducibility analysis focused on the surface asphalt layers. After determining the interfaces between the asphalt layers, the dielectric constant was computed by using two methods: 1) the ground truth method, based on the core data and time interval calculations (RADAN 7); and 2) the reflection amplitudes method, based on the magnitude difference of the GPR signal amplitudes and the dielectric constant change between the layers.

For the two approaches, equation (3.1) was resolved as follows (Evans et al. 2007):

$$d_i = \frac{ct_i}{\sqrt{\varepsilon_{r,i}}} \quad (3.1)$$

where d_i is the thickness of the i_{th} layer, t_i is the EM wave two-way travel time through the i_{th} layer, c is the speed of light in vacuum (c = 30 cm/ns), and $\varepsilon_{r,i}$ is the dielectric constant of the i_{th} layer. In this case, the ground truth method utilizes the known value of the dielectric constant d_i obtained from the drilled cores. This allows for a straightforward calculation of the dielectric constant at the measurement point, after which this value is horizontally extrapolated. Consequently, the precision of the extrapolation improves as the number of drillings increase.

As for the reflection amplitude method, it compares the signal amplitude measured at the asphalt surface with the amplitude measured in the case of the metal plates, which reflect approximately 100% of the GPR signals. The amplitude of the latter was obtained before each GPR survey by using the same antenna configuration. The dielectric constant of the asphalt surface was calculated by using Equation (3.2) (Maser and Scullion 1992):

$$\varepsilon_a = \left(\frac{1+\frac{A_1}{A_m}}{1-\frac{A_1}{A_m}}\right)^2 \quad (3.2)$$

where A_1 and A_m denote the EM wave reflection amplitudes of the asphalt surface and the metal plates on the pavement surface, respectively, while ε_a is the dielectric value of the asphalt layer.

With the obtained dielectric constant, the thickness of the asphalt layer can be calculated by using Equation (3.1). Although this approach allows for the determination of the dielectric constant and thickness for each trace along the GPR profile, it can hardly account for vertical changes in the composition of the asphalt layer. Thus, these surface values were vertically extrapolated. We also compared the calculated thickness values and real thickness data at the coring points to determine the differences between these two methods.

For the road structure analysis, depth values were exported by averaging the measured values for every 0.5 m. This data (along with the drilled cores) enabled the reconstruction of the complex structure of the investigated road. For the 2 GHz measurements, corresponding dielectric values were exported, while vertical dielectric profiles were generated to identify the compositional differences of the road structure by exporting different interfaces related to certain layers. Surface asphalt layer values were calculated by using Equation (3.2) for the subsequent layers, while macadam and cement-treated base values were calculated by using the following Equation (3.3) Al-Qadi & Lahouar, 2005; Li et al., 2013):

$$\sqrt{\varepsilon_2} = \sqrt{\varepsilon_1}\frac{1-\left(\frac{A_0}{A_m}\right)^2+\frac{A_1}{A_m}}{1-\left(\frac{A_0}{A_m}\right)^2-\frac{A_1}{A_m}} \qquad (3.3)$$

where A_1 is the reflected amplitude from the top of the subsequent layer. Moreover, a similar formula can be recursively obtained for the n^{th} layer:

$$\sqrt{\varepsilon_n} = \sqrt{\varepsilon_{n-1}}\frac{1-\left(\frac{A_0}{A_m}\right)^2+\sum_{i=1}^{n-2} y_i*\frac{A_i}{A_m}+\frac{A_{n-1}}{A_m}}{1-\left(\frac{A_0}{A_m}\right)^2-\sum_{i=1}^{n-2} y_i*\frac{A_i}{A_m}+\frac{A_{n-1}}{A_m}} \qquad (3.4)$$

where A_i is the reflected amplitude from the top of the i^{th} layer and y_i is the reflection coefficient between the i^{th} and i^{+1th} layers, which can be calculated by using the following equation (Jaselskis et al. 2003):

$$y_i = \frac{\sqrt{\varepsilon_i}+\sqrt{\varepsilon_i-1}}{\sqrt{\varepsilon_i}-\sqrt{\varepsilon_i-1}} \qquad (3.5)$$

This data, processed by using Surfer v.14 software, was used to assess the reproducibility and seasonal differences in the macadam and cement properties.

3.4.3. Volume fraction of water (f) calculations

Finally, to estimate the temporal differences in the volumetric water content of different pavement constituents, we applied the Maxwell Garnett formula, which is explicitly written for effective permittivity (ε_{eff}) as follows (Cao & Al-Qadi, 2021):

$$\varepsilon_{eff} = \varepsilon_e + 3f\varepsilon_e\frac{\varepsilon_i-\varepsilon_e}{\varepsilon_i+2\varepsilon_e-f(\varepsilon_i-\varepsilon_e)} \qquad (3.6)$$

where ε_i and ε_e denote the permittivity of the inclusion and its environment, respectively, f is a dimensionless quantity, and f = nV is the volume fraction of the inclusions in the mixture. In our calculations, ε_e stands for the measured permittivity under relatively dry conditions (3rd survey), ε_i stands for the temperature-corrected permittivity of water (Cao & Al-Qadi, 2021), and ε_{eff} represents the measured permittivity

under wetter conditions (1st and 2nd surveys). The equation was also rearranged to express *f* as the difference in the volume fraction of water between the relatively dry and wetter states. Moreover, the distribution of *f* in the surveyed profiles was displayed to identify higher moisture uptake areas (i.e., the different constituents of the road that are more exposed to damage in the long run).

3.5 Results

3.5.1 Thickness detection precision and measurement reproducibility

First, we analyzed the measurements performed on the same day. Specifically, we used the ground truth correction method to determine the difference between the actual depth values and the h_{GT} derived depths at the coring points as 0.09 cm (0.69%), −0.11 cm (−0.78%), −0.09 cm (−0.70%), and 0.00 cm (0.012%) for the first, second, third, and fourth runs, respectively. In this case, positive values represent the overestimation of actual depths, while negative values stand for the underestimation of such depths. In each run, an average of 0.06 cm (0.55%) difference was achieved. Hence, by using the ground truth method at the drilling points, the depth estimation was highly accurate, since the differences were well below the precision of using a tape to measure the core thickness. Additionally, when comparing the average core thickness calculated from the cores to the average asphalt thickness obtained by the continuous GPR measurements, the differences were 0.49 cm (3.70%), 0.17 cm (1.33%), 0.25 cm (1.19%), and 0.61 cm (4.56%) for the four consecutive measurements. This corresponds to an average difference of 0.38 cm (2.87%).

The application of 22 cores for correcting the GPR measurements is unusual in studies of this kind. Thus, we reduced the number of cores and checked the differences by only using the second run, in which the difference between the average core thickness and the average GPR-derived thickness was the lowest. Meanwhile, the number of applied cores was gradually reduced during the analysis, and the estimated h_{GT} was compared with the h_{GT} determined by using each core. In practice, employing 18 and 14 cores resulted in an average GPR-derived thickness difference of 0.51 cm (3.89%) and 0.54 cm (4.10%), respectively. When halving the number of cores and only using every second core (12 cores), the difference between the average core thickness and the average GPR-derived thickness increased to −0.55 cm (−4.19%), due to the complex road structure.

Moreover, the difference between the average core thickness and the average GPR-derived thickness by using the reduced number of cores (10 cores) was 0.78 cm

(5.85%). However, following Hungarian standards: e-UT 06.03.21 and the drilled sampling standards: MSZ EN 12 697-27 (Primusz et al., 2022), which recommend a maximum of three transversal coring profiles, sampling each lane at its midline entailed six cores for pavement analysis (personal communication by Csaba Tóth): two at the beginning, two at the middle, and two at the end of the investigated road section. In this case, the difference increased to −1.19 cm (−9.23%) between the core and the GPR average and −0.81 cm (−6.36%) between the GPR data with high-resolution control (22 cores) and the data with standard control (six cores). Finally, using two cores (one from the middle of the left lane and one from the middle of the right lane), the difference increased to 1.33 cm (10.14%).

As for the differences when using a depth estimation independent of the cores (h_{amp}), they were −0.33 cm (−2.46%), −0.36 cm (2.65%), −0.26 cm (−1.97%), and −0.14 cm (−1.14%), indicating an average of −0.28 cm (−2.06%) underestimation at the drilling points. Although the estimation at the coring points was worse than in the case of h_{GT}, it was still within the precision range of the tape measurements. Regarding the h_{amp} average thickness values obtained from the continuous GPR measurements, they were compared with the average thickness derived from the cores themselves. In this case, the differences were −1.12 cm (8.42%), −1.38 cm (10.47%), −0.91 cm (6.94%), and −1.13 cm (9.05%) for the consecutive runs, with an average value of −1.15 cm (−8.72%). This indicates that the h_{amp}-based thickness estimation was more reliable in this section of aged road. Moreover, by comparing the h_{amp} average thickness value of −1.15 cm (−8.72%) with the values obtained from the ground truth correction method using different numbers of cores, we found that the h_{amp} average thickness from the continuous measurements was more than the values obtained with 22, 18, 14, 12, and 10 validated cores. This resulted in differences of 0.38 cm (2.87%), 0.51 cm (3.89%), 0.54 cm (4.10%), 0.55 cm (4.19%), and 0.78 cm (5.85%), respectively. Meanwhile, they were lower than the values obtained with 6 and 2 validated cores, which were −1.21 cm (−9.23%) and 1.33 cm (10.14%), respectively.

To determine the reproducibility of the GPR measurements, we found that the average difference (standard deviation) of the h_{GT} continuous value was 0.20 cm for the four runs. Conversely, in the case of h_{amp}, the average difference of the continuous value was 0.19 cm for the four runs. These values slightly fluctuated between the different measurements. We also found that estimating the asphalt thickness under the same

condition in the range of ± 0.20 cm in the average value for h_{GT} and ± 0.19 cm in the average value for h_{amp} was possible.

After analyzing the data obtained on the same day, we compared the results of the three separate surveys under different environmental conditions (wet, medium-wet, and dry) on the right (Figure 3.4a) and left sides (Figure 3.4b) of the road. For the third survey, the second run was selected for comparison. When considering h_{GT} derived by using all the cores, we found that the difference between the average core thickness and the average asphalt thickness obtained by the GPR measurements was −0.92 cm (−6.96%), 0.63 cm (4.75%), and 0.25 cm (1.19%) for the three different measurements. We also obtained differences of −2.72 cm (−20.60%), −1.76 cm (13.63%), and 1.33 cm (10.14%) by using the minimum number of cores (2 cores) for the three surveys, respectively. The results indicated that the uncertainty of the GPR measurements, determined as the standard deviation of the average GPR-derived thickness values, was ± 1.81 cm and ± 2.12 cm by using 22 and 2 cores for the ground truth method, respectively.

After comparing the results of the three different surveys by using h_{amp}, we found that the difference between the average core values and the average GPR-derived asphalt thickness was −3.19 cm (−24.22%), −2.34 cm (−17.79%), and −1.38 cm (−10.47%) under wet, medium-wet, and dry conditions, respectively. We also found that the standard deviation of the h_{amp} continuous measurement for the three different measurements was 0.91 cm. Thus, it is possible to estimate the asphalt thickness under different conditions in the range of ± 0.91 cm. Moreover, we found that the difference between the dry and wet conditions, i.e., the first and third measurements, was 1.81 cm (18.1 mm).

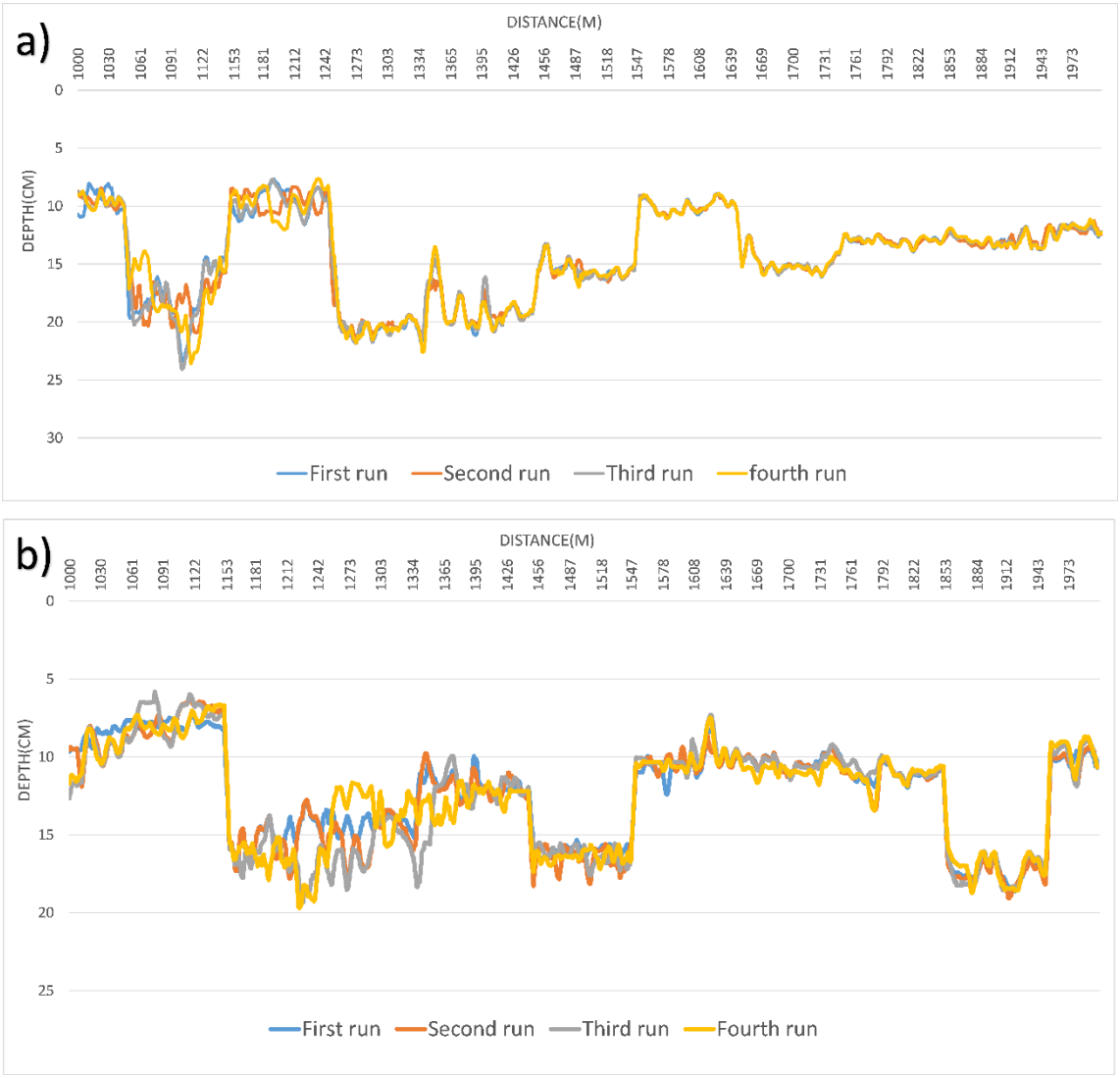

Figure 3.4 Comparison between the average GPR depth values calculated by the ground truth method (CH2) on the same day and the repeated measurement distance on a) the right side and b) left side of the road

3.5.2. Dielectric properties

3.5.2.1 Measurements on the same day

Based on the vertical dielectric values under dry conditions (3rd survey), repeatedly measured on the same day, it was clear that the composition of some sections significantly differed. Overall, three dielectric ranges, referring to the three types of pavement materials, were identified. First, the lowest dielectric values could be attributed to the macadam layer, with a mean and standard deviation of 2.68 ± 0.24. Second, the medium dielectric values could be attributed to the asphalt layer, with a mean value of 4.03 ± 0.63. In this case, the dielectric values higher than the macadam values can be explained by the higher degree of compaction, the lower size of aggregates, and the lower

porosity value (see Figure 3.5). Third, the highest dielectric values obtained from the cement-treated base included a mean dielectric value of 4.76 ± 0.36. These results indicate that the three major road components can be easily separated. However, there were some differences in the right and left lanes of the road. Based on the dielectric values, macadam was not uniform in the left lane, while some high values for the cement-treated base and asphalt layers were obtained in the right lane.

As for the standard deviation of the dielectric data, the highest variation was found in the asphalt layer. We also compared the average values of the different runs made on the same day to determine whether the lack of measurement reproducibility caused this variation in the results regarding the heterogeneity of the asphalt. Moreover, the mean dielectric values were 4.02, 4.06, 3.99, and 4.04 for the first, second, third, and fourth runs, respectively, i.e., the high standard deviation was a consequence of the heterogeneous composition of the surface course.

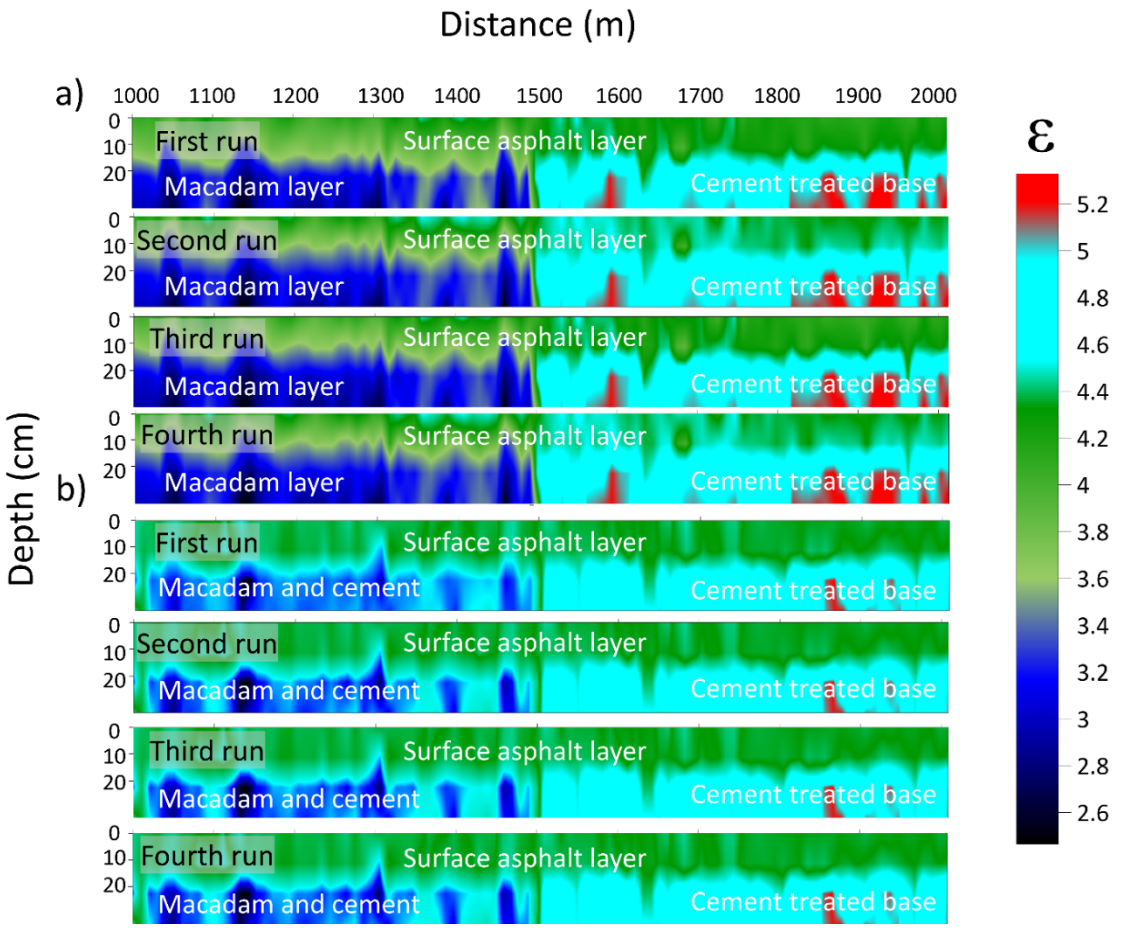

Figure 3.5 Comparison of the dielectric values for the four daily GPR measurements performed under dry conditions: a) the right side and b) left side of the road

3.5.2.2 Analysis of the dielectric properties under different conditions

We compared the data obtained on different dates under different meteorological conditions (explained in section 3.3.2) to identify the seasonal differences in the dielectric constants. The highest dielectric values were observed during the first measurement when the highest amount of precipitation preceded the survey (see Table 3.1). Thus, the average dielectric value of the surface asphalt layer under wet conditions was 8.31. A slightly lower average value (7.06) was identified for the second survey, characterized by medium-wet conditions (see Figure 3.6). Meanwhile, low dielectric values were obtained with an average value of 4.00 (see Table 3.1) for the third survey, performed under dry conditions (no precipitation during the previous week). A similar pattern was identified in the macadam and cement-treated base values. In this case, the greater the amount of water in the material, the higher the dielectric constant.

However, the degree of difference between the three main road components differed. For example, the relative difference between the dielectric values of macadam under wet and dry conditions was 25%, whereas the relative differences between the dielectric values of the surface asphalt and cement-treated base layers were 52% and 59%, respectively. These results indicate that macadam takes up less water than asphalt and cement-treated base, with the latter more sensitive to moisture content change. It is important to note that a material's moisture condition significantly affects its dielectric constant, and local moisture conditions can vary from site to site, so it is important to compare values directly between sites carefully.

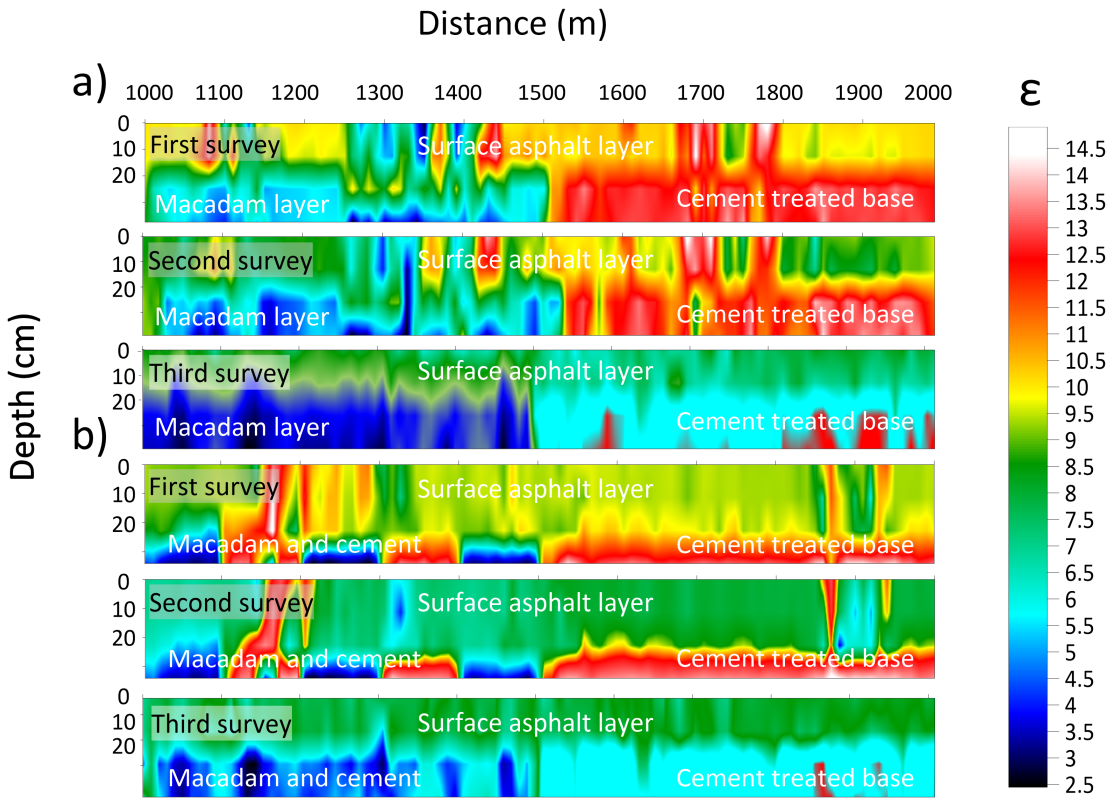

Figure 3.6 Comparison of the dielectric maps of the three GPR surveys on: a) the right side and b) left side of the road

Table 3.1 Mean and standard deviation of the dielectric constants of the three structural units under different moisture conditions

	$\varepsilon_{macadam}$	$\varepsilon_{asphalt}$	$\varepsilon_{cement\ treated\ base}$
First Survey (wet)	4.00±0.34	8.31±0.43	11.88±0.52
second survey(medium-wet)	3.30±0.34	7.06±0.23	10.88±0.52
third survey (dry)	3.00±0.24	4.00±0.63	4.83±0.36

3.5.2.3 Analysis of f

As for the volumetric water difference inside the pavement, it can be estimated by using Equation (6). For asphalt, the difference in *f* between surveys conducted under relatively dry and wet conditions was 0.06, indicating that the volumetric water content was approximately 6% higher in the latter case, while it was 0.04 under the dry and medium-wet conditions. For macadam and cement-treated base, the difference in *f* was 0.01 and 0.1 under dry and wet conditions, and 0.004 and 0.09 under dry and medium-wet conditions, respectively. These results also support that the moisture uptake of

macadam is the lowest, whereas that of the cement-treated base is the highest, with asphalt halfway in between.

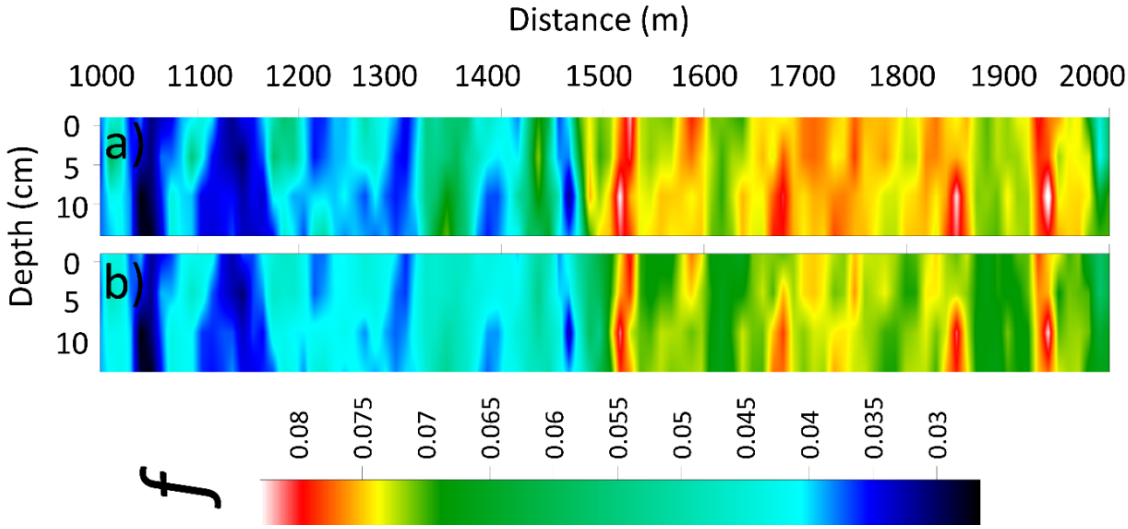

Figure 3.7 Spatial differences of *f* in the asphalt layer under relatively dry and wet conditions: a) the right side and b) left side of the road

However, temporal and spatial differences were also identified for *f*. Specifically, the asphalt layer between 1,000 and 1,500 m showed significantly lower values of *f* than that between 1,500 and 2,000 m (see Figure 3.7). There are three possible reasons for this higher fractional water uptake. First, the asphalt between 1,500 and 2,000 m is older than that between 1,000 and 1,500 m. Consequently, more water can infiltrate the pavement. Second, the high water content of the cement-treated base increases the volume of *f* content of the asphalt layer above capillary absorption. Third, the cement-treated base inhibits water infiltration into deeper layers and leads to moisture accumulation in the overlying asphalt layer. Based on the road construction data, the asphalt above the cement-treated base was laid at a later time. Thus, the second and third reason is probably more pertinent to the elevated moisture values.

Based on Spearman's correlation (Levesque, 2007) performed at a distance of 1,500 to 2,000 m, we found a weak negative correlation (−0.337248) with a high degree of significance (< 0.001) between the thickness of the cement-treated base and the volumetric difference of water within the pavement. These results indicate that high thickness affects the suggested volumetric water difference.

3.5.3 Road structure

The high-resolution horn antenna data not only allowed for the detection of interfaces between materials with high dielectric contrast, such as asphalt and cement, but

also the resolution of sub-layers within the asphalt with much lower dielectric contrast as shown in Figure 3.8 as an example of a picked part of the GPR profile (one interface in Figure 3.8a and two interfaces in Figure 3.8b). The drilling cores also confirmed the identified layers (Figures 3.8c and 3.8d). Within the short section of the asphalt, a significant variation in the thickness of the cement-treated base was observed, as shown in Figure 3.8a.

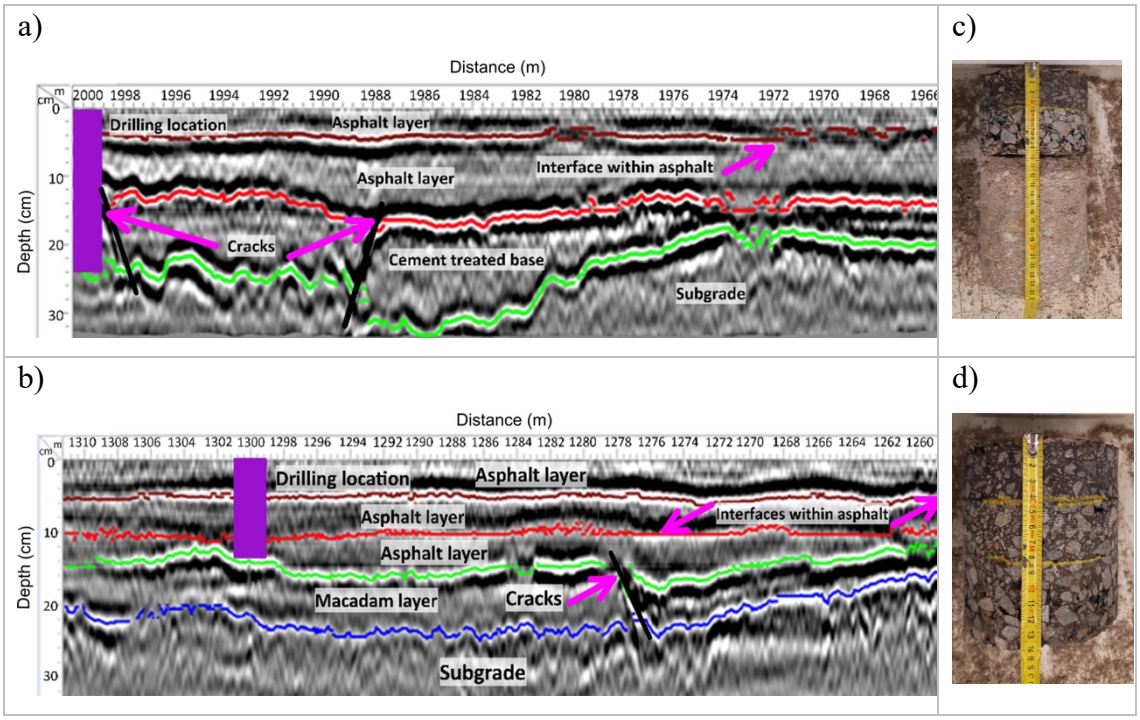

Figures 3.8 a) and b) Interpreted GPR profile showing the interfaces between the different asphalt components. c and d) core samples indicated on the profiles from the left side of the road.

The GPR data analysis, combined with the information from the drilled cores, revealed that the pavement in the study area comprised many layers of materials covering the natural ground (subgrade). Due to the complexity of the road structure on the right and left sides, the composition of each side can be explained by Figure 3.9, which illustrates the structural change between two successive sections. For the left side, a thick layer of cement-treated base at a distance of 1,100 to 1,200 m, 1,300 to 1,400 m, and 1,500 to 2,000 m were covered by an asphalt layer. The asphalt macadam was only located at three short distances: from 1,000 to 1,100 m, from 1,200 to 1,300 m, and from 1,400 to 1,500 m. The right side of the road contained a thinner cement-treated base, compared to the left side. Meanwhile, the macadam was noncontinuously located on the road's left and right sides. As for the interfaces between the cement-treated base and the

asphalt layer and between the asphalt macadam and the asphalt, they were easily observed, with a high dielectric contrast revealed by the fluctuation in echo amplitude. Overall, the interface between the subgrade and the overlaying road components produced the best contrasts because of the significant dielectric differences present.

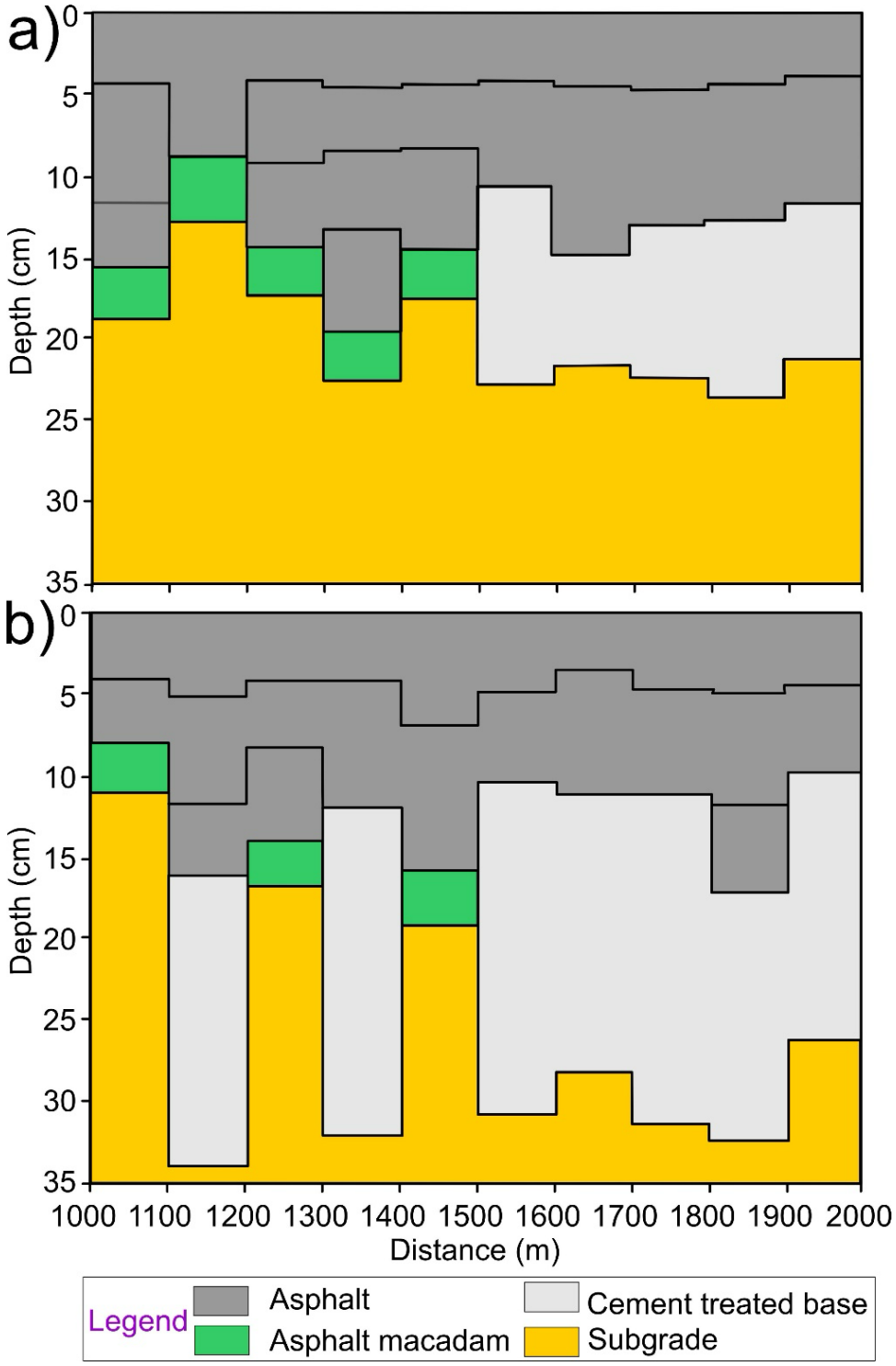

Figure 3.9 Typical longitudinal section of a) the right side and b) left side of a flexible pavement in Gyöngyös

3.6 Discussion

The applicability of GPR in assessing a road with a complex structure was tested by conducting repeated measurements on the same day and under different conditions for at-a-point and continuous measurements. Our study found that on the same day, the average thickness errors of the continuous measurements of the four runs were 2.87% for h_{GT} and −8.72% for h_{amp}. We also found that it is possible to calculate the thickness of the asphalt under the same condition, in the range of ± 0.20 cm for h_{GT} and ± 0.19 for h_{amp}, to determine the deviations in the average values. According to Al-Qadi et al. (2002), stated thickness errors ranged between 5.9% and 12%. However, their values were higher than ours because they were collected on different dates in three datasets. This disparity could also be attributed to the variations in the moisture conditions at the test sites. Another study by Holzschuher et al. (2007) found good reproducibility of the measurements under comparable circumstances. Specifically, errors in the thickness were 7.9% at low speed, 8.3% at high speed, and 6.7% during stationary observations, indicating that the survey speed did not have an impact on GPR performance.

Numerous studies, often utilizing horn antennas, have been done to determine the GPR data accuracy. In our study, when reducing the number of cores, we observed differences in the average GPR-derived thickness of 0.51 cm (3.89%) and 1.33 cm (10.14%) by using 18 and 2 cores, respectively. Similarly, Flintsch et al., (2005) found that the average absolute thickness error varied from 1.8% to 8.4%, with an overall average of approximately 4.7% when using the reflection amplitude method. We could obtain different accuracy values than these studies by using $h_{GT,}$ similar values were found by using h_{amp} in our analysis of an aged road section. Scullion and Briggs (1991) realised a reduction in the standard error from 7.6 mm (without using calibration cores) to 2.8 mm (by using one calibration core). Lalagüe et al. (2014) calculated average errors of 6%–10% without using core calibration versus 1%–5% by using core calibration. Edwards and Mason (2011) documented the percentage error of 4.5% and 7%, with and without calibrated cores (using the reflection amplitude method).

The repeatability of our measurements shows matching with Willet and Rister (2002) who repeated the measurements under dry and wet conditions and determined the number of real field cores required for precise postprocessing of radar data into thickness values. By comparing thickness of the surface layer between GPR calibrated with multiple and real measured cores, and the results were varying from 10.31% to 0.40% for asphalt less than two inches. Loizos and Plati (2007a), GPR surveys were measured twice

under the same conditions to verify the repeatability of the measured data. Based on the ground truth results, the errors ranged from 10.19% to 12.96%. Morey (1998) collected data by using a 2 GH air-coupled horn antenna, after which the percentage error was 10.3% when using the reflection amplitude method which are higher than the values obtained from the current study.

For an old pavement system, as demonstrated in Maser (1990) and Saarenketo and Scullion (2000), the data from 73 cores taken at 11 sites showed that the radar predictions were within 10% of the core data. In Fernando and Maser (1992), 14 primary test sections were selected from the different routes surveyed. The results showed accuracies of ± 5% to ± 7.5% on asphalt thickness ranging from 5.1 to 50 cm. These values are higher than our results because they covered 20 diverse pavement sections. In other words, the results were based on correlations with data from more than 200 cores. In a related study by Al-Qadi et al. (2005), measurements were taken on various pavement systems of different ages. In the case of flexible pavements, the age of the pavement increased the GPR thickness error (4.4% error for pavements 0–5 years old versus 5.8% error for pavements older than 20 years, using surfaces older than 10 years). Al-Qadi and Lahouar (2005) found that the thickness of asphalt pavement layers, which range in thickness from 280 to 350 mm for older pavement, can be estimated with an average error of 6.8%. This is similar to our results when using the ground truth method.

In our study, for the three conditions, the uncertainty of GPR measurements (determined as the standard deviation of the average GPR-derived thickness values) is reduced by using higher number of cores was ± 1.81 cm and ± 2.12 cm by using 22 and 2 cores, respectively. We also found that estimating the asphalt thickness under different conditions from h_{amp}, in the range of ± 0.91 cm, was possible. These values are also close to those obtained by Maser and Scullion (1992), in which they demonstrated that without taking a core, the thickness of the asphalt may be predicted to within ± 0.81 cm. However, the accuracy increased to ± 0.28 cm when a single calibration core was extracted at each site.

Our average dielectric values for the different road components are consistent with other researches. For instance, in Daniels (2004), the dielectric constant ranges for dry and wet asphalts were 2–4 and 6–10, respectively. Meanwhile, it was demonstrated by Evans et al. (2007) that asphalt materials that are generally comparable can have varied dielectric constant values under similar conditions. Specifically, the dielectric values of dry asphalt, wet asphalt, and concrete ranged from 2 to 4, 6 to 12, and 4 to 10, respectively.

Moreover, Roddiss et al. (1992) reported that most asphalt materials include dielectric constant values of 4–10, while those for concrete are 5–9, depending on material type and condition. In related research, according to Cao et al. (2007), concrete has a dielectric constant of 10.0 while asphalt has a dielectric constant of about 6.0, while Loizos and Plati (2007a) found that the dielectric values of the binder course were higher than those of the surface course. Additionally, they discovered that the asphalt base had an average dielectric value of 6.93 and the surface course had an average dielectric value of 6.27. The corresponding standard deviations in this instance were 0.21 and 0.29.

Finally, an analysis of the moisture represented by the constructed maps showed a clear difference among the three components of the investigated road section. The lowest difference in *f* was 0.01 for macadam, while that for asphalt was 0.06. Additionally, the highest value was observed in the cement-treated base (0.1). As mentioned by Jaselskis et al. (2003), in addition to the initial water-to-cement ratio, other elements that affect the dielectric permittivity of cement-based materials include the types of cement, pozzolan material, and aggregate. Since cement-treated base usually consists of fine grains, even a small *f* retained can result in higher dielectric permittivity values than other road components. Moreover, according to Shang et al. (1999), the effect on the dielectric constant becomes more significant and nonlinear above a moisture level of 1.2%. In our study, we found that the relative difference between the dielectric values of macadam under wet and dry conditions was 25%, while it was 52% and 59% for the surface asphalt layer and cement-treated base, respectively.

3.7 Conclusion

This study effectively demonstrates the high precision and reproducibility of Ground Penetrating Radar (GPR) measurements for assessing road thickness and structure in terms of aged pavements with a complex multilayer composition. Key findings highlight that the ground truth (h_{GT}) correction method yielded a highly accurate thickness estimation with an average deviation of 0.38 cm when validated with 22 cores. Reducing the number of calibration cores, while increasing deviations, still provided acceptable accuracy, with differences ranging from 0.51 cm using 18 cores to 1.33 cm using only 2 cores. These findings are within or outperform previous error ranges reported in similar GPR calibration studies, emphasizing the robustness of this method even with reduced calibration.

In terms of reproducibility, GPR thickness measurements showed little variation (± 0.20 cm for h_{GT}, ± 0.19 cm for h_{amp}) across repeated runs. Under different meteorological conditions, it affected largely the thickness results, with the standard deviation of GPR thickness values averaging ± 1.81 cm using 22 cores and ± 2.12 cm with 2 cores.
Comparisons of measurements under different environmental conditions (wet, medium-wet, dry) revealed significant dielectric variations, where wet conditions notably increased dielectric constants due to higher moisture uptake, particularly in the cement-treated base, which showed a 59% increase. These findings underscore the sensitivity of GPR-derived dielectric properties to moisture content, affirming the necessity of considering environmental conditions in GPR evaluations.

In conclusion, the GPR system demonstrated exceptional capability in accurately measuring pavement thickness, detecting dielectric properties, and resolving complex road structures. The minimal measurement errors, high reproducibility, and sensitivity to moisture underscore GPR's reliability for road quality assessments. The findings of this study can serve as a reference for future investigations of other roads in the world with a complex structure.

4. Assessing the Compaction Quality of Dolomitic Asphalt Pavements Using Ground Penetrating Radar

This article is published in *applied sciences MDPI* Journal as:
Enas Abdelsamei, Diaa Sheishah, Zalán Tobak, Ahmed. M. Ali, Károly Barta, Abdelouahed Fannakh, Gergő Magyar, Viktória Blanka-Végi, György Sipos Assessing the compaction quality of dolomitic asphalt pavements using ground penetrating radar," in *applied sciences MDPI*
Journal Impact Factor: 2.5 (2023)

applied sciences

MDPI

Article

Assessing the Compaction Quality of Dolomitic Asphalt Pavements Using Ground Penetrating Radar

Enas Abdelsamei, Diaa Sheishah, Zalán Tobak, Ahmed M. Ali, Károly Barta, Abdelouahed Fannakh, Gergő Magyar, Viktória Blanka-Végi and György Sipos *

Department of Geoinformatics, Physical and Environmental Geography, University of Szeged, Egyetem u. 2-6., 6722 Szeged, Hungary; enas.mohammed@nriag.sci.eg (E.A.); geo_diaa@nriag.sci.eg (D.S.); tobak@geo.u-szeged.hu (Z.T.); ahmed.mahmoud@nriag.sci.eg (A.M.A.); barta@geo.u-szeged.hu (K.B.); abdelouahed.fannakh@gmail.com (A.F.); magyar.gergo94@gmail.com (G.M.); blankav@geo.u-szeged.hu (V.B.-V.)
* Correspondence: gysipos@geo.u-szeged.hu

Abstract: The quality of newly constructed pavement depends mostly on compaction, which is essential for ensuring the pavement's longevity and performance. Traditional methods of evaluating pavement compaction and density, such as core sampling and nuclear gauge measurements, are often time-consuming and invasive and provide only a limited amount of data at a low spatial resolution on the potential air void content of the asphalt layers. The present study aimed to assess the specific gravity (G_{mb}) of a dolomitic asphalt mixture at different degrees of compaction using GPR techniques. Relative density (RD) maps were generated to visualize the spatial homogeneity of the asphalt density. Nuclear density gauging was applied for the calibration, and cores were used to validate the results. The survey was conducted on two recently paved roads in Szeged, Hungary. After testing various approaches, it was found that applying horn antennas and the surface reflection (SR) method is the most feasible way to obtain reliable and accurate dielectric permittivity (ε) data. Based on the measurements, clear relationships were found between dielectric constants, G_{mb}, and aggregate size. The findings highlight that it is possible to indirectly determine the G_{mb} of asphalts composed of dolomite and limestone aggregates using GPR, with aggregate sizes ranging from 11 mm to 25 mm and G_{mb} values between 2.43 and 2.57 g/cm^3. Consequently, a robust function was developed, which can be applied to other asphalts with similar compositions.

Keywords: Ground Penetrating Radar (GPR); dielectric permittivity; specific gravity; relative density; aggregate size

check for updates

Academic Editors: Deshan Feng, Xun Wang and Bin Zhang

Received: 4 January 2025
Revised: 20 February 2025
Accepted: 24 February 2025
Published: 26 February 2025

Citation: Abdelsamei, E.; Sheishah, D.; Tobak, Z.; Ali, A.M.; Barta, K.; Fannakh, A.; Magyar, G.; Blanka-Végi, V.; Sipos, G. Assessing the Compaction Quality of Dolomitic Asphalt Pavements Using Ground Penetrating Radar. *Appl. Sci.* **2025**, *15*, 2501. https://doi.org/10.3390/app15052501

1. Introduction

The dielectric properties of pavement materials are crucial in GPR investigations [1]. The dielectric permittivity (ε) of a substance refers to its ability to store the applied electric field, with the dielectric constant (ε_r) representing the ratio of its permittivity to that of the vacuum (ε_0) [2]. Previous studies, such as those by Loizos and Plati [3,4], proposed three calibration methods: core calibration, laboratory ε determination, and reflection amplitude calibration, all suitable for pavement evaluation. This paper distinguishes itself by using horn antennas and the surface reflection method to indirectly determine the specific gravity (G_{mb}) of dolomitic asphalt mixtures, developing a general function applicable to similar asphalt compositions and offering a more streamlined and widely applicable approach than the methods discussed.

Abstract

The quality of newly constructed pavement depends mostly on compaction, essential for ensuring pavement longevity and performance. Traditional methods of evaluating pavement compaction and density, such as core sampling and nuclear gauge measurements, are often time-consuming and invasive and provide only a limited number of data at a low spatial resolution on the potential air void content of asphalt layers. The present study aimed to assess the specific gravity (G_{mb}) of a dolomitic asphalt mixture at different degrees of compaction using GPR techniques. This way, relative density (RD) maps were generated to visualize the spatial homogeneity of asphalt density. Nuclear density gauging was applied for calibration, and cores were used to validate the results. The survey was conducted on two recently paved roads in Szeged, Hungary. After testing various approaches, it was found that applying horn antennas and the surface reflection (SR) method is the most feasible way to obtain reliable and accurate dielectric permittivity (ε) data. Based on the measurements, clear relationships were found between dielectric constants, G_{mb} and aggregate size. Findings highlight that it is possible to indirectly determine the G_{mb} of asphalts composed of dolomite and limestone aggregates using GPR, with aggregate sizes ranging from 11 mm to 25 mm and G_{mb} values between 2.43 and 2.57 g/cm³. Consequently, a robust function was developed, which can be applied to other asphalts with similar composition.

Keywords: Ground Penetrating Radar (GPR); dielectric permittivity; specific gravity relative density; aggregate size

4.1. Introduction

The dielectric properties of pavement materials are crucial in GPR investigations (Daniels, 2004). The dielectric permittivity (ε) of a substance refers to its ability to store the applied electric field, with the dielectric constant (ε_r) representing the ratio of its permittivity to that of the vacuum (ε_0) (Al-Qadi & Lahouar, 2005). Previous studies, such as those by Loizos & Plati (2007a) and Loizos & Plati (2007b), proposed three calibration methods: core calibration, laboratory ε determination, and reflection amplitude calibration, all suitable for pavement evaluation. This paper distinguishes itself by using horn antennas and the surface reflection method to indirectly determine the specific gravity (G_{mb}) of dolomitic asphalt mixtures, developing a general function applicable to similar asphalt compositions and offering a more streamlined and widely applicable approach than the methods discussed.

The ε of asphalt pavement can be measured using the time-of-flight (TOF) and the surface reflection (SR) method. The TOF method determines permittivity by analyzing the electromagnetic (EM) wave travel time or TOF within the asphalt layer, using in-situ core samples to derive the dielectric constant based on known layer thickness and GPR signal properties. The SR method estimates permittivity by measuring the SR amplitude from the GPR signal and comparing it with a calibration signal amplitude obtained from EM reflection off a metal plate on the pavement surface (Wang et al., 2024).

The main reason for variations in asphalt dielectric constants is related to the composition of the material and its physical properties (Porubiaková & Komačka, 2015; Abdelsamei et al., 2024), such as aggregate type, bulk density, bitumen content, and air void content (Sarabandi et al., 1997; Al-Qadi et al., 2001; Ghosh & Kundu, 2025; Primusz et al., 2024). Among these constituents, the aggregate type has the greatest versatility concerning the ε (Keller, 2017). A wide range of rock types are used as aggregates, though certain types are preferred due to their resistance to fragmentation and polishing. Two widely used rock types are dolomite and limestone (Sėrnas et al., 2016), with a density similar to that of volcanic and crystalline rocks but with a notably different ε (ElShafie & Heggy, 2013; Hartlieb et al., 2016).

Besides aggregate properties, the density of the asphalt mixture is also a key factor in the performance of flexible pavements. Air void content should range between 3% and 8% (Roberts et al., 1996). High air void content leads to moisture damage, binder oxidation, pavement raveling and cracking. Conversely, low air void content increases

stiffness and reduces rutting potential and possible bleeding (Brown, 1990). In dense-graded asphalt mixtures, if the air void content falls below 3%, it can lead to significant permanent deformation and shoving (Roberts et al., 1996; Brown, 1990). Asphalt pavements' G_{mb} and air void ratio are inversely related: as the air void ratio increases, the G_{mb} of asphalt decreases. Thus, the air void ratio is also used to assess asphalt density. Both parameters are largely influenced by the degree of asphalt compaction. Compaction of the asphalt layer minimizes the presence of low-ε air in the asphalt mixture, while the volumetric ratios of high-dielectric asphalt and rock are augmented. Consequently, this process leads to elevated ε values (Saarenketo, 1997; Saarenketo & Roimela, 1998).

Compaction is critical for achieving the desired density of asphalt layers; in other words, the quality of the newly constructed pavement depends mostly on the quality of compaction. In the process of asphalt pavement construction, the paver initially places the asphalt mixture on a bound or unbound base. Subsequently, compactors traverse the loose asphalt mat, eliminating air voids from the mixture. With each pass of the compactor, the air void content decreases. Previous work has demonstrated that inadequate asphalt compaction can result in excessive rutting, cracking, raveling, potholing, and water seepage (Willoughby & Mahoney, 2007).

Therefore, determining the G_{mb} or air void content of asphalt layers, i.e., assessing compaction's properness is important when evaluating pavement quality and durability. The two commonly employed approaches for the evaluation of compaction quality are 1) laboratory assessment of cores and 2) field density gauging, including nuclear and non-nuclear density measurements. Previous studies have suggested that Ground Penetrating Radar (GPR) can also be utilized as a non-nuclear method to assess compaction quality and monitor the compaction process during asphalt pavement construction (Leng et al., 2012; Shangguan et al., 2016). However, in many countries, in-situ nuclear gauge measurements are still used in standard applications (Maser, 1996; Saarenketo & Scullion, 2000; Romero & Kuhnow, 2002; Al-Qadi et al., 2010). The disadvantage of this latter method is that it gives low spatial resolution and at-a-point information on G_{mb}, and the operation of the device needs special knowledge and permissions.

The first aim of the present research was to apply different GPR techniques in the assessment of dielectric constants and to determine the most reliable and convenient way of in situ measurements using validation data obtained from nuclear gauge and laboratory pavement core tests. The extensive measurements during the repeated compaction of the investigated pavement also allowed the establishment of a function between dielectric

constants and G_{mb}. Consequently, by also involving literature data, we attempted to set up a more general model for the GPR assessment of G_{mb} and relative density (RD) on dolomitic pavements.

4.2. Description of Test Sections

The studied sections are located in Szeged, Hungary. Two newly constructed two-lane residential roads, Section I. and Section II., were chosen to conduct the survey (Figure 4.1). The length of Section I. and Section II. are 220 m and 240 m, respectively, while the width of both sections is 6 m.

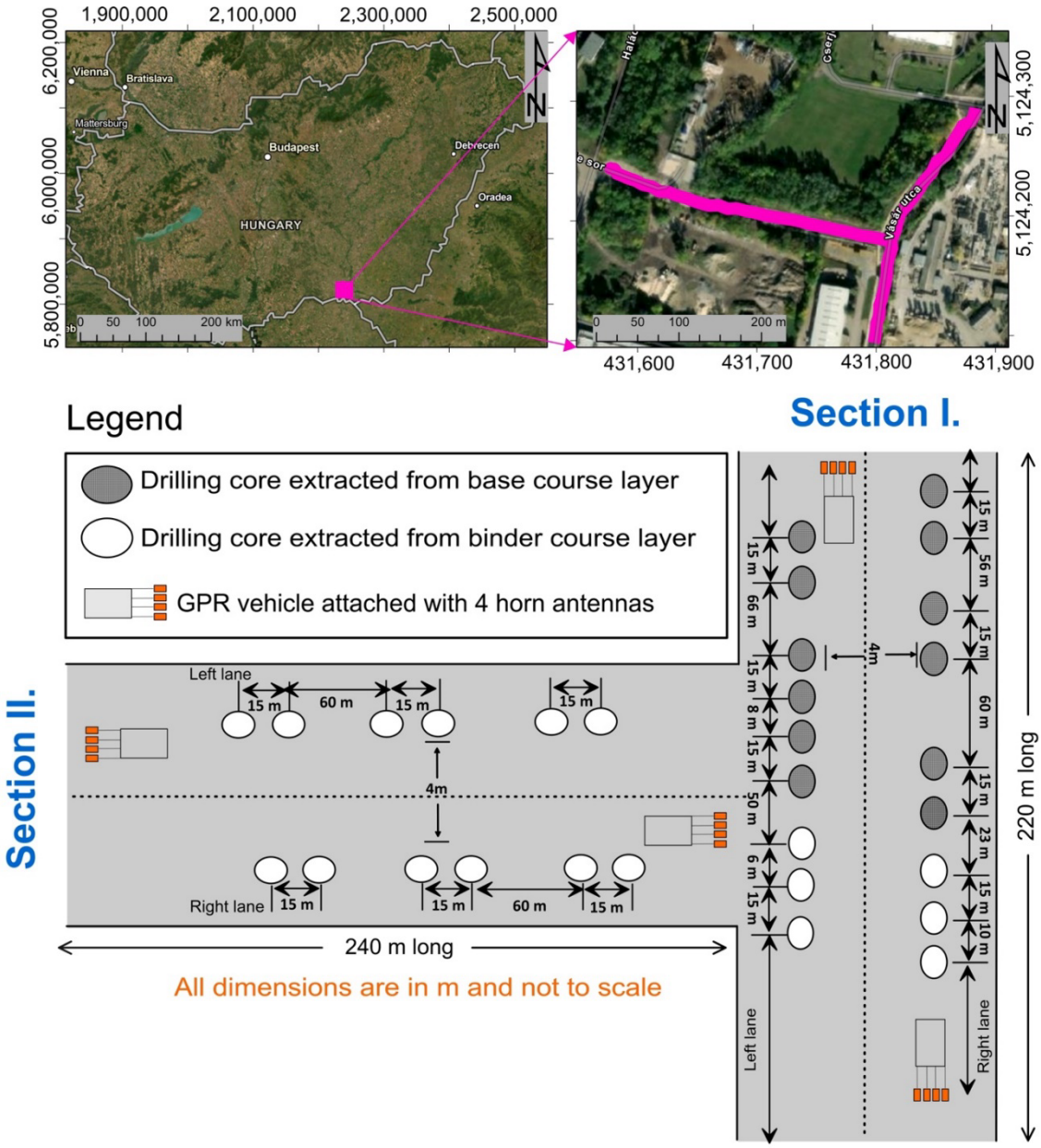

Figure 4.1 Location of the studied residential road sections.

The structure of the pavement structure of the analyzed roads was as follows (Figure 4.2):

1. 4.0 cm AC 11 wearing course.
2. 7.0 cm AC 22 binder course.
3. 8.0 cm AC 22 base course.
4. 20.0 cm FZKA 0/63 unbound granular base (refines upward from 0/63 to 0/32 until 0/22 mm.)
5. 20.0 cm sandy gravel protection layer.

In both asphalt mixes (AC 11 and AC 22), the aggregate rock type was dolomitic limestone, and the proportion of bitumen was 4.1 % by weight. The unbound granular base was also composed of dolomitic limestone (Primusz et al., 2024).

AC 11 and AC 22 are common asphalt mixes (AC) used in road construction, with the numbers indicating the grading of the aggregates AC 11 having smaller aggregates than AC 22. AC 11 is typically used for wearing courses, while AC 22 is used for binder and base courses. These mixes are standard in Europe for durable, high-performance pavements.

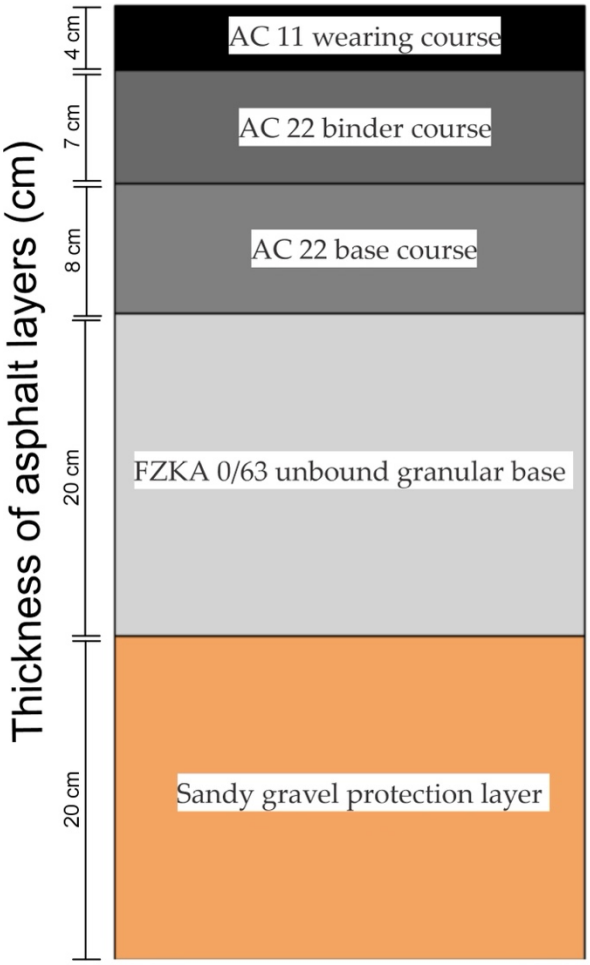

Figure 4.2 Cross-section of the pavement structure with wearing course, binder course, base course, unbound granular base, and sandy gravel protection layer.

4.3. Data and Methods

4.3.1. GPR data acquisition

GPR surveys were carried out by using two 1 GHz and two 2 GHz air-coupled GPR antennas with a SIR-30 control unit from Geophysical Survey Systems, Inc., Nashua, NH, USA (2010) to determine the relative permittivity (Figure 4.3). The horn antennas were suspended at the rear of a vehicle at 0.5 m from the pavement surface (Figure 4.4). The positioning was made using a GPS antenna mounted on the vehicle's roof. Furthermore, a high-resolution Distance Measuring Instrument (DMI) sensor was attached to the rear wheel to ensure the precise triggering of the GPR scans at predetermined intervals. The survey car was driven at a speed of 15 km/h during the survey. At the beginning of the survey, the inline and crossline offsets were manually determined to adjust the GPS location. The GPR signals were collected at a frequency of 50 scans per meter, with a scan rate of 340 scans per second. The units per mark were set

to 5, and the samples per scan were configured to 2048. A one-point gain (flat gain) was used throughout the surveys. The measurement time, or time window, was set to 30 ns for the 1 GHz antenna and 25 ns for the 2 GHz antenna. Full-coverage horn antenna GPR measurements were performed after constructing the sub-base layer, the base course, the binder course, and the wearing course; thus, the measurements were repeated four times.

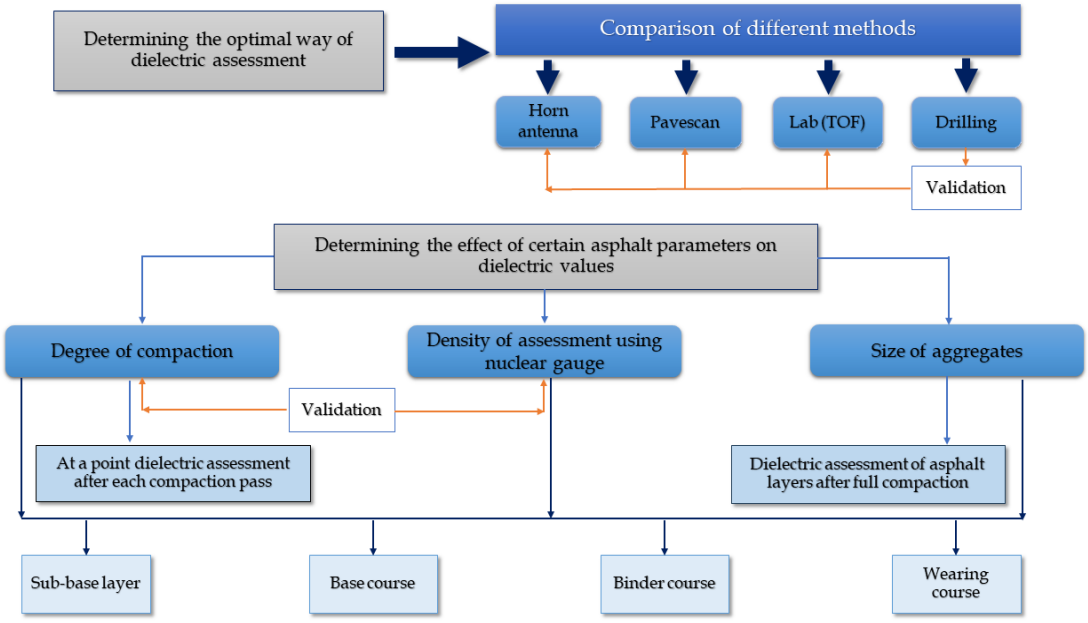

Figure 4.3 Flowchart showing the course of the analysis.

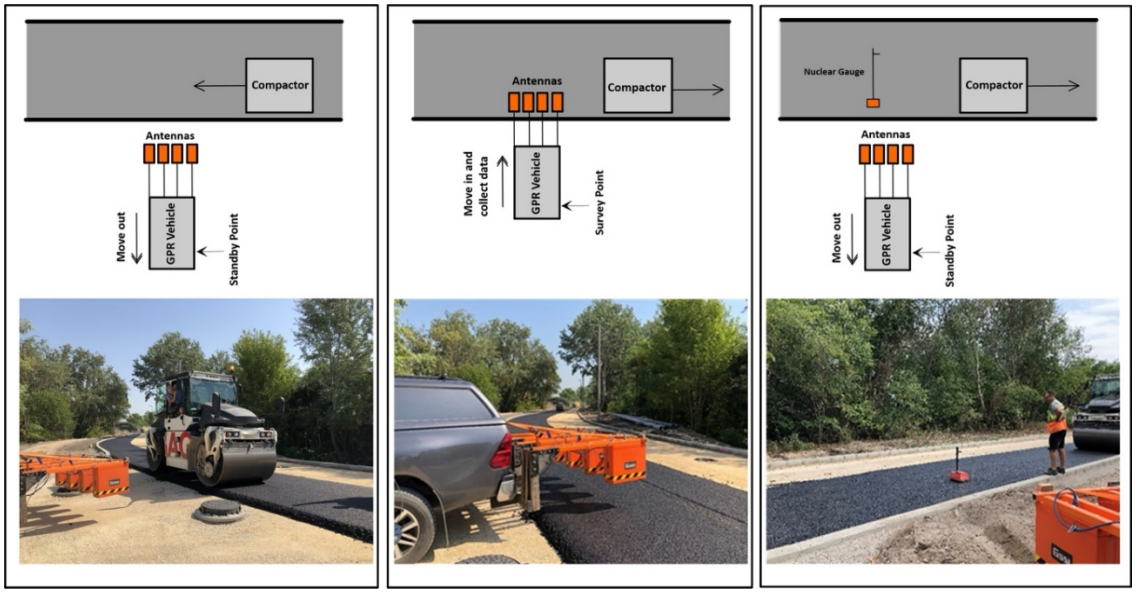

Figure 4.4 The procedure of repeated stationary GPR and nuclear gauge measurements. From left to right: vibratory roller pass, GPR horn antenna measurements, nuclear gauge measurements.

4.3.2. Pavescan data acquisition

Besides horn antennas, a PaveScan RDM 1.0 device from Geophysical Survey Systems, Inc. (2010) mounted with three sensors, was also used to determine the relative permittivity (Figure 4.3). The distance between the sensors was set to 1.2 m to cover the width of the lanes effectively. Before the data collection, the sensors were lifted 0.6 m off the ground to perform air calibration. Next, the metal plate calibration was performed by centering the plate 2.5 cm below the sensor. The distance mode was used during the survey, and the data collection speed was 5 km/h. The PaveScan measurements, covering the entire length of the road sections, were performed once after the construction of each layer.

4.3.3. Calibration and core sampling

Simultaneously with GPR data acquisition, cores were also extracted for calibration (Figure 4.1). In all, 18 cores were extracted from section I. Twelve cores after laying the base course layer and six cores after laying the binder course. In terms of Section II. Twelve cores were extracted after laying the binder course, as shown in Figure 4.1. GPS recorded the position of the cores. Cores were subjected to laboratory measurements using a SIR 3000 GPR system with a 1 GHz ground-coupled antenna. For the measurements, the cores were placed in a plastic box with a metal plate on the bottom, leading to a complete base reflection. The plastic box was then filled with crushed andesite to lessen wave diffraction and ensure the ground-coupled 1 GHz antenna was placed on a flat surface. The ε was calculated using the TOF method.

4.3.4. Compaction and ε relationship measurement

To explore the relationship between the degree of compaction and the change in the dielectric constant, stationary GPR data were collected at the same location at the construction site after each pass of a vibratory roller during the laying of each asphalt layer (Figure 4.4). For the two test sites, seven short GPR profiles were measured after each roller pass and after laying each asphalt layer. The measurements were carried out in time mode. Immediately after the compactor completed one pass, the GPR vehicle moved toward the lane to place the antenna above the pavement. The data collection was made in time mode for approximately 10 s. The GPR vehicle moved back to its original position, as shown in Figure 4.4. Following the GPR measurement, a density reading was taken by a CPN MC-3 PORTAPROBE-type nuclear gauge (InstroTek, 2002). The backscatter mode was chosen for the measurement (*Pavement In*teractive, 2002). The

device was placed on the compacted layer after warming up and determining the GPS position of the measurement point.

4.4 Data Processing

The collected GPR data was processed using GSSI's RADAN 7 software (2010). Raw data was processed to remove noise and to improve the signals. First, metal plate calibration was performed on the data files, and then inline and crossline values were edited manually to make ready GPR data files for further analysis and to determine the true track of measurements, respectively. Then, the program automatically performed reflection picking after manually selecting the reflection picking function to reduce undesired signal noise and improve reflections from the pavement layers. Processing was continued by filtering the data, including 1) a triangular finite impulse response (FIR) filter, applying a weighted moving average procedure emphasizing the filter's centre more than the ends of it, 2) a horizontal filter (stacking), merging neighbouring radar scans and delivering a single scan through a simple running average; 3) vertical filters, i.e. a low pass filter removing high-frequency noise (2 GHz and 4 GHz threshold for the 1 GHz and 2 GHz antennae, respectively) and a high pass filter to remove low-frequency noise (250 MHz and 500 MHz threshold for the 1 GHz and 2 GHz antennae, respectively). Finally, gain properties were set by applying an exponential gain function. The gain was set at 5-7 points. A horizontal background removal filter was applied in certain profiles, particularly those measured along both sections where the data exhibited significant interference or noise from unwanted reflectors—potentially obscuring critical measurements. However, this filter was not required for GPR profiles collected after each roller pass and following the placement of each asphalt layer. In this case, the filter's length must always exceed the length of the data's longest horizontal "real" reflector (GSSI, 2023).

4.5 Assessment of Physical Properties Using GPR Data

Maser, (1996) discussed the principles of using GPR reflections to compute layer properties in detail. By automatically monitoring the amplitudes and time delays between peaks, it is possible to calculate layer ε values using the SR method. The ε_{r1} is calculated by comparing the reflection amplitudes from an asphalt surface and a metal plate surface (100% reflection), as Equation (4.1) indicates.

$$\boldsymbol{\varepsilon_{r1}} = \left[\frac{1+\left(\frac{A_0}{A_p}\right)}{1-\left(\frac{A_0}{A_p}\right)}\right]^2 \qquad (4.1)$$

where ε_{r1} is the ε of the surface course layer, A_0 is the amplitude of the reflection from the surface course layer, and A_p is the amplitude of the reflection from a metal plate.

The ε of the second asphalt layer can be calculated as the following Equation (4.2) using the value ε_r computed in Equation (4.1) (Al-Qadi & Lahouar, 2005; Li et al., 2013):

$$\boldsymbol{\varepsilon_{r2} = \varepsilon_{r1}\left[\frac{1-\left(\frac{A_{0,1}}{A_p}\right)^2+\left(\frac{A_{0,2}}{A_p}\right)}{1-\left(\frac{A_{0,1}}{A_p}\right)^2-\left(\frac{A_{0,2}}{A_p}\right)}\right]^2} \quad (4.2)$$

where ε_{r2} is the ε of the second binder course layer (layer 2). $A_{0,1}$ and $A_{0,2}$ are the amplitudes of the reflection from the second binder course layer (layer 2) and first binder course layer (layer 1), respectively.

Consequently, the ε of any further layers (ε_n) can be calculated using Equation (4.3).

$$\varepsilon_n = \varepsilon_{n-1}\left[\frac{1-\left(\frac{A_{0,1}}{A_p}\right)^2+\sum_{i=1}^{n-2}\gamma_i\frac{A_{0,i+1}}{A_p}+\frac{A_{0n}}{A_p}}{1-\left(\frac{A_0}{A_p}\right)^2+\sum_{i=1}^{n-2}\gamma_i\frac{A_{0,i+1}}{A_p}-\frac{A_{0n}}{A_p}}\right]^2 \quad (4.3)$$

where γ_i is the reflection coefficient at the interface between the two following layers, and n stands for the specific layer and can be calculated using Equation (4.4) (Al-Qadi & Lahouar, 2005).

$$\mathbf{y_i} = \frac{\sqrt{\varepsilon_{r,i}}-\sqrt{\varepsilon_{r,i+1}}}{\sqrt{\varepsilon_{r,i}}+\sqrt{\varepsilon_{r,i+1}}} \quad (4.4)$$

Where $\varepsilon_{r,i}$ is ε of the i^{th} layer. A function was established for the G_{mb} and ε of each asphalt layer using density gauge measurements during the asphalt compaction and simultaneous GPR measurements. This function was applied to map the asphalt G_{mb} on the investigated road section spatially. The quality assessment of road structures is primarily based on the percent of the air void (AV) of the asphalt layers, and this parameter was estimated using Equation (4.5).

$$AV = G_{mm} - G_{mb}/G_{mm} \quad (4.5)$$

Laboratory measurements were made on samples from the AC 11 (wearing course) and the AC 22 (binder and base courses) asphalt mixtures (Primusz et al., 2024). The measured theoretical maximum G_{mb} of the samples was as follows: G_{mm} AC 11 = 2436 kg/m^3, G_{mm} AC 22 = 2572 kg/m^3.

G_{mm} is the theoretical maximum specific gravity measured in the laboratory of the HMA**,** and G_{mb} is the specific gravity, which is estimated in the field using GPR measurements. Finally, the in situ RD of the analyzed layers was calculated using the following formula:

$$RD = 1 - AV = G_{mb}/G_{mm} \quad (4.6)$$

The obtained values for the above parameters were spatially interpolated using kriging and visualized with Surfer v.16.

4.6 Results

4.6.1 Comparability and accuracy of ε measurements

We conducted a comparative study using field and laboratory validation to determine the most efficient measurement approach—specifically, the horn antenna or PaveScan—for further analysis of pavement characteristics. By comparing the results (Table 4.1), we found that the average ε values of the base course, binder course, and wearing course, calculated by the horn antenna and PaveScan for Sections I. and II., yielded similar results.

Table 4.1 Comparison of average ε values for different pavement layers using horn antenna and PaveScan in sections I. and II.

	Section I.		**Section II.**	
Layer	**Horn Antenna**	**PaveScan**	**Horn Antenna**	**PaveScan**
Base Course	5.87	5.86	5.65	5.67
Binder Course	6.1	6.09	5.63	5.76
Wearing Course	4.42	4.73	4.52	4.23

When validating the above results of the base course and binder course layers using cores (the wearing course was not cored), it was found that for Section I, the relative deviation of PaveScan dielectric values from core-derived laboratory data was considerably higher than the relative deviation experienced in the case of GPR horn antenna measurements as shown in Table 4.2, for Section II. It was found that the relative deviation of PaveScan dielectric values from core-derived data was also considerably higher than the relative deviation experienced based on horn antenna measurements, as shown in Table 4.2. It was also noticed that the dielectric constants of the surface course had the lowest values, which were surveyed by either the horn antenna or the PaveScan device, most probably because the smallest grain size characterized this layer compared to the other layers.

Table 4.2 Comparison of relative deviation (%) between PaveScan and horn antenna dielectric values and core-derived laboratory data for base and binder course layers in sections I and II.

		Section I.			**Section II.**		
Layer	**Measurement Method**	**Min Deviation (%)**	**Max Deviation (%)**	**Mean Deviation (%)**	**Min Deviation (%)**	**Max Deviation (%)**	**Mean Deviation (%)**
Base Course	PaveScan	1.03	6.36	4.46	0.14	2.81	1.58
Binder Course		0.42	4.94	2.45	0.39	7.88	3.84
Base Course	Horn Antenna	0.31	2.41	1.4	0.22	1.94	1.05
Binder Course		0.39	3.16	1.88	0.2	7.72	3.34

In general, horn antenna values fell closer to core data. This means that horn antenna measurements can estimate dielectric constants very well, and their accuracy is higher than PaveScan measurements. However, in the case of both devices, the assessment of ε_r was made using the SR method, while the laboratory assessment was made using the TOF method. Still, the results underline the flexible use of horn antenna systems in determining the ε_r of pavement layers (Figure 4.5).

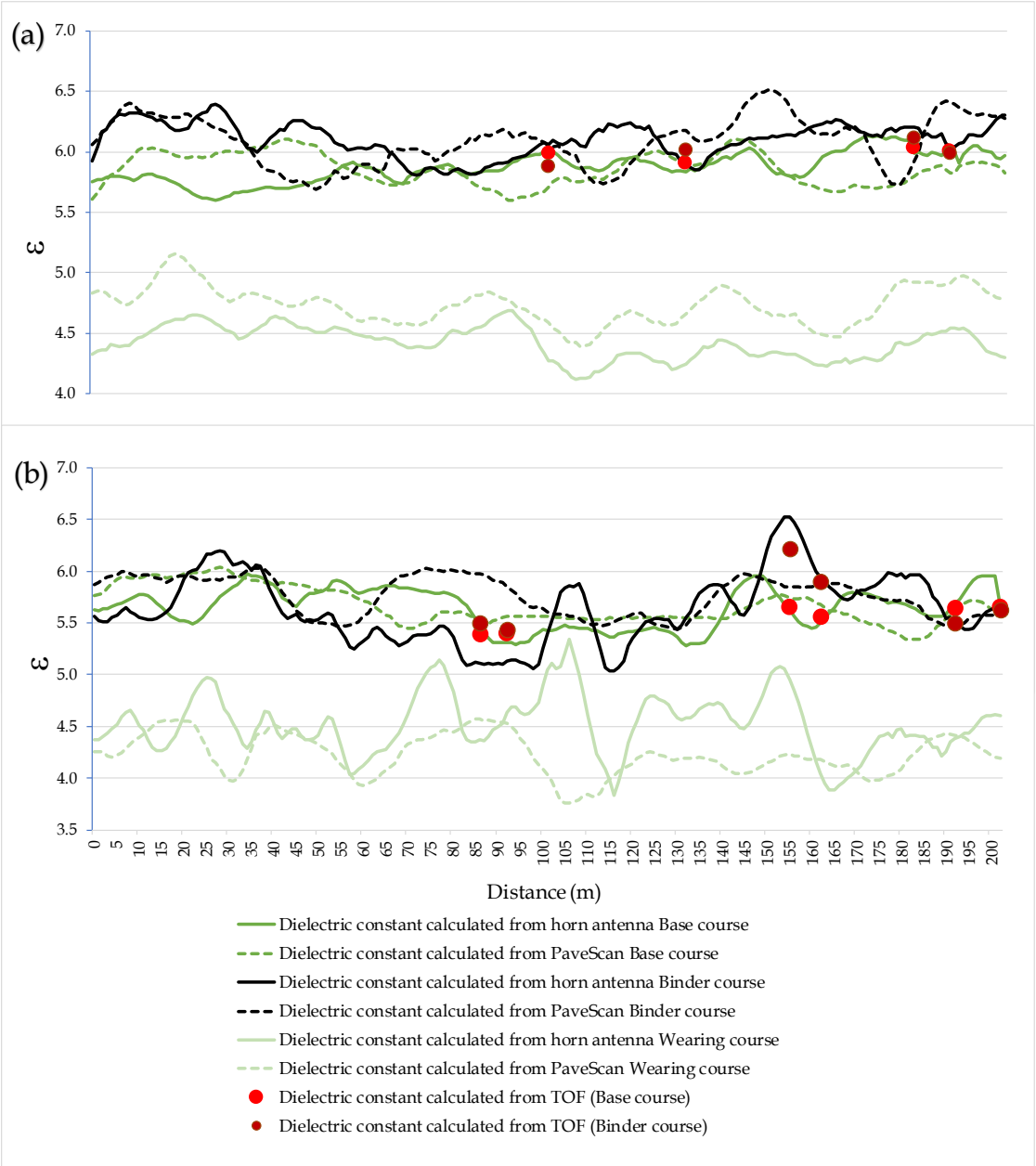

Figure 4.5 Longitudinal profile of ε values measured by the horn antenna and the PaveScan device, a) Section I., b) Section II. Red and maroon dots represent core derived ε values at coring locations.

To assess the accuracy of the horn antenna and PaveScan instruments applied in the field, a detailed comparison was made between laboratory test measurements, performed for each layer separately, and field data obtained by horn antenna and PaveScan measurements after the compaction of each layer (Figure 4.6). All core samples were applied to investigate comparability. Laboratory measurements were made to provide an independent ε value for the comparisons. Initially, we established a relationship between the on-site ε values obtained by horn antenna measurements just before the coring was made using the SR method and the ε values obtained in the lab from

the cores themselves by the ground coupled antenna, using the TOF method, (Figure 4.6a). Results showed a direct proportional relationship with a high coefficient of determination ($R^2 = 0.83$), indicating a strong correlation between the ε values obtained by the two approaches. Subsequently, we plotted the at-a-point results of the PaveScan measurements using the SR method against laboratory data (Figure 4.6b). A very similar coefficient of determination was obtained in this case ($R^2 = 0.82$). However, the regression line in terms of horn antenna results approximates the line of equality much better than the regression obtained using PaveScan measurements, meaning that ε obtained by using the horn antenna exhibits a closer agreement with the laboratory measurements. Based on these findings, we can confidently conclude that the SR horn antenna values can be effectively utilized for the reliable investigation of ε, and the data obtained are reliable for further analyses in this study.

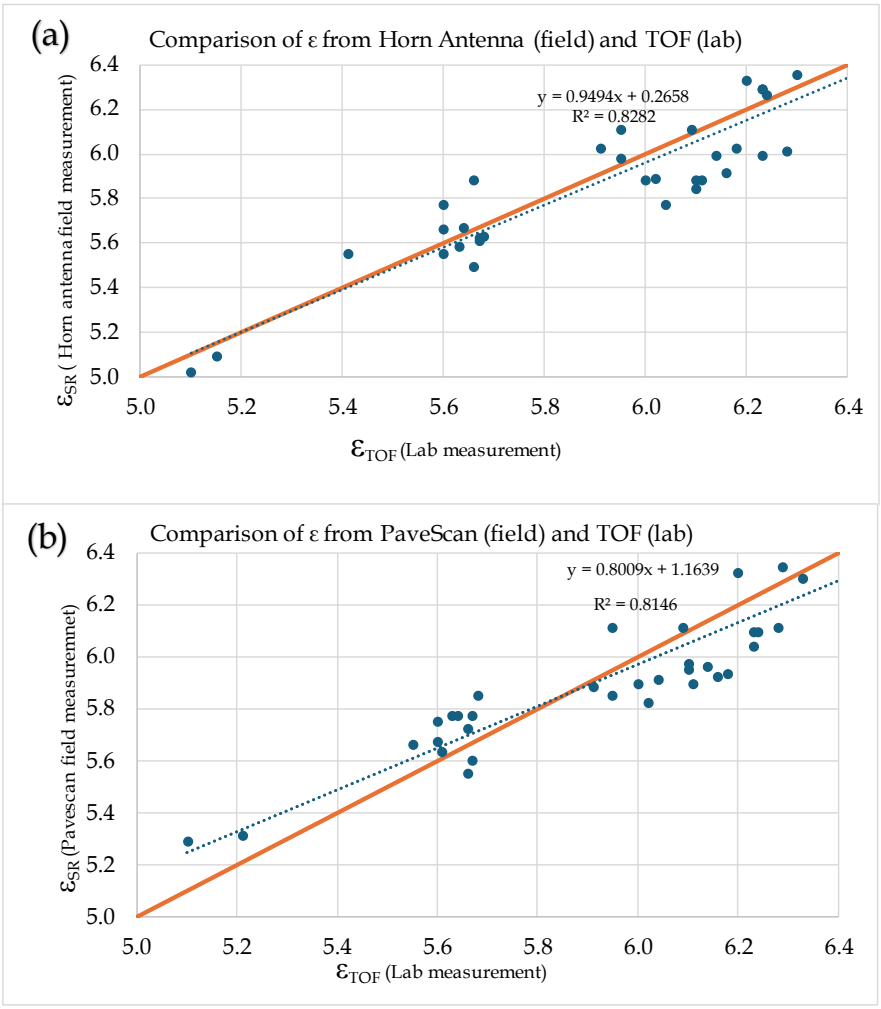

Figure 4.6 Comparison of ε from a) SR from horn antenna (field measurement) and TOF (lab measurement) methods b) SR from PaveScan (field measurement) and TOF (lab measurement) method by using core samples. The line with orange color represents the line of equality.

4.6.2. Effect of G_{mb}, aggregate size and compaction on ε

By understanding how G_{mb} and aggregate size affect dielectric values, a valuable tool can be developed to assess the compaction quality, material homogeneity, and the prediction of the structural performance of the pavement. Nuclear gauge G_{mb} data was plotted against GPR results on ε to set up relationships between the above parameters. (Figure 4.7). G_{mb} was measured on each layer after each compaction pass. In the case of each layer, a clear, direct relationship was found between density and ε, and the coefficient of determination was, in most cases, higher than 0.9. The layers appeared at different parts of the graph, and the slope of the linear functions between the plotted parameters was also different for each. This is because the variation in slope indicates that different asphalt layers have unique dielectric-density relationships, which are influenced by material properties such as aggregate size (d_{max}), compaction level, and asphalt content. Understanding these distinctions is important for accurately interpreting GPR results. The highest G_{mb} and ε values were found in terms of the sub-base course (ρ: 2.60–2.80 g/cm3 and ε: 8.77–10.88), the binder and base course exhibited medium values ((ρ: 2.30–2.54 g/cm3 and ε: 5.13–6.46)) in average, while the wearing course had the lowest values (ρ: 2.11–2.29 g/cm3 and ε: 3.77–4.70). The results show a clear relationship between aggregate size (d_{max}) and dielectric values.

We can read from Figure 4.7 that larger aggregates generally lead to higher G_{mb} because they reduce overall porosity. However, smaller aggregates allow for a more uniform and efficient compaction process, which enhances density but may also retain a higher concentration of air voids if not adequately compacted. The compaction process was efficient in the case of the wearing course, which contained smaller aggregates. Still, it did not fully eliminate air voids, leading to slightly lower G_{mb} than coarser layers. In contrast, the binder course and base course layers, characterized by a moderate aggregate size, contained moderate air voids. Consequently, the binder course and base course showed better compaction during compaction, leading to higher density than the wearing course. The high dielectric values of the sub-base course are primarily due to its larger aggregate size, which influences air void distribution and compaction efficiency. While dolomitic aggregates may have a naturally higher dielectric constant, the dominant factor in this context is the aggregate size, as it directly affects the layer's density and air void content. Six compaction passes reached the maximum density and dielectric values (Table 4.3). We found that the ε for all layers reached a relatively stable value, indicating the achievement of maximum mixture densities. These compaction curves can serve as a

valuable reference for determining the optimal number of compaction passes required to achieve maximum mixture density. Additionally, the point at which the dielectric and density values show negligible changes—observed after six compaction passes—could be a reference for future research studies. Overall, the assessment revealed the relationship between ε and G_{mb}, providing insights into the compaction and characteristics of the different asphalt layers.

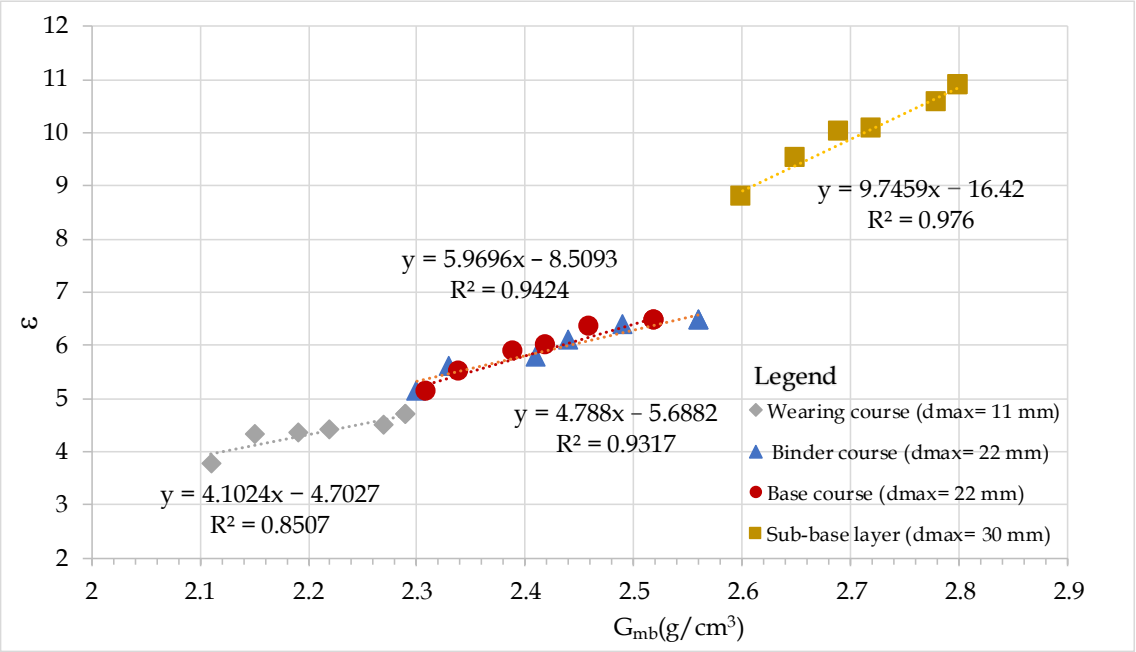

Figure 4.7 The relationship between G_{mb}, measured by the nuclear gauge and ε measured by horn antenna during the compaction process of each layer (1, 2, 3, 4, 5, 6 and 7 corresponds to the number of compaction passes).

Table 4.3 G_{mb} and ε values during the compaction process for each pavement layer.

Number of compaction passes	Sub-base course		Base course		Binder course		Wearing Course	
	G_{mb}	ε	G_{mb}	ε	G_{mb}	ε	G_{mb}	ε
1	2.6	8.77	2.31	5.11	2.3	5.11	2.11	3.77
2	2.65	9.5	2.34	5.49	2.33	5.49	2.15	4.31
3	2.69	9.99	2.39	5.88	2.41	5.88	2.19	4.36
4	2.72	10.05	2.42	5.99	2.44	5.99	2.22	4.41
5	2.78	10.55	2.46	6.33	2.49	6.33	2.27	4.50
6	2.8	10.88	2.52	6.44	2.56	6.44	2.29	4.70
7	2.8	10.88	2.52	6.44	2.56	6.44	2.29	4.70

4.6.3. The RD of Asphalt Layers

Standardised at-a-point nuclear gauge measurements provide only a limited number of data and a low spatial resolution on the potential air void content of asphalt layers. Based on the systematic tests made during the compaction process and the equations determined, detailed maps were generated on the RD of the different asphalt layers to visualise the parameter's spatial homogeneity. RD maps can be important in predicting the pavement's long-term performance, supporting maintenance strategies, and facilitating the detection of different defects.

In general, we found that the RD values show significant differences across the pavement's depth and along the roadway section. Across the depth of the pavement, the lowest RD values were experienced regarding the wearing course (Table 4.3 and Figure 4.8). Based on the relationships in Figure 4.7, this is because the AC 11 mixture can incorporate more air voids, which simultaneously decreases its density and ε compared to the applied AC 22 mixture.

In the case of both sections, the RD of the base course was higher than the RD of the binding course, even though both layers were constructed from the same mixture, and the same number of roller passes were applied during their construction. This suggests that the compaction of the binding and wearing courses led to the additional compaction of the base course, even though the base course cooled down by the time of the construction of the overlying layers. Consequently, the RD of the base course was found to be the highest of the investigated layers. However, in the meantime, the base course had the highest variability, or standard deviation (SD) of RD values (Table 4.3 and Figure 4.8), referring to a less uniform compaction, probably due to the uneven sub-base layer. At the same time, the most uniform compaction was achieved in the case of the binding course.

Besides layer-to-layer differences in RD values, a significant within-layer inhomogeneity was also apparent in the investigated courses (Table 4.3). This is most striking when right and left lanes, compacted separately, are compared to each other (Figure 4.7). The greatest difference in the compaction of separate lanes can be seen in terms of the wearing course, e.g. at section II. a 3.6% difference was identified between the average RD of the two lanes (Figure 4.8b). In the meantime, density variation can also be significant along the same lane as well (Figure 4.8a and b), suggesting that the temperature of the asphalt mixture was changing during the construction process. Based

on the results, additional roller passes should have been made during the construction of the wearing course, especially on the left lane at Section II. (Figure 4.8b). Although the general condition of the investigated section is good, the identified spatial differences in compaction quality call for continuous monitoring of the road structure.

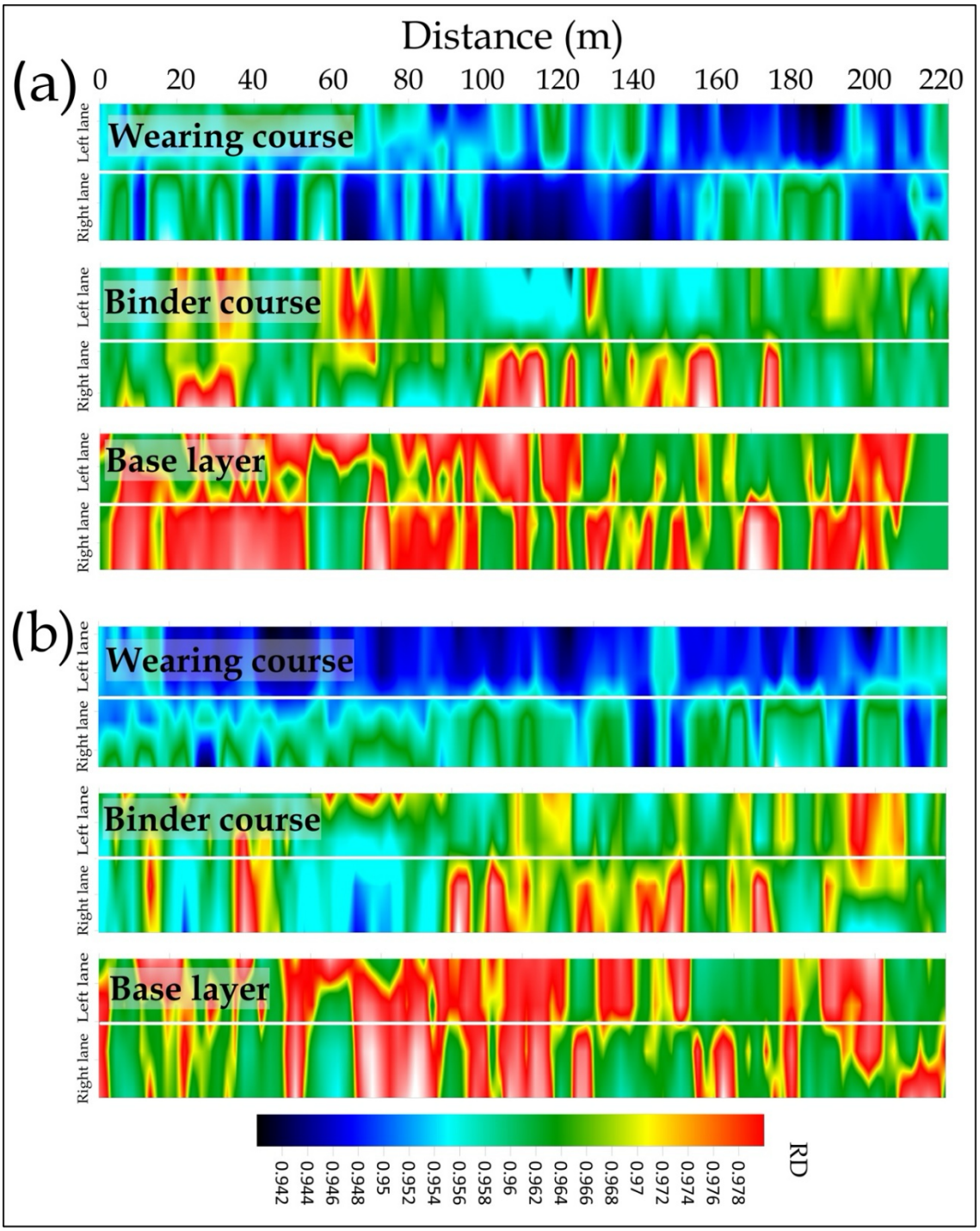

Figure 4.8 Horizontal variation of RD in terms of the investigated layers: a) Section I. b) Section II.

4.7. Discussion

The assessment of pavement conditions is essential for efficient transportation infrastructure management. GPR technology provides different alternatives to assess the dielectric properties of asphalt layers. However, these alternatives may yield significantly different results. Porubiaková and Komačka (2015) found differences between SR and TOF methods. The present study found that the SR method fits laboratory results better. On the other hand, Wang et al. (2024) found that a certain type of TOF method can provide equally good results. However, the common-mid point (CMP) allows for a real-time TOF-accurate estimation method, which involves more complex data acquisition and processing than simpler GPR survey techniques. It requires careful planning and execution and sophisticated processing software, which can increase the overall cost and time needed for the survey. Thus, SR was the simpler method that produced reliable measurements.

The study of the relationship between ε and G_{mb} revealed a strong linear correlation regarding the wearing course, with a coefficient of determination (R^2) of 0.85. Similar findings were reported by several other authors, such as Chang et al. (2011) and Popik et al. (2010), using the same antenna frequency (2 GHz), and also by Xiong et al. (2021). However, they did not indicate the frequency of the applied antenna. These authors found R^2 values of 0.73, 0.71 and 0.81 respectively. However, the slope of their functions is different from those in the present study (Figure 4.9). The differences in slope can be attributed to several factors, including aggregate composition and gradation, asphalt binder content, air voids, and compaction efficiency as discussed by Chang et al. (2011) in detail. Although G_{mb} was measured using different methods (density prediction model, non-nuclear density gauge, and nuclear density gauge), the obtained values were within a range of ±0.05 g/cm³, showing high consistency across the studies.

When plotting the data of the above studies in Figure 4.9. It is clear that even though the investigated HMA mixtures have different characteristics (Table 4.4), most of the data plot to the same region (Figure 4.9) and provide the means of determining a more general function between ε and G_{mb} (Figure 4.10). We found that in the case of our study (Wearing course, Binder course, Base course) and the survey made by Xiong et al. (2021) (AC 13, AC 20, AC 25) the data are located in the same range. However, in the present study, in the case of sub-base layers, we found that the data falls outside the expected range of dielectric values (ε) due to the larger aggregate size (d_{max} = 30 mm). Additionally, asphalt content plays a significant role in these deviations, as higher asphalt

content generally results in lower dielectric values due to reduced volumetric proportions of mineral filler and aggregate.

Table 4.4 Mean, minimum, and maximum values and range and standard deviation of RD for investigated asphalt layers.

	Course Type	Mean RD	Min RD	Max RD	Range RD	SD
Section I.	Wearing course	0.949	0.944	0.956	0.012	0.033
	Binder course	0.964	0.960	0.971	0.011	0.022
	Base course	0.976	0.972	0.978	0.006	0.041
Section II.	Wearing course	0.944	0.942	0.954	0.012	0.037
	Binder course	0.963	0.962	0.974	0.012	0.029
	Base course	0.974	0.971	0.977	0.006	0.043

The impact of asphalt binder content on dielectric values is particularly important in interpreting the results shown in Figure 4.8. Asphalt content influences the density and compaction of asphalt mixtures, thereby affecting the dielectric response. As seen in other studies (Chang et al. 2011; Popik et al. 2010), an increase in asphalt binder content tends to decrease the overall dielectric constant due to the lower permittivity of the binder compared to the mineral aggregate. This relationship must be considered when comparing different datasets and developing generalized functions for dielectric estimation. Therefore, variations in asphalt binder content should be explicitly analyzed alongside other influencing factors such as air voids, compaction efficiency, and aggregate gradation.

Finally, for asphalt pavements with aggregate sizes ranging from 11 mm to 25 mm, composed of limestone-dolomite and within the same percentage of asphalt binder content as detailed in (Table 4.5), we propose a generalized function between ε and G_{mb} for these specific conditions (Figure 4.10). The influence of asphalt content on these correlations further highlights the necessity of considering binder properties in future analyses.

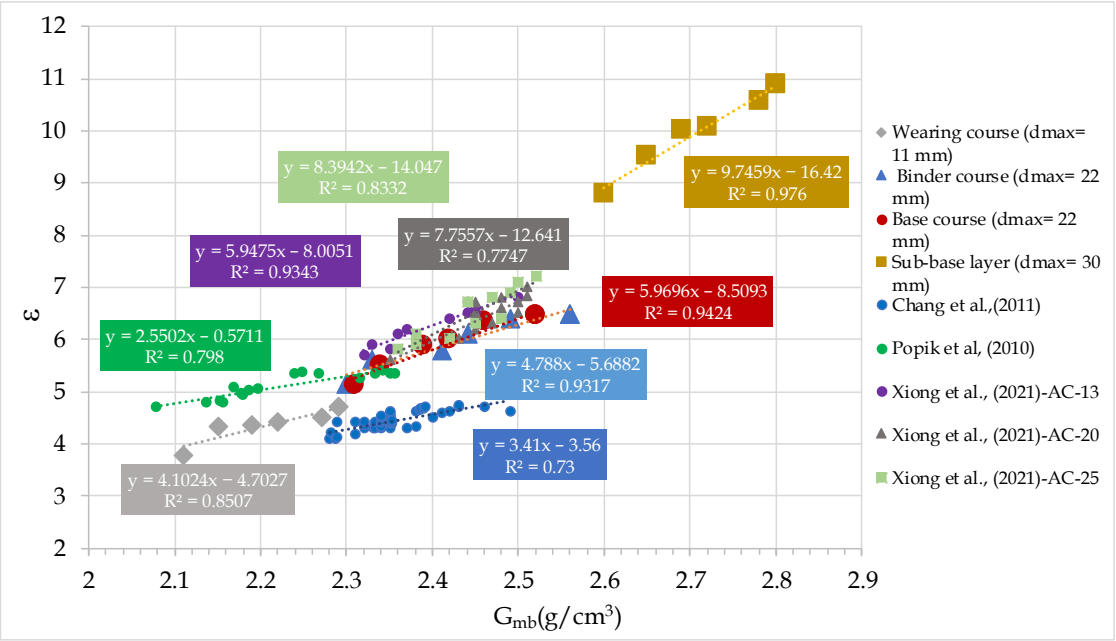

Figure 4.9 Comparison of the relationship between ε and G_{mb} resulted from this study and other authors' studies.

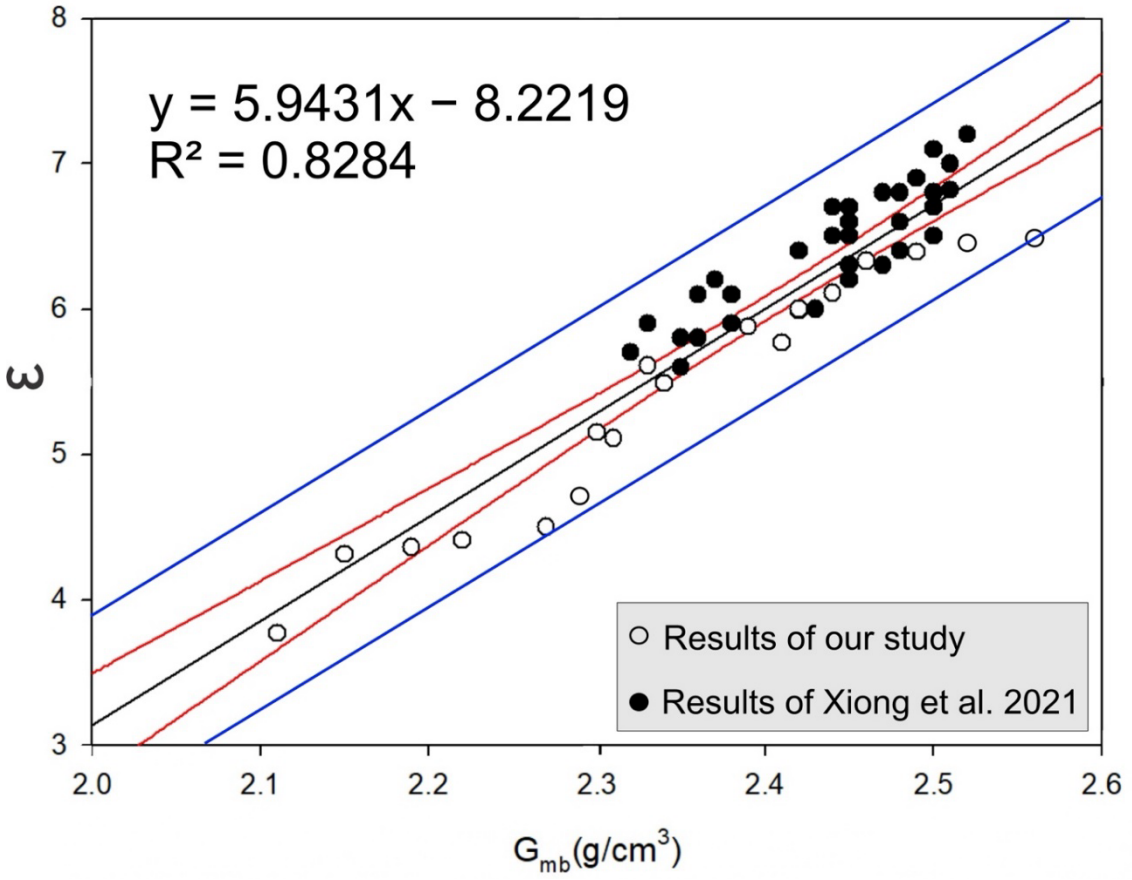

Figure 4.10 Plot of the function between ε and G_{mb} derived from our study and Xiong et al. (2021)

Table 4.5 Mineral composition, aggregate size, asphalt Binder, mean ε, G_{mb} and other information regarding the studies the results of which are plotted on Figure 4.9.

	This study	**Popik et al. (2010)**	**Xiong et al. (2021)**	**Chang et al. (2011)**
Mineral composition	Dolomitic limestone	Granite	Limestone	Sandstone
Aggregate size	AC 11, AC 22	AC 13-19 mm	AC 13, AC 20, AC 25	AC 20
Asphalt Binder	4.1%	5.1%	4.5%, 4.1%, 3.8%	4%, 5%, 6%
Mean ε	2.36	2.23	2.44	2.35
G_{mb}	5.45	5.11	6.43	4.44
Other	Binder RD: 1.050 g/cm^3	35% Recycled Asphalt Pavement (RAP)	8 % Air voids, 0.44 % Moisture content	2-10 % Air voids

Based on our study, reflection amplitudes become relatively constant after six compaction passes. This finding was reinforced by Leng et al. (2012), indicating that the maximum mixture densities can be achieved when the number of compactions passes reaches six. Another study by Zhao et al. (2021) revealed that the rolling resistance and energy utilization coefficient values were less than 0 when the numbers of roller passes were 7, 9, and 10 since the value of compaction energy density was at a very low level when the number of roller passes exceeded 6.

Despite the observed variations, the RD of asphalt layers in the investigated road section ranged between 0.94 and 0.98, which is considered close to the optimum value. These results are consistent with those reported by Popik et al. (2010), who found that over 80% of the surveyed area exhibited RD values between 0.90 and 0.95. Another study by Zhao et al. (2021) found that the degree of compaction ranged between 0.93 and 0.99; when they used different rollers, they found the compaction effect for the same number of roller passes was different. Beainy et al. (2012) found that about 99 % of three other sites were compacted between a density of 0.93 and 0.96 by using the intelligent asphalt compaction analyzer (IACA); they also found that less than 1% of the completed pavement was under compacted.

Finally, Commuri et al. (2011) found that the RD values ranged between 0.91 and 0.93 when using a nonnuclear density gauge. All the above results reiterate that most of the construction was of high quality.

Our results showed that the ε and RD values of the binder course were higher than those of the wearing course. This suggests that, beyond the influence of D_{max} and other factors, the wearing course exerted pressure on the binder course. Loizos and Plati (2007a) also found that the dielectric properties of the wearing course can influence the estimated values of the binder course. This can be explained by several factors: the weight of asphalt layers increases compression in underlying layers, raising their density and affecting dielectric properties. Temperature differences between layers may also influence ε, as shown by Kassem et al. (2012), who found that lower compaction temperatures increased air voids in both HMA and WMA. Additionally, material composition variations and possible chemical or physical interactions between layers could contribute to changes in dielectric properties.

4.8. Conclusion

In the comparative analysis of dielectric values derived from pavescan and horn antenna measurements, the dielectric values measured by the horn antenna were more closely aligned with the core data. This suggests that the horn antenna measurements are highly effective in estimating ε, demonstrating superior accuracy compared to pavescan measurements. Based on lab findings, we concluded that the SR derived from the horn antenna method can be effectively utilized for reliable pavement investigations.

Asphalt density assessment can be spatially extended by calibrating GPR dielectric data using nuclear gauge measurements, and atomic measurements can be substituted. This is especially true regarding larger projects, where the same or similar AC mix is used on longer road sections. We concluded that the ε depended on the density of the asphalt mixture—higher density reduced air voids, leading to an increased dielectric constant. Additionally, we proposed a generalized function to describe the relationship between ε and bulk G_{mb} under specified conditions, such as asphalt pavements with aggregate sizes ranging from 11 mm to 25 mm and composed of dolomite or limestone.

Therefore, we concluded that the asphalt content influenced the dielectric constant, as the density of Hot Mix Asphalt (HMA) was influenced by the components of air, mineral filler, aggregate, and asphalt binder. The compaction curve helps determine the required number of compaction passes to achieve the maximum asphalt mixture density, and the GPR measurement corresponding to the maximum density can be used as a reference to examine the density levels at other locations.

The presented RD maps demonstrated that the relative compactness of in situ asphalt materials is not uniform. Variations in density within the same layer suggest variations in compaction efficiency during construction. Specifically, Section II's left lane exhibited lower compaction quality, indicating that additional roller passes should have been made during the construction of the wearing course. Although the general condition of the investigated section is good, the identified spatial differences in compaction quality, particularly in Section II., justify continuous monitoring of the road structure. This need for monitoring is further supported by observed density variations beyond an acceptable threshold, which could impact long-term performance. Incorporating literature on pavement monitoring decision-making could further strengthen this justification.

We concluded that a method for density assessment was developed using GPR by surveying asphalt at different degrees of compaction. This way, more accurate RD maps were generated to visualize the spatial homogeneity of density. The survey findings highlight that it is possible to indirectly determine the G_{mb} of asphalts composed of dolomite and limestone aggregates using horn antenna GPR measurements calibrated with nuclear gauge data, as these methods demonstrated superior accuracy and reliability in estimating ε and assessing asphalt density. Also, RD maps generated in this study are important in predicting the long-term performance of the pavement, supporting maintenance strategy and facilitating the detection of different defects.

5. Overall Conclusions

The studies demonstrate that GPR is a highly effective tool for assessing various aspects of infrastructure and road quality. In the context of levee assessment, GPR combined with ERT proved valuable for evaluating levee integrity and seepage dynamics. These methods successfully delineated seepage pathways and identified subsurface features, offering a reliable approach for flood risk assessment in Hungary and similar flood-prone areas worldwide.

For road assessment, GPR showed exceptional capability in accurately measuring pavement thickness, detecting dielectric properties, and resolving complex road structures. The minimal measurement errors, high reproducibility, and sensitivity to moisture underscore GPR's reliability for road quality assessments. GPR proved particularly useful for evaluating aged roads with complex structures. The findings demonstrate that reasonably accurate assessments of pavement thickness, structure, dielectric values, and amplitude of aged roads can be achieved using GPR surveys under various conditions. The study also highlighted the importance of considering environmental conditions, as moisture content significantly impacted GPR measurements.

For newly constructed pavements, GPR was shown to be an effective method for assessing compaction quality. The research demonstrated that it is possible to indirectly determine the specific gravity of asphalts composed of dolomite and limestone aggregates using GPR. This allows for the generation of relative density maps to visualize the spatial homogeneity of asphalt density, which is important for predicting long-term pavement performance and supporting maintenance strategies.

Overall, these studies highlight the versatility and effectiveness of GPR as a non-destructive testing method for various infrastructure applications. The findings can serve as a reference for future investigations of roads and other structures with complex compositions.

5.1 Summary of key findings

By addressing the research hypotheses to achieve the research objective, my study has achieved the following key findings:

Study 1. The study successfully demonstrated the effectiveness of combining Electrical Resistivity Tomography (ERT) and Ground Penetrating Radar (GPR) for assessing levee integrity. Three-dimensional (3D) ERT profiles successfully delineated seepage pathways as the tank filled, while 3D GPR profiles indicated areas of increased amplitude,

corresponding to seepage zones and the water table. Validation through drilling confirmed the geophysical findings, underscoring the accuracy of ERT and GPR in non-destructively identifying subsurface features and seepage channels. The results highlight the applicability of these methods for evaluating levee integrity and seepage dynamics, offering a reliable approach for flood risk assessment in Hungary and similar flood-prone areas worldwide.

Study 2. The research revealed that GPR measurements showed high accuracy and reproducibility for assessing road thickness and structure in aged pavements with complex multilayer compositions. The average error of thickness on the same day between continuous GPR and the core data were 2.87% using the ground truth correction method and 8.72% using the amplitude method respectively. Environmental conditions significantly affected GPR measurements of pavement properties, with dielectric values varying under different moisture conditions. For example, the average dielectric values of surface asphalt layer were 4.00, 7.06, and 8.31 under dry, medium-wet, and wet conditions, respectively. The study also found clear relationships between GPR-derived dielectric constants and road composition factors, with the dielectric constant depending on the density of the asphalt mixture.

Study 3. The research demonstrated that it is possible to indirectly determine the specific gravity of asphalts composed of dolomite and limestone aggregates using GPR. Applying horn antennas and the surface reflection (SR) method proved to be the most feasible way to obtain reliable and accurate dielectric constant data. Clear relationships were established between dielectric constants, specific gravity, and aggregate size. The study showed that higher density resulted in reduced air voids, leading to an increased dielectric constant. A robust function was developed, which can be applied to other asphalts with similar composition. The research also demonstrated that by calibrating GPR dielectric data using nuclear gauge measurements, asphalt density assessment can be spatially extended, and nuclear measurements can be substituted. This approach is particularly valuable for larger projects where the same or similar asphalt concrete mix is used on longer road sections.

5.2 Cross-cutting Findings:

Across all three studies, GPR proved to be a versatile and effective non-destructive testing method for infrastructure assessment. The research highlighted the importance of considering environmental conditions, particularly moisture content, in

GPR measurements. The studies also demonstrated the value of integrating GPR with other assessment methods, such as ERT for levee assessment and nuclear gauge measurements for asphalt compaction quality assessment. The generation of spatial maps (e.g., seepage pathway maps for levees and relative density maps for asphalt pavements) from GPR data provided comprehensive visualizations of infrastructure conditions, offering valuable tools for assessment and maintenance planning.

5.3 Implications

The successful application of GPR and ERT in assessing levee integrity has significant implications for flood risk management. These non-destructive techniques offer a reliable approach for evaluating levee conditions, potentially reducing the risk of unexpected failures. The ability to delineate seepage pathways and identify subsurface features without invasive methods allows for more frequent and comprehensive assessments, enhancing overall flood protection strategies. The integration of these geophysical methods with traditional geotechnical approaches provides a more holistic understanding of levee structures. This comprehensive assessment can lead to more targeted and cost-effective maintenance and reinforcement strategies, ultimately improving the longevity and reliability of flood protection infrastructure.

The application of GPR to aged road assessment has important implications for infrastructure management and maintenance planning. The ability to accurately measure pavement thickness and structure in complex, multilayered aged pavements allows for more precise evaluation of road conditions. This can lead to better-informed decisions regarding rehabilitation and reconstruction efforts, potentially extending the service life of existing road infrastructure. The demonstrated sensitivity of GPR measurements to environmental conditions, particularly moisture, highlights the importance of considering temporal variations in pavement assessment. This understanding can lead to more nuanced maintenance schedules and improved accuracy in long-term performance predictions for road infrastructure.

The development of GPR-based methods for assessing asphalt compaction quality has significant implications for pavement construction and quality control processes. The ability to indirectly determine the specific gravity of asphalt mixtures using GPR offers a non-destructive alternative to traditional core sampling and nuclear density gauge measurements. This can lead to more comprehensive and efficient quality assessments during and after construction, potentially improving overall pavement quality and

longevity. The generation of relative density maps using GPR data provides a powerful tool for visualizing spatial variations in compaction quality. This capability has implications for identifying areas of potential weakness in newly constructed pavements, allowing for targeted remediation efforts and improved overall pavement performance.

5.4. Cross-cutting Implications:

Across all three applications, the use of GPR demonstrates the potential for more frequent, comprehensive, and non-destructive assessments of critical infrastructure. This shift towards non-invasive evaluation techniques could lead to more proactive maintenance strategies, reducing the likelihood of unexpected failures and extending the service life of infrastructure assets.

The improved spatial resolution and coverage offered by GPR techniques, compared to traditional point-measurement methods, allows for a more complete understanding of infrastructure conditions. This comprehensive view can inform more effective resource allocation for maintenance and rehabilitation efforts, potentially leading to significant cost savings in long-term infrastructure management.

Furthermore, the development of these advanced GPR applications contributes to the broader field of smart infrastructure management. By providing detailed, quantitative data on infrastructure conditions, these techniques support data-driven decision-making processes in infrastructure planning and maintenance. This aligns with the growing trend towards digitalization and intelligent management of civil infrastructure systems, potentially leading to more resilient and sustainable infrastructure networks.

5.5. Limitations, Recommendations and Future Research

GPR has shown limited capability to investigate the depth of levee structures due to their high clay content. ERT, while providing greater penetration depth, has the disadvantage of lower spatial resolution. The "3D effect" in ERT, where resistivity variations outside the survey plane impact readings along the ERT line, can lead to interpretation challenges, especially in complex environments like river embankments.

Another limitation the accuracy of GPR measurements may decrease with the age of the pavement, as noted in some studies. Environmental conditions, particularly moisture content, significantly affect GPR measurements of pavement properties, which can lead to variations in results under different weather conditions.

Lastly, the study was limited to dolomitic and limestone asphalt mixtures, and the applicability of the developed methods to other aggregate types may require further

validation. The relationship between dielectric constants and specific gravity may vary with different asphalt compositions and environmental conditions.

For recommendation to integrate multiple geophysical methods, such as GPR and ERT, along with geotechnical measurements for a comprehensive understanding of levee conditions. Careful consideration should be given to the placement of ERT profiles to minimize 3D effects.

Additionally, when assessing aged roads, it is advisable to conduct GPR surveys under various environmental conditions to account for the impact of moisture on measurements. The use of multiple GPR frequencies can provide a balance between resolution and penetration depth.

For large-scale projects, it is recommended to calibrate GPR dielectric data using nuclear gauge measurements to extend asphalt density assessment spatially. The generation of relative density (RD) maps is advised to visualize the spatial homogeneity of asphalt density and identify areas of potential compaction issues.

For future research, it is needed to develop advanced 3D inversion techniques for ERT to better handle complex levee geometries. Research into the integration of GPR and ERT data with machine learning algorithms could enhance the detection and characterization of seepage pathways.

Another important area for future research should focus on developing robust algorithms for automatically detecting and characterizing defects in aged pavements using GPR data. Studies exploring the long-term changes in GPR signatures of pavements could provide insights into the aging process and help in predictive maintenance.

Additionally, Future work should extend the study to a wider range of asphalt mixtures and aggregate types to develop a more comprehensive model for specific gravity estimation using GPR. Research into real-time GPR assessment during the compaction process could lead to improved quality control in pavement construction.

Across all applications, there is a need for standardization of GPR data collection and processing methods to ensure consistency and comparability of results across different studies and locations. Additionally, the development of user-friendly software tools for GPR data interpretation could facilitate wider adoption of these techniques in infrastructure assessment and management.

Acknowledgements

I am profoundly grateful to my supervisor, Dr. Gyorgy Sipos, for his exceptional guidance, steadfast support, and unwavering inspiration throughout my PhD journey. His mentorship over the past four years has been invaluable, and this research would not have been possible without his extensive assistance and encouragement.

I would also like to express my sincere gratitude to the Hungarian government for providing financial support through the Stipendium Hungaricum scholarship. This opportunity significantly enriched my experience of studying and living in Hungary. My heartfelt thanks go to my fellow students for their encouragement and camaraderie throughout my academic career. Special acknowledgment is due to the Department of Physical and Environmental Geography at the University of Szeged for creating an outstanding research environment. I am equally thankful to the faculty, administrators, and doctoral candidates from diverse backgrounds for their kindness and support.

I am deeply appreciative of all individuals and organizations who contributed to the success of this research. I extend my sincere thanks to the Hungarian National Research, Development, and Innovation Office for funding the TKP2021-NVA-16 project, which played a pivotal role in enabling this study.

Special gratitude is owed to the Digital Water Management System (DWMS) for providing critical meteorological data that greatly enriched the analysis. I am also thankful to the local authorities and road management agencies in Szeged and Gyöngyös, Hungary, for granting access to the study sites and sharing valuable information about the road structures.

I acknowledge the invaluable assistance of laboratory staff at our institutions for their expertise in core sample analysis and geotechnical testing. I am grateful for the collaborative efforts of all team members involved in field surveys, data processing, and interpretation, which were essential to the success of this research.

Additionally, I extend my heartfelt thanks to the anonymous reviewers whose insightful comments and constructive feedback significantly enhanced the quality of the research papers.

I am deeply grateful to my husband, Dr. Diaa Sheishah, for his unwavering support, patience, and encouragement throughout my PhD journey. His steadfast belief in me, coupled with his constant motivation and understanding, has been a source of strength during the most challenging moments. I also wish to express my heartfelt appreciation to my beloved parents, whose unconditional love, guidance, and sacrifices

have shaped my path, as well as to my family and close friends for their unwavering support, understanding, and encouragement, especially during the challenging COVID-19 pandemic. Their presence has been a constant source of strength, helping me overcome difficulties and reach this milestone. Although I may not always express these sentiments, I deeply cherish and value each of them.

References

Abdelsamei, E., Sheishah, D., Runa, B., Balogh, O., Tóth, C., Primusz, P., ... & Sipos, G. (2024). Application of Ground Penetrating Radar in the Assessment of Aged Roads: Focus On Complex Structures Under Different Weather Conditions. *Pure and Applied Geophysics*, 1-19. https://doi.org/ 10.1007/s00024-024-03604-y

Abu-Hassanein Z. S., C. H. Benson, and L. R. Blotz, 1996. "Electrical resistivity of compacted clays," Journal of Geotechnical Engineering - ASCE, vol. 122, pp. 397-406. https://doi.org/10.1061/(ASCE)0733-9410(1996)122:5(397)

Alakukku, L., 1996. Persistence of soil compaction due to high axle load traffic. I. Short-term effects on the properties of clay and organic soils. European Journal of Soil Science, 37, 211–222. https://doi.org/10.1016/0167-1987(96)01017-3

Al-Qadi, I. L., & Lahouar, S. (2005). Measuring layer thicknesses with GPR–Theory to practice. Construction and building materials, 19(10), 763-772. https://doi.org/10.1016/j.conbuildmat.2005.06.005

Al-Qadi, I. L., Lahouar, S., Jiang, K., McGhee, K. K., & Mokarem, D. (2005). Accuracy of ground-penetrating radar for estimating rigid and flexible pavement layer thicknesses. *Transportation research record*, 1940(1), 69-78. https://doi.org/10.1177/036119810519400010

Al-Qadi, I. L., Lahouar, S., & Loulizi, A. (2001). In situ measurements of hot-mix asphalt dielectric properties. *NDT & e International*, *34*(6), 427434.https://doi.org/10.1016/S09638695(01)00010-X

Al-Qadi, I.L., Lahouar, S. & Loulizi, A., (2002). Ground Penetrating Radar Evaluation for Flexible Pavement Thickness Estimation. In *Proceedings*

Al-Qadi, I. L., Lahouar, S., & Loulizi, A. (2003). Successful application of ground-penetrating radar for quality assurance-quality control of new pavements. *Transportation research record, 1861(1)*, 86-97. https://doi.org/10.3141/1861-10

Al-Qadi, I. L., Leng, Z., Lahouar, S., & Baek, J. (2010). In-place hot-mix asphalt density estimation using ground-penetrating radar. *Transportation research record*, *2152(1)*, 19-27.https://doi.org/10.3141/2152-03

Ameri, M., Kashani Novin, M., & Yousefi, B. (2014). Comparison of the field measurements of asphalt concrete densities obtained by ground-penetrating radar, pavement quality indicator and the borehole coring methods. *Road Materials and Pavement Design, 15(4)*, 759-773.

Antoine, R., Fauchard, C., Fargier, Y., & Durand, E. (2015). Detection of leakage areas in an earth embankment from GPR measurements and permeability logging. *International Journal of Geophysics,* 2015. https://doi.org/10.1155/2015/610172.

Ball, J., Chambers, J., Wilkinson, P., & Binley, A. (2023). Resistivity imaging of river embankments: 3D effects due to varying water levels in tidal rivers. *Near Surface Geophysics*, *21*(1), 93-110. https://doi.org/10.1002/nsg.12234

Barnes, C. L., & Trottier, J. F. (2002). Phenomena and conditions in bridge decks that confound ground-penetrating radar data analysis. Transportation research record, 1795(1), 57. https://doi.org/10.3141/1795-0

Beainy, F., Commuri, S., & Zaman, M. (2012). Quality assurance of hot mix asphalt pavements using the intelligent asphalt compaction analyzer. *Journal of Construction Engineering and Management*, *138*(2), 178-187. https://doi.org/10.1061/(ASCE)CO.1943-7862.0000420

Beck, Y.L., Lopes, S. P., Ferber, V., and Côte, P., (2011). Microstructural Interpretation of Water Content and Dry Density Influence on the DC-Electrical Resistivity of a Fine-Grained Soil. *Geotechnical Testing Journal, 34(6)*:694–707. https://doi.org/10.1520/GTJ103763

Bezina, Š., Stančerić, I., Domitrović, J., & Rukavina, T. (2021). Spatial Representation of GPR Data—Accuracy of Asphalt Layers Thickness Mapping. *Remote Sensing, 13(5),* 864. https://doi.org/10.3390/rs13050864

Birchak, J. R., C. G. Gardner, J. E. Hipp, and J. M (1974). Victor, High dielectric constant microwave problems for sensing soil moisture, Proc. IEEE, 62, 93-98.

Blanchy G., Saneiyan S., Boyd J., McLachlan P. and Binley A. (2020). "ResIPy, an Intuitive Open Source Software for Complex Geoelectrical Inversion/Modeling." Computers & Geosciences, February, 104423. https://doi.org/10.1016/j.cageo.2020.104423.

Brown, E. (1990). Density of asphalt concrete-how much is needed? https://doi.org/10.21949/1404494

Busato, L., Boaga, J., Peruzzo, L., Himi, M., Cola, S., Bersan, S., & Cassiani, G. (2016). Combined geophysical surveys for the characterization of a reconstructed river embankment. Engineering Geology, 211, 74–84. https://doi.org/10.1016/j.enggeo.2016.06.023

Cao, Q., & Al-Qadi, I. L. (2021). Effect of moisture content on calculated dielectric properties of asphalt concrete pavements from ground-penetrating radar measurements. Remote Sensing, 14(1), 34. https://doi.org/10.3390/rs14010034

Cao, Y., Dai, S., Labuz, J., & Pantelis, J. (2007). Implementation of ground penetrating radar.

Chang, C. M., Chen, J. S., & Wu, T. B. (2011). Dielectric modeling of asphalt mixtures and relationship with density. *Journal of Transportation Engineering*, *137*(2), 104-111.https://doi.org/10.1061/(ASCE)TE.1943-5436.000020

Chen, Q., Zhang, L.M., (2006). Three-dimensional analysis of water infiltration into the Gouhou rockfill dam using saturated unsaturated seepage theory. Can. Geotech. J. 43(5), 449–461.

Chlaib, H. K., Mahdi, H., Al-Shukri, H., Su, M. M., Catakli, A., & Abd, N. (2014). Using ground-penetrating radar in levee assessment to detect small-scale animal burrows. Journal of Applied Geophysics, 103, 121–131. https://doi.org/10.1016/j.jappgeo.2014.01.011

Commuri, S., Mai, A. T., & Zaman, M. (2011). Neural network–based intelligent compaction analyzer for estimating compaction quality of hot asphalt mixes. *Journal*

of Construction Engineering and Management, *137*(9), 634-644. https://doi.org/10.1061/(ASCE)CO.1943-7862.0000343

Constable, S.C., Parker, R.L., Constable, C.G., (1987). Occam's inversion: a practical algorithm for generating smooth models from electromagnetic sounding data. Geophysics 52, 289–300. https://doi.org/10.1190/1.1442303

Cosenza P., E. Marmet, F. Rejiba, Y. Jun Cui, A. Tabbagh, and Y. (2006). Charlery, "Correlations between geotechnical and electrical data: A case study at Garchy in France," Journal of Applied Geophysics, vol. 60, pp. 165-178. https://doi.org/10.1016/j.jappgeo.2006.02.0030

Dane, J. H., & Hopmans, J. W. (2002). Laboratory Methods of soil analysis: Part 4 physical methods, 5, 675-720.

Daniels, D. J. (Ed.). (2004). Ground penetrating radar (Vol. 1). Iet.

De Groot-Hedlin, C., Constable, S., (1990). Occam's inversion to generate smooth, two-dimensional models from magnetotelluric data. Geophysics 55, 1613–1624. https:// doi.org/10.1190/1.1442813.

Dezert, T., Fargier, Y., Palma Lopes, S., & Côte, P., (2019). Geophysical and geotechnical methods for fluvial levee investigation: A review. Engineering Geology, 260(March 2018), 105206. https://doi.org/10.1016/j.enggeo.2019.105206

Domitrović, J., & Rukavina, T. (2013). Application of GPR and FWD in Assessing Pavement Bearing Capacity. Romanian Journal of Transport Infrastructure, 2(2), 11–21. https://doi.org/10.1515/rjti-2015-0015

Domitrovi´c, J.; Rukavina, T.; Bezina, Š.; Stanˇceri´c, I. (2019). Mapping of Runway Pavement Layers Thickness by GPR. In Proceedings of the International Conference on Sustainable Materials, Systems and Structures (SMSS2019)—Challenges in Design and Management of Structures, Rovinj, Croatia, 20–22; Ivankovi´c, A.M., Kušter Mari´c, M., Strauss, A., Kiši ˇcek, T., Eds.; RILEM Publications, S.A.R.L.: Paris, France, 2019; pp. 208–215.].

DWMS (2024) Hungarian Drought and Water Scarcity Monitoring System https://vizhiany.vizugy.hu/

Edwards, L. & Mason, Q., (2011). Evaluation of Nondestructive Methods for Determining Pavement Thickness, US Army Corps of Engineers: ERDC/GSL TR-11-41.

ElShafie, A., & Heggy, E. (2013). Dielectric and hardness measurements of planetary analog rocks in support of in-situ subsurface sampling. *Planetary and Space Science*, *86*, 150-154.

Evans, R., Frost, M., Stonecliffe-Jones, M., & Dixon, N. (2007). Assessment of in situ dielectric constant of pavement materials. Transportation Research Record, 2037, 128–135. https://doi.org/10.3141/2037-12

Fernando, E. G., & Maser, K. R. (1992). Development of a procedure for the automated collection of flexible pavement layer thicknesses and materials: Phase i: Demonstration of existing ground penetrating radar technology. Florida DOT State Project, 99700, 7550.

Fetter, C. W. (2001). Properties of aquifers. Applied hydrogeology, 625p. University of Wisconsin, Oshkosh. https://arjzaidi.files.wordpress.com/2015/09/unimasr-com_e7ce669a880a8c4c70b4214641f93a02.pdf

Flintsch, G. W., Al-Qadi, I. L., Loulizi, A., Lahouar, S., McGhee, K. K., & Clark, T. (2005). Field investigation of high-performance pavements in Virginia. Virginia Center for Transportation Innovation and Research.

Fukue, M., Minatoa, T., Horibe, H. and Taya, N., (1999). The micro-structure of clay given by resistivity measurements. Eng. Geol. 54, 43-53.

García-Tomillo, A., Figueiredo, T.De, Dafonte, J.D., Almeida, A., Paz-Gonz´alez, A., (2018). Effects of machinery trafficking in an agricultural soil assessed by Electrical Resistivity Tomography (ERT). Open Agric. 3, 378–385. https://doi.org/10.1515/opag-2018-0042

Geophysical Survey Systems Incorporation (GSSI) (2010) RADAN 7 software, accessible at: https:// www. geophysical. com/ software

Geophysical Survey Systems Incorporation (GSSI) (2017) RADAN 7 manual. Published by Geophysical Survey Systems, Inc. 40 Simon Street Nashua, New Hampshire 03060–3075 USA https:// www.geophysical.com/wp-content/uploads/2017/10/GSSI- RADAN-7-Manual.pdf

Geophysical Survey Systems Incorporation (GSSI). *RADAN 7 Manual (2023)*; Geophysical Survey Systems, Inc.: Nashua, NH, USA, 2017. Available online: https://www.geophysical.com/wp-content/uploads/2017/10/GSSI-RADAN-7-Manual.pdf

Ghosh, S., & Kundu, S. (2025). Fluvial anomaly as indicator of tectonically active landscapes: A study in the Darjeeling Sikkim Himalaya, India. *DYSONA-Applied Science*, *6*(1), 70-85.

Giao, P. H., Chung, S. G., Kim, D. Y., and Tanaka, H. (2003). *Electric imaging and laboratory resistivity testing for geotechnical investigation of Pusan clay deposits.* Journal of Applied Geophysics, 52(4):157–175. https://doi.org/10.1016/S0926-9851(03)00002-8

Goodman, D. (2017). GPR-SLICE Software. https://gpr-survey.com/

Goyal, V.C., Gupta, P.K., Seth, P.K. and Singh, V.N., (1996). Estimation of temporal changes in soilmoisture using resistivity method. Hydro. Proces. 10, 1147-1154. (14) (PDF) Electrical resistivity survey in soil science: A review. Available from: https://www.researchgate.net/publication/222649758_Electrical_resistivity_survey_in_soil_science_A_review [accessed Jul 18 2022].

GSSI. RADAN 7 software; 2018. https://www.geophysical.com/ software.

Gupta, S.C. and Hanks, R.J., (1972). Influence of wa ter content on electrical conductivity of the soil.Soil Sci. Soc. Am. Proc. 36, 855-857.

Hadzick Z.Z., A.K. Guber, Y.A. Pachepsky, R.L. Hill, (2011). Pedotransfer functions in soil electrical resistivity estimation. Geoderma 164. 195–202. https://doi.org/10.1016/j.geoderma.2011.06.004

Hartlieb, P., Toifl, M., Kuchar, F., Meisels, R., & Antretter, T. (2016). Thermo-physical properties of selected hard rocks and their relation to microwave-assisted comminution. *Minerals Engineering*, *91*, 34-41.

Himi, M., Casado, I., Sendros, A., Lovera, R., Rivero, L., & Casas, A. (2018). Assessing preferential seepage and monitoring mortar injection through an earthen dam settled over a gypsiferous substrate using combined geophysical methods. Engineering Geology, 246(September), 212–221. https://doi.org/10.1016/j.enggeo.2018.10.002.

Hojat, A. (2024). An iterative 3D correction plus 2D inversion procedure to remove 3D effects from 2D ERT data along embankments. *Sensors*, *24*(12), 3759. https://doi.org/10.3390/s24123759

Holzschuher, C., Lee, H. S., & Greene, J. (2007). Accuracy and Repeatability of Ground Penetrating Radar for Surface Layer Thickness Estimation of Florida Roadways. Florida Department of Transportation, Gainesville, Florida.

Hugenschmidt, J. (1996). Ground Penetrating Radar for road engineering. Materials and Structures/Materiaux et Constructions, 31(207), 192–194. https://doi.org/10.1007/bf02480399

InstroTek, I. (n.d.). ***MC-3 Elite^{TM} \| InstroTek, Inc.*** **Retrieved April 10, (2022)**, from https://www.instrotek.com/products/mc-3-elite

Iravani M. A., Deparis J., Davarzani H., Colombano S., Guérin R. and Maineult A.,(2020a). The influence of temperature on the dielectric permittivity and complex electrical resistivity of porous media saturated with DNAPLs: a laboratory study: Journal of Applied Geophysics, 172, 103921.

Iravani, M. A., Deparis, J., Davarzani, H., Colombano, S., Guérin, R., & Maineult, A. (2020b). Complex Electrical Resistivity and Dielectric Permittivity Responses to Dense Non-aqueous Phase Liquids' Imbibition and Drainage in Porous Media: A Laboratory Study. Journal of Environmental and Engineering Geophysics, 25(4), 557–567. https://doi.org/10.32389/JEEG20-050

Jaselskis, E. J., Grigas, J., & Brilingas, A. (2003). Dielectric Properties of Asphalt Pavement. Journal of Materials in Civil Engineering, 15(5), 427–434. https://doi.org/10.1061/(ASCE)0899-1561(2003)15:5(427)

Jerabek, J., Zumr, D., Dost´al, T., (2017). Identifying the plough pan position on cultivated soils by measurements of electrical resistivity and penetration resistance. Soil Tillage Res. 174, 231–240. https://doi.org/10.1016/j.still.2017.07.008.

Jodry, C., Palma Lopes, S., Fargier, Y., Sanchez, M., & Côte, P., (2019). 2D-ERT monitoring of soil moisture seasonal behaviour in a river levee: A case study. Journal of Applied Geophysics, 167, 140–151. https://doi.org/10.1016/j.jappgeo.2019.05.008

Kassem, E., Scullion, T., Masad, E., & Chowdhury, A. (2012). Comprehensive evaluation of compaction of asphalt pavements and a practical approach for density predictions. *Transportation research record*, *2268*(1), 98-107. https://doi.org/10.3141/2268-12

Keller, G. V. (2017). Electrical properties of rocks and minerals. In *Handbook of Physical Properties of Rocks (1982)* (pp. 217-294). CRC Press.

Keller, G.V. and Frischknecht F.C.,(1966). Electrical methods in geophysical prospecting. Pergamon Press Inc., Oxford: pp 517.

Kiss, T., Fiala, K., Gy, Sipos, Szatmári, G., (2019). *Long-term hydrological changes after various river regulation measures: are we responsible for flow extremes* Hydrol. Res. 50 (2), 417–430. https://doi.org/10.2166/nh.2019.095.

Kiss, T., Nagy, J., Fehérvári, I., Amissah, G. J., Fiala, K., & Sipos, G. (2021). *Increased flood height is driven by local factors on a regulated river with a confined floodplain, Lower Tisza, Hungary.* Geomorphology, 389, 107858. https://doi.org/10.1016/j.geomorph.2021.107858

Lalagüe, A., Lebens, M. A., & Hoff, I. (2014). Accuracy of Ground-penetrating Radar in Pavement Thickness Evaluation: Impact of Interpretation Errors. Materials and Infrastructures 1, 5, 227-237. https://doi.org/10.1002/9781119318583.ch17

Lászlóffy, W., (1982). *The Tisza. Akadémiai Kiadó,* Budapest, p. 610 (in Hungarian).

Laurens, S., Balayssac, J. P., Rhazi, J., Klysz, G., & Arliguie, G. (2005). Non-destructive evaluation of concrete moisture by GPR: Experimental study and direct modeling. Materials and Structures/Materiaux et Constructions, 38(283), 827–832. https://doi.org/10.1617/14295

Lee, B., Oh, S., & Yi, M. J. (2020). Mapping of leakage paths in damaged embankment using modified resistivity array method. Engineering Geology, 266, 105469. https://doi.org/10.1016/j.enggeo.2019.105469

Lee, D.-W., Lee, K.-S., Lee, Y.-H., (2011). Seepage analysis of agricultural reservoir due to raising embankment. Korean J. Agric. Sci. 38(3), 493–504.

Leng, Z., Al-Qadi, I. L., Shangguan, P., & Son, S. (2012). Field application of ground-penetrating radar for measurement of asphalt mixture density: Case study of Illinois route 72 overlay. *Transportation research record*, *2304*(1), 133-141. https://doi.org/10.3141/2304-1

Levesque, R. (2007). SPSS programming and data management: A guide for SPSS and SAS users.

Li, J., Walubita, L. F., Simate, G. S., Alvarez, A. E., & Liu, W. (2013). Use of ground-penetrating radar for construction monitoring and evaluation of perpetual pavements. IEEE Region 10 Annual International Conference, Proceedings/TENCON, 2–5. https://doi.org/10.1109/TENCON.2013.6718938

Liu, L., & Guo, T. (2003). Determining the condition of hot mix asphalt specimens in dry, water-saturated, and frozen conditions using GPR. Journal of Environmental & Engineering Geophysics, 8(2), 143-149. https://doi.org/10.4133/JEEG8.2.143

Loizos, A., & Plati, C. (2006). Field and laboratory test for assigning dielectric constants of asphalt pavement materials. Road materials and pavement design, 7(4), 513-532. https://doi.org/10.1080/14680629.2006.9690049

Loizos, A. & Plati, C., (2007a). Accuracy of Ground Penetrating Radar Horn-Antenna Technique for Sensing Pavement Subsurface. Sensors Journal, 7(5), pp.842–850.Technique for Sensing Pavement Subsurface. *Sensors Journal*, 7(5), pp.842–850. 10.1109/JSEN.2007.894152

Loizos, A. & Plati, C., (2007b). Accuracy of pavement thicknesses estimation using different ground penetrating radar analysis approaches. *NDT & E International*, 40(2), pp.147– 157.https://doi.org/10.1016/j.ndteint.2006.09.001

Loke, M. H., (2004). Tutorial: 2-D and 3-D Electrical Imaging Surveys, 2004 Revised Edition. Tutorial: 2-D and 3-D Electrical Imaging Surveys, (July), 136.

Loke, M.H., Barker, R.D., (1996). Rapid least-squares inversion of apparent resistivity pseudosections by a quasi-Newton method. Geophys. Prospect. 44, 131–152. https://doi.org/10.1111/j.1365-2478.1996.tb00142.x

Loken, M. C. (2007). Use of ground penetrating radar to evaluate Minnesota roads (No. MN/RC-2007-01).

Maser, K. (1990). Automated detection of pavement layer thickness and subsurface moisture using ground penetrating radar. Infrasense, Incorporated.

Maser, K. R. (1996). Condition assessment of transportation infrastructure using ground-penetrating radar. *Journal of infrastructure systems*, *2*(2), 94-101. https://doi.org/10.1061/(ASCE)1076-0342(1996)2:2(94)

Maser, K. R., & Scullion, T. (1992). Influence of asphalt layering and surface treatments on asphalt and base layer thickness computations using radar.

Mezősi, G. (2022). Natural Hazards and the Mitigation of their Impacts. Springer International Publishing AG, Switzerland,p. 260 https://doi.org/10.1007/978-3-031-07226-0

Michot, D., Dorigny, A. and Benderitter, Y., (2000). Mise en évidence par r ésistivité électrique desécoulements préférentiels et de l'assèchement par le maïs d'un calcisol de Beauce irrigué.C.R.Acad.Sci., 332, 29-36. (14) (PDF) Electrical resistivity survey in soil science: Areview. Available from: https://www.researchgate.net/publication/222649758_Electrical_resistivity_survey_in_soil_science_A_review [accessed Jul 18 2022].

Morey, R. M. (1998). Ground penetrating radar for evaluating subsurface conditions for transportation facilities, ‖ NCHRP Synthesis 255, Transportation Research Board, Washington D.C.

Oludayo, I. (2021). Effect of Grain Size Distribution on Field Resistivity Values of Unconsolidated Sediments. 7(1), 12–18.

Ožbolt, M., Rukavina, T., & Domitrović, J. (2012). Comparison of the pavement layers' thickness measured by georadar and conventional methods–examples from Croatia. The Baltic Journal of Road and Bridge Engineering, 7(1), 30-35. 10.3846/bjrbe.2012.0

Pavement Interactive (2002). *Nuclear Density Gauge - Pavement Interactive*. https://pavementinteractive.org/reference-desk/construction/compaction/nuclear-density-gauge/

Pereira, J.O., Defossez, P. & Richard, G. (2007). Soil susceptibility to compaction as a function of some properties of a silty soil as affected by tillage system. European Journal of Soil Science, 58, 34–44. https://doi.org/10.1111/j.1365-2389.2006.00798.x

Perri, M. T., Boaga, J., Bersan, S., Cassiani, G., Cola, S., Deiana, R., Simonini, P., & Patti, S., (2014). River embankment characterisation: The joint use of

geophysical and geotechnical techniques. Journal of Applied Geophysics, 110, 5–22. https://doi.org/10.1016/j.jappgeo.2014.08.012

Popik, M., Maser, K., & Holzschuher, C. (2010). Using high-speed ground penetrating radar for evaluation of asphalt density measurements. In Proceedings of the Annual Conference & Exhibition of the Transportation Association of Canada, Halifax, NS, Canada (pp. 26-29).

Porubiaková, A., & Komačka, J. (2015). A comparison of dielectric constants of various asphalts calculated from time intervals and amplitudes. *Procedia Engineering, 111(TFoCE)*, 660–665. https://doi.org/10.1016/j.proeng.2015.07.129.

Primusz, P., Abdelsamei, E., Ali, A. M., Sipos, G., Fi, I., Herceg, A., & Tóth, C. (2024). Assessment of In Situ Compactness and Air Void Content of New Asphalt Layers Using Ground-Penetrating Radar Measurements. *Applied Sciences*, *14*(2), 614. https://doi.org/10.3390/app14020614

Primusz P., Runa B., Balogh O., To´th Cs (2022). U´j e´pı´te´su} asz- faltre´tegek vastagsa´ga´nak e´s to¨mo¨rse´ge´nek meghata´roza´sa fo¨ldradarral. U´tu¨gyi lapok. Makada´m 2000 Kft., 2022, 10(16), 38–52. (In Hungarian)

Radzicki, K., Gołębiowski, T., Ćwiklik, M., & Stoliński, M. (2021). A new levee control system based on geotechnical and geophysical surveys including active thermal sensing: A

Rahimi, S., Wood, C. M., Coker, F., Moody, T., Bernhardt-Barry, M., & Mofarraj Kouchaki, B. (2018). The combined use of MASW and resistivity surveys for levee assessment: A case study of the Melvin Price Reach of the Wood River Levee. Engineering Geology, 241(May), 11–24. https://doi.org/10.1016/j.enggeo.2018.05.009.

Reynolds, J. M. (2011). An introduction to applied and environmental geophysics. A John Wiley & Sons, Ltd., Publication. 2nd Edition

Reynolds, W. D., & Elrick, D. E. (2002). Constant head well permeameter (vadose zone). Methods of Soil Analysis: Part 4 Physical Methods, 5, 844-858.

Richards, K.S., Reddy, K.R., (2010). New approach to assess piping potential in earth dams and levees. ASCE NEWS, 51(6) (pp. A1, A4, A5, andA10).

Robain, H., Descloitres, M., Ritz, M., and Atangana, Q. Y., (1996). A multiscale electrical survey of a lateritic soil system in the rain forest of Cameroon. Journal of Applied Geophysics, 34(4):237–253. https://doi.org/10.1016/0926-9851(95)00023-2

Roberts, F. L., Kandhal, P. S., Brown, E. R., Lee, D. Y., & Kennedy, T. W. (1996). Hot mix asphalt materials, mixture design and construction.

Roddis, W. M., Maser, K., & Gisi, A. J. (1992). Radar pavement thickness evaluations for varying base conditions. Transportation Research Record, (1355).

Romero, P., & Kuhnow, F. (2002). Evaluation of new nonnuclear pavement density gauges with data from field projects. *Transportation research record*, *1813*(1), 47-54. https://doi.org/10.3141/1813-06

Saarenketo, T. (1997). Using ground-penetrating radar and dielectric probe measurements in pavement density quality control. *Transportation Research Record*, *1575*(1), 34-41. https://doi.org/10.3141/1575-05

Saarenketo, T., & Roimela, P. (1998). Ground penetrating radar technique in asphalt pavement density quality control. In *Proceedings of the seventh international conference on ground penetrating radar* (Vol. 2, pp. 461-466).

Saarenketo, T., & Scullion, T. (2000). Road evaluation with ground penetrating radar. *Journal of applied geophysics*, *43*(2-4), 119-138. https://doi.org/10.1016/S0926-9851(99)00052-X.

Salazar, F., Toledo, M.Á., Oñate, E., Suárez, B., (2016). Interpretation of dam deformation and leakage with boosted regression trees. Eng. Struct. 119, 230–251.

Samouelian, A. Cousin, I., Tabbagh, A. Bruand, A. and Richard, G. (2005). Electrical resistivity survey in soil science: a review. Soil and Tillage Research, vol. 83, pp. 173-193.

Sarabandi, K., Li, E. S., & Nashashibi, A. (1997). Modeling and measurements of scattering from road surfaces at millimeter-wave frequencies. *IEEE Transactions on Antennas and Propagation*, *45*(11), 1679-1688.https://doi.org/10.1109/8.650080

Schweitzer F. (2001), Pleisztocen. In: Karatson D. (szerk.) Pannon enciklopedia Kertek,Budapest,130-135.https://docplayer.hu/1721975-A-magyarorszagi-folyoszabalyozasok-geomorfologiai-vonatkozasai.html

Scullion, T., & Briggs, R. C. (1991). Use of Radar Technology for Pavement Layer Evaluation. Texas Transportation Institute, Texas A & M University System.

Sener, J. C., Smith, R. M., Garz, M. D., Murgel, G. A., Hamilton, R. W., & Haws, D. 68.R. (1998, March). Pavement thickness evaluation by GPR survey in Idaho. In Structural Materials Technology III: An NDT Conference (Vol. 3400, pp. 236-249). SPIE. https://doi.org/10.1117/12.300095

Sentenac, P., Benes, V., Budinsky, V., Keenan, H., & Baron, R. (2017). Post flooding damage assessment of earth dams and historical reservoirs using non-invasive geophysical techniques. Journal of Applied Geophysics, 146, 138–148.

Šernas, O., Vorobjovas, V., Šneideraitienė, L., & Vaitkus, A. (2016). Evaluation of asphalt mix with dolomite aggregates for wearing layer. *Transportation Research Procedia*, *14*, 732-737.

Shangguan, P., Al-Qadi, I., Coenen, A., & Zhao, S. (2016). Algorithm development for the application of ground-penetrating radar on asphalt pavement compaction monitoring. *International Journal of Pavement Engineering*, *17*(3), 189-200. https://doi.org/10.1080/10298436.2014.973027

Shang, J. Q., Umana, J. A., Bartlett, F. M., & Rossiter, J. R. (1999). Measurement of complex permittivity of asphalt pavement materials. Journal of transportation engineering, 125(4), 347-356. https://doi.org/10.1061/(ASCE)0733-947X(1999)125:4(347)

Sheishah, D., Kiss, T., Borza T., Fiala K., Kozák P., Abdelsamei E., Tóth C., Grenerczy G., Páll, D. G., & Sipos G. (2023a). Mapping subsurface defects and surface deformation along the artificial levee of the Lower Tisza River, Hungary. Natural Hazards journal 117, 1647–1671 (2023). https://doi.org/10.1007/s11069-023-05922-1

Sheishah, D., Sipos, G., Barta, K., Abdelsamei, E., Hegyi, A., Onaca, A., & Abbas, A. M. (2023b). Comparative evaluation of the material of the artificial levees.

Journal of Environmental Geography, 16(1–4), 1–10. https://doi.org/10.14232/jengeo-2023-44452

Sheishah, D., Sipos, G., Hegyi, A., Kozák, P., Abdelsamei, E., Tóth, C., Onaca, A., & Páll, D. G. (2022). Assessing the Structure and Composition of Artificial Levees Along the Lower Tisza River (Hungary). Geographica Pannonica, 26(3), 258–272. https:// doi: 10.5937/gp26-39474

Solla, M., Lagüela, S., González-Jorge, H., & Arias, P. (2014). Approach to identify cracking in asphalt pavement using GPR and infrared thermographic methods: Preliminary findings. NDT and E International, 62, 55–65. https://doi.org/10.1016/j.ndteint.2013.11.006

Sudha K., M. Israil, S. Mittal, and J. Rai, (2009)."Soil characterisation using electrical resistivity tomography and geotechnical investigations," Journal of Applied Geophysics, vol. 67, pp. 74-79.

Szlávik, L (2000). Az Alföld árvízi veszélyeztetettsége (Flood hazard in the Great Hungarian Plain). In A Vízs Zerepe és Jelent˝osége (Role and Significance of Water in the Great Hungarian Plain); Pálfai, J., Ed.; Nagyalföld Alapítvány: Békéscsaba, Hungary; pp. 64–84. (In Hungarian).

Szűcs P., Nagy L., Ficsor J., Kovács S., Szlávik L., Tóth F., Keve G., Lovas A., Padányi J., Balatonyi L., Baross K., Sziebert J., Ficzere A., Göncz B., & Dobó K., (2019) Árvízvédelmi ismeretek = Flood Protection, available at: http://hdl.handle.net/20.500.12944/13490 (in Hungarian)

Tabbagh, J., Samouëlian, A., Tabbagh, A., and Cousin, I., (2007). *Numerical modelling of direct current electrical resistivity for the characterisation of cracks in soils.* Journal of Applied Geophysics, 62(4):313–12 323. https://doi.org/10.1016/j.jappgeo.2007.01.004

Topp, G. C., J. L. Davis, and A. P. Annan (1980). Electromagnetic determination of soil water content: Measurement in coaxial transmission lines, Water Resource. Res., 16, 574-582.

Tresoldi, G., Arosio, D., Hojat, A., Longoni, L., Papini, M., & Zanzi, L., (2019). Long-term hydrogeophysical monitoring of the internal conditions of river levees. Engineering Geology, 259 (August 2018), 105139. https://doi.org/10.1016/j.enggeo.2019.05.016

Wang, S., Leng, Z., Sui, X., Zhang, W., Ma, T., & Zhu, Z. (2024). Real-Time Asphalt Pavement Layer Thickness Prediction Using Ground-Penetrating Radar Based on a Modified Extended Common Mid-Point (XCMP) Approach. *IEEE Transactions on Intelligent Transportation Systems.* https://doi.org/10.1109/TITS.2023.3343196

Website 1: https://vizhiany.vizugy.hu/

Willett, D. A., Mahboub, K.C., & Rister, B. (2006). Accuracy of ground-penetrating radar for pavement-layer thickness analysis. Journal of Transportation Engineering, 132(1), 96–103. https://doi.org/10.1061/(ASCE)0733-947X(2006)132:1(96)

Willoughby, K. and Mahoney, J. (2007). An assessment of wsdot's hot-mix asphalt quality control and assurance requirements. resreport WA-RD 517.2, Washington State Department of Transportation, Olympia, WA, USA.

Xiong, X., Xiao, S., Tan, Y., Zhang, X., Zhang, D., Han, M., & Wang, W. (2021). Estimation of density and moisture content in asphalt mixture based on dielectric property. *Construction and Building Materials*, *298*, 123518. https://doi.org/10.1016/j.conbuildmat.2021.123518

Yoon G. L. and Park J. B., (2001). "Sensitivity of leachate and fine contents on electrical resistivity variations of sandy soils," Journal of Hazardous Materials, vol. 84, pp. 147-161.

Zhao, Y., Xie, S., Gao, Y., Zhang, Y., & Zhang, K. (2021). Prediction of the number of roller passes and degree of compaction of asphalt layer based on compaction energy. *Construction and Building Materials*, *277*, 122274. https://doi.org/10.1016/j.conbuildmat.2021.122274

Zhu, J.J., Kang, H.Z., Gonda, Y., (2007). Application of Wenner configuration to estimate soil water content in pine plantations on sandy land. Pedosphere 17, 801–812. https://doi.org/10.1016/S1002-0160(07)60096-4.

Zorkóczy, Z., (1987). Árvízvédelem = Flood protection. Budapest: Országos Vízügyi Hivatal (in Hungarian).

Summary

The dissertation titled "Performance of Shallow Geophysical Techniques in The Assessment of Earth and Road Structures" specifically focuses on the application of Ground Penetrating Radar (GPR) and Electrical Resistivity Tomography (ERT) in assessing the integrity of earthern levees and the quality of road structures. The study evaluates the effectiveness of these non-destructive techniques in delineating seepage pathways in levees and measuring pavement thickness, structure, and moisture content in aged road sections with complex multilayer compositions. Additionally, the research explores the potential of GPR in determining the specific gravity and relative density of asphalt mixtures, aiming to develop a method for assessing compaction quality and generating spatial maps of asphalt density. The hypotheses proposed in this dissertation were as follows:

1. How effective are electrical resistivity tomography (ERT) and ground-penetrating radar (GPR) in delineating seepage pathways and accurately identifying subsurface features in levees?
2. How do the results of geophysical surveys, particularly Ground Penetrating Radar (GPR) and Electrical Resistivity Tomography (ERT), compare with validation through drilling, and what are the relative strengths and limitations of these methods in assessing infrastructures such as levees and pavements?
3. How accurate and reproducible are GPR measurements for assessing road thickness and structure in aged pavements with a complex multilayer structure?
4. How do different environmental conditions and pavement properties affect GPR measurements and the obtained dielectric constant values?
5. What is the optimal procedure to map dielectric constants and related physical properties through field and laboratory comparisons?
6. How can Ground Penetrating Radar (GPR) be effectively utilized to determine the specific gravity and relative density of asphalts?
7. Is it possible to develop a general function between dielectric properties and specific gravity for dolomitic pavements to facilitate compaction quality mapping?

The dissertation employed a diverse range of data collection techniques, including a controlled tank experiment to simulate flood conditions along a 37-meter levee section, and extensive GPR surveys on aged road sections and newly constructed pavements. For data analysis, the study utilized specialized software such as RADAN 7 for GPR data

processing, RES2DINV for ERT data inversion, and Surfer for spatial interpolation and visualization of results. The research also incorporated validation methods, including borehole drilling for levee assessment, core sampling for road thickness verification, and nuclear gauge measurements for calibrating GPR-derived asphalt density data, ensuring the accuracy and reliability of the geophysical findings.

The dissertation yielded significant findings in the assessment of levee integrity using combined GPR and ERT techniques. Three-dimensional ERT profiles successfully delineated seepage pathways as the experimental tank was filled, while 3D GPR profiles indicated areas of increased amplitude corresponding to seepage zones and the water table. Validation through drilling confirmed the accuracy of these geophysical methods in non-destructively identifying subsurface features and seepage channels. The study demonstrated that the levee body primarily comprised fine silts, with low-to-medium resistivity values indicating a homogeneous nature. However, saturated hydraulic conductivity measurements revealed a non-aquitard nature, suggesting susceptibility to concentrated seepage despite the homogeneous structure.

In the assessment of aged road structures, GPR proved highly effective in measuring pavement thickness and structure in complex, multilayered compositions. The average error of thickness measurements between continuous GPR and core data was 2.87% using the ground truth method and 8.72% using the amplitude method . The study revealed significant variations in dielectric values under different moisture conditions, with the surface asphalt layer exhibiting average dielectric values of 4.00, 7.06, and 8.31 under dry, medium-wet, and wet conditions respectively. These findings highlighted the importance of considering environmental factors when interpreting GPR data for road assessments. The research also demonstrated that GPR could effectively differentiate between various road components, including macadam, asphalt, and cement-treated base, based on their dielectric properties.

For newly constructed pavements, the dissertation explored the potential of GPR in assessing asphalt compaction quality. The study established clear relationships between dielectric constants, specific gravity, and aggregate size. A robust function was developed to indirectly determine the specific gravity (G_{mb}) of asphalts composed of dolomite and limestone aggregates using GPR, applicable to aggregate sizes ranging from 11 mm to 25 mm and G_{mb} values between 2.43 and 2.57 g/cm³. The research also demonstrated the capability of GPR to generate relative density (RD) maps, visualizing the spatial homogeneity of asphalt density. These maps revealed significant variations in

compaction quality across pavement depth and along roadway sections, with RD values ranging between 0.94 and 0.98, considered close to the optimum value. The study concluded that GPR-based density assessment, when calibrated with nuclear gauge measurements, could effectively extend asphalt density evaluation spatially, offering a non-destructive alternative to traditional core sampling and nuclear density gauge measurements.

The results of this study have significant implications for flood risk management and infrastructure assessment. The demonstrated effectiveness of combined GPR and ERT techniques in evaluating levee integrity and seepage dynamics offers a reliable approach for flood risk assessment in Hungary and similar flood-prone areas worldwide, potentially reducing the risk of unexpected levee failures. In road infrastructure management, the high precision of GPR in assessing pavement thickness, structure, and moisture content in aged roads with complex compositions allows for more accurate evaluation of road conditions, leading to better-informed decisions regarding rehabilitation and maintenance efforts. Furthermore, the development of GPR-based methods for assessing asphalt compaction quality and generating relative density maps has important implications for pavement construction and quality control processes, potentially improving overall pavement quality, longevity, and long-term performance prediction.

In conclusion, this dissertation demonstrates the versatility and effectiveness of shallow geophysical techniques, particularly GPR and ERT, in assessing earth and road structures. The research provides comprehensive evidence of the applicability of these non-destructive methods for evaluating levee integrity, assessing aged road conditions, and determining asphalt compaction quality in newly constructed pavements. By offering improved spatial resolution and coverage compared to traditional point-measurement methods, this study contributes to the broader field of smart infrastructure management, supporting data-driven decision-making processes in civil engineering and potentially leading to significant cost savings in long-term infrastructure maintenance and rehabilitation.

Declaration

I, Enas Muhammed Abdelrazek Abdelsamei, affirm that the dissertation presented for the doctoral degree at the Doctoral School of Geosciences, University of Szeged, is entirely my own work and has not been previously submitted for any academic degree elsewhere. I assure that all assistance received in its preparation and all sources utilized have been fully acknowledged and referenced.